Using Dissolved Gas Analysis to Investigate the Performance of Permeable Reactive Barriers

by

Randi Lee Williams

B.Sc., The University of Wisconsin – Madison, 2001

A THESIS SUBMITTED IN PARTIAL FULFILLMENT OF THE REQUIREMENTS FOR THE DEGREE OF

MASTER OF APPLIED SCIENCE

in

THE FACULTY OF GRADUATE STUDIES

(Geological Engineering)

THE UNIVERSITY OF BRITISH COLUMBIA

MARCH 2005

ABSTRACT

The strongly reducing nature of permeable reactive barrier (PRB) treatment materials can lead to gas production, potentially resulting in the formation of gas bubbles and ebullition. For this work degassing in the saturated zone of PRB systems due to the production of gases (primarily CO_2 and CH_4) is investigated using the depletion of Ar and N_2, naturally present non-reactive gases, in order to identify, confirm, and possibly quantify chemical and physical processes occurring. Dissolved gas sampling and analysis were conducted at three PRB sites designed for the treatment of groundwater contaminated by mining and industrial activities: the Nickel Rim Mine Organic Carbon PRB Site (Site I), the Campbell Mine Zero-Valent Iron (Fe^0)/ Organic Carbon Test Cell PRB (Site II), and the Columbia Nitrogen Fe^0/ Organic Carbon Mixed PRB Site (Site III).

At Site I, residence times within the PRB are sufficiently long to allow gas production and degassing. A simple four-gas degassing model was used to analyze the data set, and the results indicate that sulfate reduction is by far the main process of organic carbon consumption within the barrier. The data provided additional information to delineate rates of microbially mediated sulfate reduction and to determine slow and fast flow zones within the barrier. Degassing was incorporated into reactive transport simulations for Site I in order to model 8 years of barrier operation. The simulations adequately reproduce observed dissolved gas trends, although no information on the volume change due to bubble formation or the fate of the trapped gas could be obtained.

At Site II, residence times were short and the dissolved gas data could be used primarily as a transport tracer. Zones of preferential and of low flow could be identified within the PRB. At Site III, the strong resemblance of water composition upgradient and

downgradient of the PRB suggested that residence times are long and that there is little flow through the PRB. The dissolved gas data could primarily be used as a reaction tracer. The data suggested that gas production and reaction rates are relatively insignificant in the barrier system.

The success and failures at Sites I-III could be used to create a set of criteria under which dissolved gas analysis is useful for PRB systems. Treatment material composition, dissolved gas composition in the groundwater influent to the PRB, and residence times through the PRB are important factors to consider.

TABLE OF CONTENTS

LIST OF TABLES

LIST OF FIGURES

ACKNOWLEDGEMENTS

I would like to acknowledge all those who made my thesis work possible.

Thanks to my advisors, Dr. Uli Mayer and Dr. David Blowes. Uli was a wonderful mentor, always providing support and guidance, and it was a privilege to work with him. Dr. Blowes allowed me to conduct interesting field work, and provided insights along the way.

Thanks to professors Dr. Roger Beckie and Dr. Leslie Smith for their constructive criticism and comments. They were great instructors throughout my studies.

A very special thanks to my colleagues at UBC, particularly Craig Thompson, Rich Amos, Sergi Molins, and Jasmin Caton, for their conversation, influences, and/or help with field work from the beginning. I would also like to thank Jeff Bain and David Smyth of U of Waterloo, and Ralph Ludwig of the EPA for all of their contributions and help coordinating field work.

This project was made possible by funding from the Canadian Water Network (CWN).

Chapter I: Introduction

1.1 Introduction

Permeable reactive barriers (PRB's) offer a passive approach for the remediation of contaminated groundwater. These remediation systems are often composed of treatment mixtures containing zero-valent iron (Fe^0) or organic carbon, with the objective to induce reducing conditions which are suitable for the treatment of a variety of contaminants (Benner et al., 1999; Blowes et al., 2000; Schipper and Vojvodić-Vuković, 2001; Nikolaidis et al., 2003). The strongly reducing nature of treatment materials may lead to gas production in permeable reactive barriers (PRB's), potentially resulting in the formation of gas bubbles and ebullition.

The formation of gas bubbles has been observed previously in laboratory columns containing organic carbon (Soares et al., 1988 and 1991) and Fe^0 (Kamolpornwijit et al., 2003), and in Fe^0 treatment cells (Morrison et al, 2002). Mackenzie et al. (1999) demonstrated that hydrogen gas production and entrapment could occur within the iron media. Long-term column studies conducted by Vikesland et. al (2003) showed that precipitate formation and gas pocket accumulation could alter transport properties of a column filled with granular iron media. The vertical transport conditions of most column experiments, however, do not correspond to field conditions, and gas bubble formation, entrapment, exsolution, and ebullition are expected to be different in field situations (Vikesland et al., 2003).

Although gas production may have negative effects on barrier permeability (Fryer and Schwartz, 1998; Mackenzie et al., 1999; Liang et al., 2000; Kamolpornwijit et al., 2003) and contaminant treatment (Morrison, 2003; Vikesland et al., 2003), the formation

of gas bubbles will likely affect the gas composition in the pore water, and therefore may be a useful indicator in helping to delineate physical transport and biogeochemical reaction processes occurring within and down-gradient of PRB systems. Precipitation water is typically in equilibrium with atmospheric gases prior to infiltration into the subsurface. Subsequently, microbially mediated processes may either consume (O_2 by aerobic respiration) or produce gases (e.g.: N_2 by denitrification, H_2S and CO_2 by sulphate reduction, CH_4 and CO_2 by methanogenesis), while altering the dissolved gas composition. Inorganic reactions, such as carbonate mineral dissolution-precipitation may also affect the ratio of gases dissolved in groundwater.

Blicher-Mathiesen et al. (1998) demonstrated that in the saturated zone naturally occurring non-reactive dissolved gases (i.e., argon) could be used to estimate the degree of denitrification and degassing taking place within a Danish riparian wetland. Amos et al. (2005) applied the use of non-reactive dissolved gases at a degrading petroleum hydrocarbon contaminated site. These authors also demonstrated that when denitrification is negligible, Ar and N_2 could effectively be used to better understand and quantify physical and chemical processes related to methanogenic activity. Specifically, Amos et al. (2005) showed that the production of methane could induce degassing, thus causing depletion in dissolved Ar and N_2. The signature of Ar and N_2 depletion could therefore be used to infer degassing rates and provide a better estimate of the rate of methanogenesis, and also suggested that attenuation of methane along the flow path, and into the down gradient aquifer, is largely controlled by physical processes. Fortuin and Willemsen (2005) used the hydrogeochemical transport model PHREEQC to simulate organic carbon decomposition, CH_4 formation and subsequent N_2 and Ar exsolution.

They correlated the model results to their field data, collected throughout pristine Dutch and Belgian aquifers, to determine the total historical organic carbon decomposition needed to account for the observed dissolved gas concentrations. While the use of non-reactive gases (i.e., Ar and N_2) to investigate physical and chemical processes occurring within aquifers has been demonstrated in various settings, to our knowledge this method has not been applied within a PRB system.

For example, Figure 1.1 demonstrates the effect that gas production may have in an organic carbon permeable reactive barrier designed for the treatment of acid mine drainage. Though the gases produced (or consumed) within PRBs of different treatment materials may vary, the effect is generally applicable to all PRB systems. In Figure 1.1a, initial anoxic groundwater is shown, with N_2, and Ar at atmospheric levels, and slightly elevated CO_2. Figure 1.1b shows that H_2S, CO_2 and CH_4 gases are being produced, as a result of sulfate reduction and methanogenesis, thus increasing the total gas pressure in the system. In Figure 1.1c, a critical pressure threshold is reached, considered here to be the hydrostatic pressure, causing a gas bubble to form. Dissolved gases equilibrate into the gas phase according to Henry's Law, and this process will lead to the depletion of the non-reactive gases Ar and N_2. In Figure 1.1d the gas bubble is mobilized, which may occur if the bubble reaches a critical size and buoyancy forces overcome capillary forces. Bubble transport may lead to ebullition and the removal of the bubble from the system. The degree of depletion of Ar and N_2 can be used to infer the scale of which the other reaction processes are occurring.

1.2 Thesis Objectives

The objectives of this work include the use of dissolved gas analysis to investigate the performance of permeable reactive barriers, specifically, to test if the gas composition can be used to identify, confirm, and possibly quantify chemical and physical processes occurring within PRB systems. Specifically, dissolved gas analysis will be used in this study to answer the following questions:

- *Does the occurrence of degassing leave a signature within and downgradient of a PRB?*
- *Can the gas composition be used as a proxy for residence time in order to provide additional information on the existence of preferential flow within a PRB?*
- *Can dissolved gas data be used to determine the treatment material consumption attributed to each reaction process occurring within a PRB?*
- *Can dissolved gas data be used to delineate the rates of the reaction processes occurring within a PRB?*
- *Does the occurrence of degassing imply that ebullition is taking place at a site?*
- *Can we use this study to determine a set of criteria under which dissolved gas analysis is (particularly) useful within a PRB system?*

To address these objectives, dissolved gas sampling and analysis were conducted at three PRB sites designed for the treatment of groundwater contaminated by mining and industrial activities: the Nickel Rim Mine Organic Carbon PRB Site (Site I), the

Campbell Mine Zero-Valent Iron (Fe^0)/ Organic Carbon Test Cell PRB (Site II), and the Columbia Nitrogen Fe^0/ Organic Carbon Mixed PRB Site (Site III).

1.3 References

Amos, R.T., K.U. Mayer, B. A. Bekins, G. N. Delin, R. L. Williams, 2005. Use of dissolved and vapour-phase gases to investigate methanogenic degradation of petroleum hydrocarbon contamination in the subsurface. *Wat. Resour. Res.* 41, W02001, doi:10.1029/2004WR003433.

Blicher-Mathiesen, G., G. W. McCarty, L. P. Nielsen, 1998. Denitrification and degassing in groundwater estimated from dissolved dinitrogen and argon, *J. Hydrol.*, 208, 16-24.

Blowes, D. W., C. J. Ptacek, S. G. Benner, C. W. T. McRae, T. A. Bennet, R. W. Puls, 2000. Treatment of inorganic contaminants using permeable reactive barriers. *J. Contam. Hydrol.*, 45, 123-137.

Fortuin, N., and A. Willemsen, 2005. Exsolution of nitrogen and argon by methanogenesis in Dutch ground water. *J. Hydrol.*, 301, 1-13.

Fryar, A. E and F. W. Schwartz, 1998. Hydraulic-conductivity reduction, reaction-front propagation, and preferential flow within a model reactive barrier. *J. Contam. Hydrol.*, 32, 333-351.

Kamolpornwijit, W., L. Liang, O. R. West, G. R. Moline, A. B. Sullivan, 2003. Preferential flow path development and its influence on long-term PRB performance: column study. *J. Contam. Hydrol.*, 66, 161-178.

Liang, L., N. Korte, B. Gu, R. Puls, C. Reeter, 2000. Geochemical and microbial reactions affecting the long-term performance of in situ 'iron barriers'. *Adv. Environ. Res.*, 4, 273-286.

Mackenzie, P. D., D. P. Horney, T. M. Sivavec, 1999. Mineral precipitation and porosity losses in granular iron columns. *J. Haz. Mat.*, 68, 1-17.

Morrison, S. J., D. R. Metzler, B. P. Dwyer, 2002. Removal of As, Mn, Mo, Se, U, V, and Zn from groundwater by zero-valent iron in a passive treatment cell: reaction progress modeling. *J. Contam. Hydrol.*, 56, 99-116.

Morrison, Stan J., 2003. Performance evaluation of a permeable reactive barrier using reaction products as tracers. *Environ. Sci. Technol.*, 37, 2302-2309.

Nikolaidis, N. P., G. M. Dobbs, J. A. Lackovic, 2003. Arsenic removal by zero-valent iron: field, laboratory and modeling studies. *Water Res.*, 37, 1417-1425.

Schipper, L. A. and M. Vojvodić-Vuković, 2001. Five years of nitrate removal, denitrification and carbon dynamics in a denitrification wall. *Water Res.*, 35, 3473-3477.

Soares, M. I. M, S. Belkin and A. Abeliovich, 1988. Biological groundwater denitrification: Laboratory studies. *Wat. Sci. Tech.*, 20, 189-195.

Soares, M. I. M., C. Braester, S. Belkin, and A. Abeliovich, 1991. Denitrification in laboratory sand columns: Carbon regime, gas accumulation and hydraulic properties. *Water Res.*, 25, 325-332.

Vikesland, P. J, J. Klausen, H. Zimmermann, A. L. Roberts, W. P. Ball, 2003. Longevity of granular iron in groundwater treatment processes: changes in solute transport properties over time. *J. Contam. Hydrol.*, 64, 3-33.

Figures

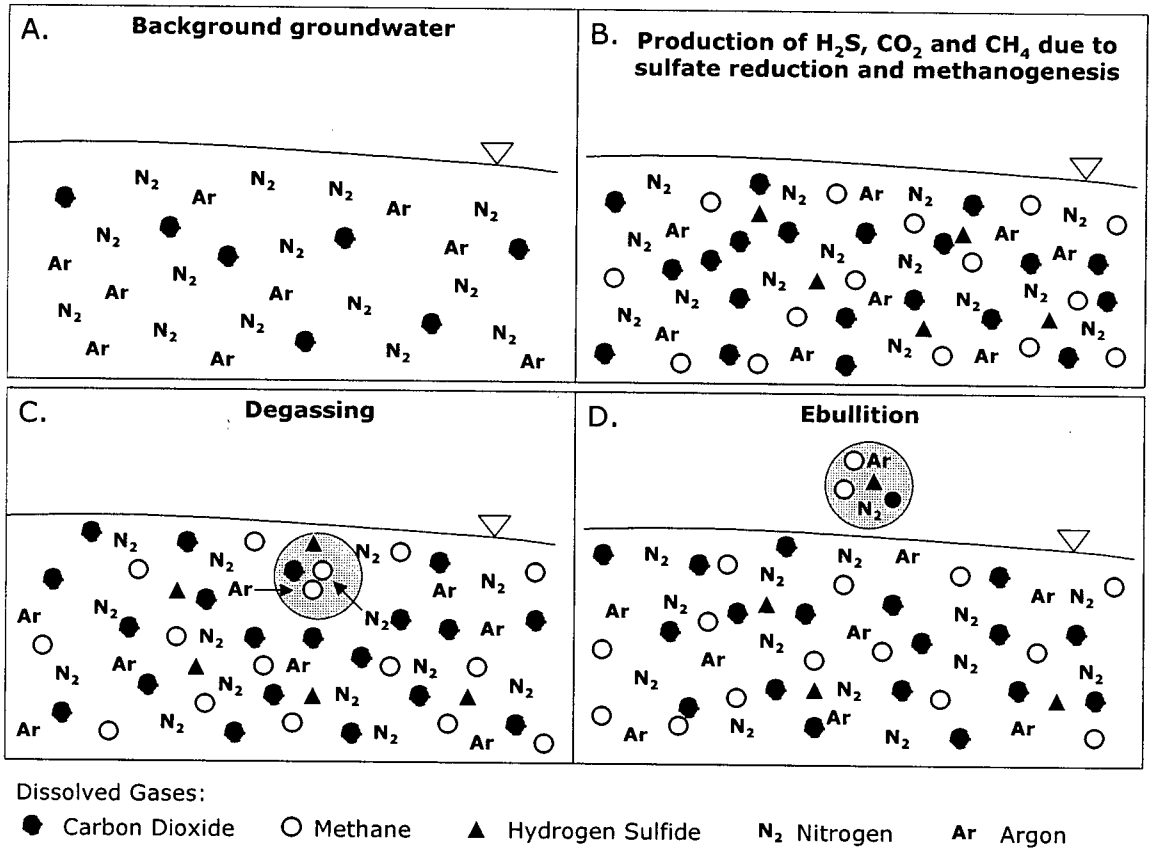

Figure 1.1 Conceptual diagram of: (A) typical groundwater, N_2 and Ar present near atmospheric levels; (B) gas production (i.e., increasing H_2S, CO_2 and CH_4) resulting from sulfate reduction and methanogenesis; (C) gas accumulation and degassing of all gases in groundwater; and (D) ebullition. Assuming no other sources of argon or nitrogen concentrations in groundwater, both (C) and (D) result in depletion of atmospheric gases nitrogen and argon.

Chapter II: Methods

2.1 Introduction

The following sections describe dissolved gas sampling and analysis procedures conducted at three PRB sites: the Nickel Rim Mine Organic Carbon PRB Site (Site I), the Campbell Mine Zero-Valent Iron (Fe^0)/ Organic Carbon Test Cell PRB (Site II), and the Columbia Nitrogen Fe^0/ Organic Carbon Mixed PRB Site (Site III). Deviations from the methods discussed in the following sections will be discussed in the following chapters that are specific to each site.

2.2 Dissolved Gas Sampling

Groundwater samples were collected at three different PRB sites using peristaltic pumps. Samples were analyzed in the field at Site I and Site II. Samples collected from Site III were analyzed in the Earth & Ocean Science Hydrogeology Laboratory at the University of British Columbia. All samples were analyzed for dissolved CH_4, CO_2, Ar, N_2, O_2, and H_2 gases using a Varian Micro CP-4900 portable gas chromatograph (GC). Additionally, dissolved oxygen was also analyzed using CHEMets colorimetric field kits (0-1 ppm, 1-10 ppm) (CHEMets, Inc., Calverton, Va). Sulfide samples were analyzed using CHEMets sulfide field kits (0-1 ppm, 1-10 ppm, with activation solution A-9500) (CHEMets, Inc., Calverton, Va). Duplicate samples were collected and analyzed at several locations at each site. Samples were also analyzed for dissolved H_2S at Site I.

Peristaltic pumps were the chosen method of groundwater extraction, due to the small tubing (1/4-inch) within bundle piezometers at all sites, and the small diameters within the wells (1 inch- to- 1 ¼ inch) at Sites I and II. At least 3 well volumes were

purged at low flow rates (25 ml min^{-1} to 200 ml min^{-1}) prior to sample collection at well points. Low pumping rates were used to avoid degassing, which would jeopardize dissolved gas analysis. Bubbles were rarely observed in the line while pumping.

2.3 Dissolved Gas Analysis Method

Dissolved gases were analyzed in the field (Site I and II) or laboratory (Site III) using the headspace method described by Amos et al. (2005). Sampling of dissolved gas species was performed by flushing groundwater at low flow rates in an airtight 125 ml glass flask (Site I) or 250 ml glass bottle (Sites II and III) before sample collection. After the bottle had been sufficiently flushed and capped with a septum cap, the bottle was inverted and a 15 ml aliquot of UHP helium was injected through the rubber septum as equal parts of the sample were removed. The sample was then agitated for 10 minutes to allow for dissolved gases to equilibrate with the headspace. After equilibration, a 10 ml gas sample was collected from the headspace with a gas-tight syringe for injection into the field gas chromatograph (GC). The GC was calibrated each sampling day using calibration gas (Sigma-Aldrich 5% CO_2, CO, N_2, and O_2; 4% H_2, CH_4, and He) and air.

2.4 Dissolved Gas Data Corrections

GC analysis results are reported for CH_4, CO_2, Ar, N_2, O_2, H_2, and H_2S as mole fractions. These data are converted to partial pressures based on flask pressure (measured by inserting a pressure gauge into the flask influent tubing line), atmospheric pressure for the ground elevation at each site, and groundwater temperature (degrees Kelvin). Due to the anaerobic nature of the samples and their susceptibility to be contaminated by atmospheric gas, a correction is applied to the partial pressure to compensate for this source of error. For this correction the O_2 concentration of the water is measured by an

alternate means (i.e., CHEMets kits (CHEMets, Inc., Calverton, Va)) and taken to be the true value. The difference between the true value and the value obtained through GC analysis can then be used to estimate the amount of atmospheric contamination in the sample. For the non-atmospheric gases the contamination of the sample by atmospheric gases results in dilution of the sample, which is generally small. The corrected partial pressure A_{g-C} is calculated as follows;

$$A_{g-C} = A_g(1+(A_{O_2} - \overline{A_{O_2}})/0.21) \tag{2.1}$$

where A_g is the uncorrected partial pressure, A_{O_2} is the value of O_2 obtained from the GC, $\overline{A_{O_2}}$ is the true value and 0.21 is the mole fraction of O_2 in the atmosphere. For the atmospheric gases Ar and N_2 the contamination of the sample results in dilution plus an additional increment of the particular gas added to the sample so that the extra Ar or N_2 must be subtracted from the measured value using the following;

$$A_{g-C} = A_g - X_{g-A}((A_{O_2} - \overline{A_{O_2}})/0.21) \tag{2.2}$$

where X_{g-A} is the mole fraction of the gas in the atmosphere. This correction was not applied at Site III. Atmospheric contamination of the gas chromatography samples was typically low (<8%, on average < 5% at Site I; < 9 % on average, < 2 % at Site II).

To calculate dissolved gas concentrations in the sample water using the headspace technique the following equation is used;

$$[A]_{aq} = \frac{([A]_g V_g) + ([A]_w V_w)}{V_w} \div MW \tag{2.3}$$

where;

$$[A]_g = A_g / RT$$

$$[A]_w = K_H A_g$$

and $[A]_g$ (mol L^{-1}) is the concentration of the gas in the headspace, $[A]_w$ (mol L^{-1}) is the concentration of the gas in the water in the sample flask, V_g and V_w are the volume of the headspace and volume of the water in the sample flask respectively, MW is the molecular weight of the gas, K_H (M atm^{-1}) is the Henry's law constant for the gas at the sample temperature, R is the ideal gas constant, and T is the sample temperature. All Henry's law constants used are from the CRC Handbook (2001) except CH_4, which is from Yamamoto et al. (1976).

2.5 Blanks Samples

Field blanks of deionised water were pumped through the sampling equipment, and then analyzed using the same procedures described above. Field blanks demonstrated that the sampling methods described above did not introduce contamination to the samples. Dissolved gas data was near atmospheric for Ar, CO_2, N_2, and O_2, and SO_4 and Fe collected at Site I were below the detection limits.

2.6 Additional Site Specific Methods

2.6.1 Site I

In addition to dissolved gas data collection and analysis, sulfate (Hach SulfaVer 4 Sulfate reagent (citric acid and barium chloride)) and ferrous iron (Hach Ferrous Iron Reagent) samples were analyzed by passing samples through 0.22-μm filters (Millipore 33 mm Millex Syringe filters) and using a portable data logging spectrophotometer (Hach DR/2010). Determinations of pH (Fisher Scientific Accumet AP25 meter and Orion refillable probe) were made at each piezometer. The pH probe was calibrated and

regularly checked using pH 4.0 and pH 7.0 buffer solutions, which encompassed the range of observed pH-values.

Ebullition of gas bubbles was visible above the PRB in standing water at the site after rain events. Flasks were placed above the location to collect the gas, and triplicate samples were analyzed.

Argon depletion for each sample was calculated by normalizing the measured value at each well with respect to the average of the background well concentrations of argon (i.e., up gradient well nests RW21, RW23, RW22, and RW24), which were close to atmospheric Ar-contents.

2.6.2 Site II

Four vapour sampling wells were constructed of 2 cm OD stainless steel tubing with a porous tip. The porous tip was located within the unsaturated zone just above the water surface within the reactive media, and just below the clay cap. Gas samples were collected in a 50 ml gas tight syringe using a peristaltic pump after purging of a minimum of 3 well volumes.

2.6.3 Site III

Atmospheric contamination did appear to affect the data collected at site III, likely as a result of the lapse in time between collection and sample analysis, and due to changes in temperature from collection (approximately 26 degrees C in situ) to sample storage (approximately 6 degrees C), which caused a small bubble to form in the bottles due to volume loss. CHEMets DO data had been collected at the site, and in general the site conditions are anoxic. Sample contamination appeared to be small, such that the site

trends in the dissolved gas data (i.e., Ar, N_2, CH_4, and CO_2) are significant and still allow a conclusive analysis.

2.7 References

Amos, R.T., K.U. Mayer, B. A. Bekins, G. N. Delin, R. L. Williams, 2005. Use of dissolved and vapour-phase gases to investigate methanogenic degradation of petroleum hydrocarbon contamination in the subsurface. *Water Resour. Res.*, 41, W02001, doi:10.1029/2004WR003433.

Lide, D. R., editor-in-chief, 1994. *CRC Handbook of Chemistry and Physics, 75th Edition*; CRC Press, Inc.: Boca Raton, Florida.

Yamamoto, S., J. B. Alcauskas, T. E. Crozier, 1976. Solubility of methane in distilled and sea water. *J. Chem. Eng. Data*, 21, 78-80.

Chapter III:

Using dissolved gas analysis for investigating the performance of an organic carbon permeable reactive barrier for the treatment of acid mine drainage

3.1 Introduction

Drainage waters from mine tailings derived from sulfidic ore deposits are elevated in concentrations of SO_4 and Fe and other metals (Zn, As, Pb, etc.). The present study was conducted at the Nickel Rim organic carbon PRB site near Sudbury, Ontario, which was designed to treat acid mine drainage (Waybrant, 1995; Benner et al., 1997; Waybrant et al., 1998; Benner et al., 1999; Benner et al., 2002). As groundwater high in sulfate and ferrous iron enters the organic carbon PRB, microbially mediated reduction of sulfate occurs (Benner et al., 1997):

$$SO_4^{2-} + 2CH_2O + 2H^+ \rightarrow H_2S + 2CO_{2(g)} + 2H_2O \quad (3.1)$$

and ferrous iron then rapidly reacts with sulfide to form metal sulfides within the barrier (Benner et al., 1997):

$$Fe^{2+} + H_2S \rightarrow FeS_{(s)} + 2H^+ \quad (3.2)$$

Another naturally occurring reaction within the barrier, though not a part of the treatment process, is the decomposition of the organic carbon coupled with methanogenesis (Stumm and Morgan, 1996):

$$2CH_2O \rightarrow CO_{2(g)} + CH_{4(g)} \quad (3.3)$$

Both equations (3.1) and (3.3) lead to the consumption of the organic carbon treatment material, and the possible production of gases (i.e., CO_2, CH_4, and H_2S).

A significant amount of gas production may induce degassing and possibly ebullition, which may also affect dissolved gas composition, as was discussed in the introductory chapter (Figure 1.1).

Multicomponent reactive transport modeling efforts to date (Mayer et al., submitted) conducted at the Nickel Rim PRB have focused on the quantitative evaluation of the conceptual model for the site based on aqueous phase geochemical data (Benner et al., 2002) and solid phase sulfur geochemistry (Herbert et al., 2000). Mayer et al. (submitted) assessed the performance of the PRB over a 3.5 year time period, and considered spatial and seasonal variability. Although extensive fieldwork and modeling analysis have been conducted at this site, a detailed analysis of dissolved gases to assess barrier performance has not been conducted to date.

The specific objectives of the current work are outlined in Chapter 1. In addition, a four-gas degassing model was developed to determine the ratio between the dominant terminal electron accepting processes (TEAPs) occurring within the PRB, and reactive transport simulations were conducted using the reactive transport code MIN3P (Mayer et al., 2002) to assess the suitability of a simple equilibrium-degassing model to describe the process of gas exsolution at this site. These simulations also provide further insight into the long-term performance of organic carbon PRB's.

3.2 Site Description

Dissolved gas data was collected at the organic carbon PRB near the Nickel Rim mine site, in Sudbury, Ontario (Figure 3.1, after Benner et al., 2002). The hydrogeology of the site has been well characterized by Johnson (1993), Bain et al. (1995), and Bain (1996). The installation of the PRB took place in August 1995 (Benner et al., 1997).

Contaminant treatment, geochemistry, microbiology, and flow processes within the PRB, are described in Benner et al. (1997, 1999, 2000, 2002), Herbert Jr. et al. (2000), and Daignault (2002).

Groundwater originating from the tailings impoundment follows two paths ending at Moose Lake. Approximately half of the water from the tailings dam flows within the alluvial aquifer, passing through the PRB. The remaining water from the tailings seeps out of the base of the tailings dam and reaches Moose Lake as surface water (Benner et al., 1997). The plume from the tailings dam is high in Fe and SO_4 concentrations (500 to 2000 mg L^{-1} Fe and 1000 to 7000 mg L^{-1} sulfate) and is slightly acidic (pH 4-6) (Bain, 1996). The aquifer is bounded by bedrock to the north, south, and base, and groundwater velocities are estimated to be 15 m a^{-1} (Bain et. al., 1995). As shown in Figure 3.1, monitoring points have been installed along three transects, A-A', E-E', and F-F', passing through the PRB (Benner et al., 1999). Sampling locations along cross-section A-A' are shown in Figure 3.2 (after Benner et al., 1999). The site ground elevation is 315 m (0.941 atm).

3.3 Methods

The sampling conducted at Nickel Rim took place in the area between the monitoring wells just up gradient of the organic carbon PRB and Moose Lake July 9 through July 19, 2003. Monitoring points were sampled at well nests RW21, RW22, RW23, and RW24 up-gradient of the PRB; nests RW29, RW30, RW31, RW81, RW78 within the PRB; and nests RW26, RW71, RW76, RW36, RW28, RW32, and RW35 down-gradient of the PRB (Figure 3.2). The depth to groundwater at the site was approximately 0.5 meters during sample collection for this work.

Within the barrier, monitoring points within nests RW29, RW30, RW31, and RW81 are 1¼-inch wells, and all other points are bundle piezometers. Mini-packers were placed within the 1¼-inch wells just above the screen in order to minimize the volume of water being purged and to avoid atmospheric contamination of the samples.

3.4 Four-Gas Analytical Model

A four-gas degassing model considering nitrogen (N_2), argon (Ar), carbon dioxide (CO_2) and methane (CH_4) was developed based on the governing equations by Cirpka and Kitanidis (2001), and described in Amos et al. (2005). The degree of Ar and N_2 depletion measured in the PRB is used here to determine the ratio between microbially mediated sulfate reduction and methanogenesis. The groundwater at the site is anaerobic, which allowed oxygen to be disregarded in the model calculations. The governing equations are formulated as functions of total concentrations, ideal gas behaviour is assumed, and equilibrium partitioning between the phases is described by Henry's law. The total concentration of each gas in the system is calculated by;

$$T_i = C_{i(aq)} S_w + C_{i(g)} S_g \tag{3.4}$$

where T_i (mol L^{-1}) is the total mass of gas i per pore volume, $C_{i(aq)}$ (mol L^{-1}) is the concentration of the gas in the aqueous phase, $C_{i(g)}$ (mol L^{-1}) is the concentration of the gas in the gas phase and S_w and S_g are the water and gas saturations, respectively. Given the total concentration, a theoretical partial pressure for each gas can be calculated assuming $S_g = 0$, and therefore $T_i = C_{i(aq)} S_w$;

$$\bar{p}_i = T_i / K_i \tag{3.5}$$

where K_i is the Henry's law constant (mol L^{-1} atm^{-1}) of gas i. Table 3.1 provides Henry's Law constants used for each gas. If the sum of the theoretical gas pressures of all the

gases present in the system is less than the total pressure, P_T, then no gas phase is present. If the sum of the theoretical pressure exceeds the total pressure then a gas phase is present and then S_g can be calculated so that the following condition is satisfied;

$$P_T = \sum_{i=1}^{N_g} p_i \tag{3.6}$$

where p_i (atm) is the partial pressure of gas i and N_g is the number of gases in the system. In practical terms, this implies that the four considered gas partial pressures used in the model, N_2, Ar, CO_2, and CH_4, equal the total gaseous phase pressure. Substituting the relations;

$$C_{i(aq)} = p_i K_i \tag{3.7}$$

and

$$C_{i(g)} = p_i / RT \tag{3.8}$$

into Equation (3.4) and solving for p_i yields;

$$p_i = \frac{T_i}{K_i S_w + S_g / RT} \tag{3.9}$$

where R is the gas constant (0.08206 atm L mol^{-1} K^{-1}) and T (K) is temperature. Substituting Equation 3.9 into Equation 3.6, S_g can be determined. Subsequently $C_{i(aq)}$ and $C_{i(g)}$ can be calculated using Equations 3.7 and 3.8, respectively.

Due to the incompressibility of water the formation of a gas phase displaces a volume of water equal to the gas saturation so that at each reaction step the water saturation is updated by;

$$S_w = 1 - S_g \tag{3.10}$$

maintaining a constant volume. This results in a loss of gas from the system equal to $S_g \times C_{i(aq)}$ at each step.

For each step update of the model, production of CH_4 and CO_2 increase the total pressure until a critical threshold is reached, and bubble formation and degassing occurs. We assume that this threshold is the hydrostatic pressure. All gases dissolved in the water partition into the bubble according to Henry's Law, and dissolved concentrations of natural gases present, i.e., N_2 and Ar, therefore decrease (see Figure 1.1).

CO_2-production due to microbially mediated reduction of sulfate is described by equation (3.1). Increases in CO_2 and CH_4 due to methanogenesis are described by equation (3.3). By assuming all CH_4 measured is a result of equation (3.3), a 1:1 ratio of CH_4 to CO_2 observed is assumed to be a product of methanogenesis. The remaining CO_2 measured is assumed to be a product of sulfate reduction. The model allows the use of different ratios of sulfate reduction to methanogenesis to optimize the fit to measured partial pressures at each sampling point within the PRB, and thus optimize the estimate for the contribution of sulfate reduction for the various sampling locations. If only the existing dissolved CH_4 and CO_2 concentrations are used, an underestimation will occur because a considerable amount of all gases are lost to the gas phase during degassing (Amos et al., 2005).

The pH measured within the barrier ranged from 6.3 to 6.9, which required including the speciation of dissolved CO_2 into bicarbonate using the equation (Stumm and Morgan, 1996):

$$CO_{2(aq)} + H_2O \rightarrow H^+ + HCO_3^- \qquad \log K_1 = -6.40 \; for \; T = 17°C \qquad (3.11)$$

where T is temperature and K_1 is the equilibrium constant for the reaction, respectively. Model calculations were based on a groundwater temperature of 17 degrees Celsius (290 K), which is consistent with temperature values reported by Benner et al., (2002) for mid July. Groundwater temperatures within the aquifer and barrier exhibit large seasonal variations, with an annual change of 17 degrees C (Benner et al., 2002). Sulfate reduction is complex and is likely limited by fermentative activity when groundwater exhibits colder temperatures. Model calculations for July do not, therefore, represent annual barrier performance.

The four-gas model assumes an initial amount of sulfate, based on observed concentrations up gradient of the barrier (20- to- 40 mmol L^{-1}). Sulfate reduction is initially assumed to be independent of sulfate concentrations, but the sulfate reaction rates start to decrease with decreasing sulfate concentrations (Benner et al., 2002), suggesting that a Monod-type expression is suitable. Therefore, for the 4-gas model, a new ratio of sulfate reduction to methanogenesis is calculated within the model as the initial sulfate concentration declines. The new ratio (R_{new}) is calculated as a fraction of the initial ratio (R_{int}) using the expression

$$R_{new} = R_{\text{int}} \cdot \left(\frac{[SO_4]}{K_{SO_4} + [SO_4]} \right) \qquad (3.12)$$

where $[SO_4]$ is the total concentration of dissolved sulfate [mol L^{-1}] and the half saturation constant (K_{SO_4}) equals 1.62 x 10^{-3} mol L^{-1} based on literature data (Boudreau and Westrich 1984; Roychoudhury et al., 1998).

Chloride data and flow modeling boundary and initial conditions from Benner et al. (2002) were used to estimate residence times for the points sampled within the barrier.

These residence times were used in conjunction with values of sulfate reduced at each data point using the four-gas model, which allowed the estimation of sulfate reduction rates.

3.5 Reactive Transport Modeling

3.5.1 Model Framework

Mayer et al. (submitted) conducted reactive transport modeling of the Nickel Rim PRB over a 3.5-year time period. The chemical and physical framework for the modeling simulations conducted in this study are nearly identical to that described in Mayer et al. (submitted). Here, methanogenesis was included to facilitate the simulation of degassing and to improve the long-term modeling over 8 years of barrier operation. For details on the modeling setup not described in the following sections (model and chemical framework, boundary and initial conditions, accounts for the influence of seasonal temperature variation, etc.), refer to Mayer et al. (submitted).

3.5.2 Chemical Framework

As described by Mayer et al. (submitted), sulfate-reduction results in organic carbon oxidation (i.e., consumption) and the production of hydrogen sulfide and elemental sulfur. A multi-modal Monod-type rate expression was used to simulate the observed long-term decline in barrier reactivity and rate dependence on sulfate concentration. The rate expression is defined as:

$$R_{SO_4-H_2S} = -\sum_{i=1}^{N_{org}} k_{i,SO_4-H_2S} \left(\frac{[SO_4]}{K_{SO_4} + [SO_4]} \right) \tag{3.13}$$

where N_{org} is the number of organic carbon fractions with different reactivity and k_{i,SO_4-H_2S} is the effective rate coefficient for fraction i [mol dm^{-3} s^{-1}]. [SO_4] is the total

concentration of dissolved sulfate [mol L^{-1}] and the half saturation constant (K_{SO_4}) equals 1.62 x 10^{-3} mol L^{-1} based on literature data (Boudreau and Westrich 1984; Roychoudhury et al., 1998). Previous work did not consider consumption of the organic carbon treatment material by processes other than sulfate reduction; however, in the current simulations organic carbon also undergoes methanogenesis by the following reaction:

$$CH_2O + \frac{1}{2}H_2O \rightarrow \frac{1}{2}CH_{4(aq)} \frac{1}{2}CO_3^{2-} + H^+ \qquad (3.14)$$

Due to the lack of information on reaction intermediates, the fermentation of organic carbon and the consumption of the fermentation products by sulfate reduction and by methanogenesis are described as overall reactions. The rate expression used to simulate the observed long-term decline in barrier reactivity assumes that the most reactive organic carbon fraction is consumed first, causing the overall reactivity to decline asymptotically, an approach consistent with the widely accepted model of natural organic carbon as composed of a continuum of reactivities to oxidation (Westrich and Berner, 1984; Boudreau and Ruddick, 1991). Based on a series of preliminary simulations, the number of organic carbon fractions was set to $N_{org} = 4$, representing fractions of decreasing reactivity (with fraction 1 being the fastest and fraction 4 being the slowest to react).

3.5.3 Degassing of Ar, CH_4, CO_2, and N_2

Degassing of Ar, CH_4, CO_2, and N_2, and was included in the simulations, because neglecting the process would lead to simulated concentrations of these gases which over predict field observed N_2(aq), CO_2(aq) and CH_4(aq). The following equation incorporated into the MIN3P code was used to calculate the degassing rate (Mayer et al., 2001):

$$R_d = k_d \max\left[\left(\frac{\sum_{i=1}^{Ng} p_i^g}{p_a + 9.869 \cdot 10^{-6} \rho_w g(h_i - z_i)} - 1\right), 0\right] \quad (3.15),$$

where k_d defines the rate constant for the degassing reaction (5×10^{-9} mol L^{-1} H_2O s^{-1}, calibrated), g the gravitational acceleration (m s^{-2}), p_a is the atmospheric pressure (atm), and ρ_w identifies the density of water (kg m^{-3}). The confining pressure is calculated on the basis of the nodal hydraulic head obtained from the flow solution (h_i (m) and the elevation head z_i (m). Calibration of the degassing rate involved achieving a simulation in which the first term in the brackets of equation 3.15 is close to zero, representative of equilibrium conditions. Henry's Law equilibrium values were calculated with changing temperature via the Van't Hoff Equation. The transport of gas bubbles was not considered; it was assumed that gas bubbles leave the saturated zone instantaneously and exit to the atmosphere.

3.6 Results and Discussion

3.6.1 Dissolved Gases and Water Chemistry

Dissolved gas results show that argon and nitrogen are generally depleted within the PRB at Nickel Rim, relative to groundwater up gradient of the barrier (Figures 3.3 to 3.6), confirming our hypothesis and indicating that degassing is taking place. Depletion of argon and nitrogen was seen down gradient of the PRB (Figure 3.3) as well, though the depletion was less than that seen within the top and base of the PRB. The depletion of argon and nitrogen correlates well with elevated concentrations of dissolved methane (0.45 mg L^{-1} to 20.57 mg L^{-1}) and CO_2 (140.81 mg L^{-1} to 810.09 mg L^{-1}) within the PRB relative to up gradient methane (below the detection limit of 0.01 mg L^{-1} to 0.08 mg L^{-1}) and CO_2 concentrations (103.10 mg L^{-1} to 224.41 mg L^{-1}), and less elevated

concentrations of methane (0.28 mg L^{-1} to 14.59 mg $L^{-1)}$ and CO_2 (256.07 mg L^{-1} to 726.79 mg L^{-1}) down gradient of the PRB. Within the PRB, the greater depletion of argon and nitrogen in the top and bottom portions of the barrier correlates well with the more elevated concentrations of dissolved CH_4 and CO_2 at these locations. Overall, the groundwater is anoxic throughout the studied area, and dissolved hydrogen gas is below the detection limit of 1 mg L^{-1}. H_2S gas odors were present at several sampling locations within the barrier, but were only detected at two locations (RW30-a at 10.2 mg L^{-1} and RW24-4 at 4.1 mg L^{-1}). Alternative analysis using CHEMets kits also showed that total sulfide was not present up gradient or down gradient of the barrier, but was also measured at RW30-a (3 mg L^{-1}), and at RW29-2 as well (0.1 mg L^{-1}). In addition, sulfide was detected along cross-section E-E' at RW81-x (3.0 mg L^{-1}) and at RW76-4 (0.1 mg L^{-1}). Ferrous iron data collected in 2003 ranged from 169 mg L^{-1} to 1,200 mg L^{-1} up gradient of the barrier, 0.88 mg L^{-1} to 219 mg L^{-1} within the PRB, and 28 mg L^{-1} to 860 mg L^{-1} down gradient of the PRB. Corresponding sulfate concentrations ranged from 1,500 mg L^{-1} to 5,400 mg L^{-1} up gradient of the barrier, 660 mg L^{-1} to 3,500 mg L^{-1} within the PRB, and 5 mg L^{-1} to 4,900 mg L^{-1} down gradient of the PRB. The observed pH measurements ranged from 5.5 to 6.3 up gradient of the barrier, 6.3 to 6.9 within the barrier, and from 6.3 to 6.5 down gradient of the barrier. Observed pH values were higher within the top and bottom portions of the barrier than pH values observed in the central portion of the barrier. The pH values downgradient of the barrier appeared to be consistent with pH values observed within the central portion of the barrier.

3.6.2 Ratio Between Sulfate Reduction and Methanogenesis

The four-gas analytical model was used to reproduce observed dissolved N_2, Ar, CH_4, and CO_2 at each location sampled within the barrier along transect A-A'. The simulations were carried out for assumed pH values of 6.5 and 6.9 to account for the effect of carbonate speciation under different pH-conditions. Observed pH-values within the barrier in July 2003 ranged from approximately 6.3 to 6.9. Using a pH of 6.5 lead generally to a better agreement between observed and simulated data, and these results are discussed here. The results using a pH of 6.9 are shown in Appendix A for completeness. Observed gas partial pressures are presented in Figure 3.7 for well nest 29 through 31, corresponding to the portion of cross section A-A' that is located within the PRB, and are plotted in direct comparison to the results of the 4-gas model. Each "step" corresponds to a specified amount of CO_2 and CH_4 added to the system produced through sulfate reduction and methanogenesis and thus defines reaction progress. Using a ratio of sulfate reduction to methanogenesis of 16: 1, the best overall fit to the gas results from within the barrier was achieved. This ratio was determined by visual assessment of trial simulations, but appears to be a reasonable estimate, as it was also the average of the specific ratios for individual sampling locations, discussed below. The errors between observed and simulated results using this ratio are shown in Table A1 of Appendix A. The error results show that observed N_2 and Ar partial pressures could be matched very well, but small variations in CH_4 and CO_2 lead to large errors.

In general, Figure 3.7 shows that observed gas compositions from zones of elevated CH_4 and CO_2 (29-2, 30-a, 30-3, 31-2, 31-a, as indicated from Figures 3.3 and

3.4) are comparable with simulated data for a relatively large number of degassing "steps". Assuming constant sulfate and methanogenesis rate coefficients, "steps" are proportional to residence times within the PRB. Simulated N_2 partial pressures are much lower than atmospheric levels and Ar depletion is greater at these sampling locations, generally corresponding well with observed data, and indicating a significant degree of degassing. Observed gas partial pressures for sampling locations with less elevated CH_4 and CO_2, and less depletion of N_2 and Ar (29-8, 30-4, 30-b, 31-4, 31-b, as indicated from Figures 3.3 and 3.4) tend to correlate with the model results for fewer "steps".

The goodness of fit estimates shown in Table A1 of Appendix A indicates that the ratio of 16:1 between sulfate reduction and methanogenesis is not equally applicable for all sampling locations. Observed values were moved along the "step" axis until the best match to the simulated N_2 and Ar was found, and therefore N_2 and Ar average error results were low at 3.8 and 7.2 percent, respectively, while CO_2 and CH_4 average error results were 25 and 50 percent, respectively (Table A1). For this reason, the four-gas model was also used to match each data point individually using a sampling location specific ratio of sulfate reduction to methanogenesis to improve the match between observed and simulated gas partial pressures. For example a lower ratio of sulfate reduction to methanogenesis of 7:1 provides a better fit to the observed results for well 31-2 (Figure 3.8). In general, the observed data for sampling locations with a greater degree of degassing were better fit to the model using lower ratios of sulfate reduction to methanogenesis than for sampling locations with a lower degree of degassing, indicating that more organic carbon is consumed by methanogenesis in zones of advanced reaction progress, due possibly to sulfate transport limitations to these zones. Table 3.2

summarizes the calibrated ratios of sulfate reduction to methanogenesis for sampling locations along A-A' within the barrier. Plots including observed data and model results at specific locations are included in Appendix A. Using this approach the average relative error between observed and simulated data ranges between 5.1 % and 9.3% for the various gases (Table A2). The ratios for all sampling locations are greater than or equal to 5:1, indicating that the majority of the organic carbon throughout the barrier is being consumed by sulfate reduction.

The average ratio of sulfate reduction to methanogenesis in zones of significant degassing is 8:1, while the average ratio for sampling locations in zones of limited degassing was 24:1 (Table 3.2). Assuming the overall average of sulfate reduction to methanogenesis of 16:1 (Table 3.2) is representative to the average ratio throughout the barrier, and using equations (3.1) and (3.3), it can be estimated that 94 percent of organic carbon is consumed by sulfate reduction, and 6 percent is consumed by methanogenesis, or, 97% of the CO_2 produced is generated by sulfate reduction, while methanogenesis contributes only 3%. Using the same calculation for the zones of significant and limited degassing estimates, 89% and 96% of the organic carbon is consumed by sulfate reduction, respectively.. This calculation confirms that the dominant TEAP within the barrier is by far sulfate reduction.

The relatively consistent agreement between observed and simulated gas compositions suggests that the equilibrium-based degassing model captures the process of gas exsolution adequately. The results also indicate that the samples from various locations have undergone a different degree of reaction progress, relatively independent from the distance of the sampling location from the up gradient end of the barrier. The 4-

gas model does not include ebullition, which will likely affect the results. If bubbles leave the system by ebullition, the model may underestimate the CH_4 and CO_2 production.

3.6.3 Relative Residence Times

Assuming that maximum reaction rates are relatively homogeneous throughout the barrier, the presence of zones of significant and limited degassing suggests that reaction progress and therefore residence time of the sampled pore water differs significantly between the different sampling locations. Dissolved gas data supports the existence of fast and slow flow zones within the barrier, as discussed by Benner et al. (2002). Using argon and nitrogen depletion as a proxy for residence time it can be seen that low flow zones exist at the top and base of the barrier (Figure 3.3) along cross-section A-A'. H_2S was only detected at the base of the barrier along cross section A-A', indicating that this is an area of very slow moving pore water, with slower velocities and, hence, longer residence times than measured elsewhere within the barrier (Figure 3.4). These results are consistent with low concentrations of Fe and SO_4 that were previously observed along cross section A-A' at the top and bottom of the barrier, also indicating increased residence times (Benner et al., 2002). Iron and sulfate results from the current sampling round were consistent with previously observed trends (data not shown).

Fewer sampling locations were available within the barrier along transects E-E' and F-F', but the available data for N_2, Ar, CO_2, and CH_4 are shown in Figures 3.5 and 3.6, respectively. Along transect E-E', greater N_2 and Ar depletion were seen at the top of the barrier (Figure 3.5). Benner et al. (2002) showed that the lowest SO_4 and Fe measured within the barrier were also at the top. Along transect F-F', greater N_2 and Ar

depletion were generally seen in the center of the barrier (Figure 3.6), though data was not collected from very shallow depths (nothing less than 1.6 m below ground surface) in the barrier along this transect, so the trends could not be accurately defined.

3.6.4 Reaction Rates and Treatment

For each "step" of the 4-gas model, sulfate reduction can be estimated, by assuming that for every 2 moles of CO_2 produced as defined by equation (3.1), 1 mole of sulfate is reduced, and reacts with 1 mole of iron as defined in equation (3.2) to form FeS precipitate. Model results indicate the amount of sulfate removed at specific points within the barrier (Table 3.3). One could also calculate the amount of Fe that could potentially precipitate by equation (3.2). Equation (3.1) and (3.2), do not, however, describe the system fully. Though previous studies indicate that the dominant sink for SO_4 and Fe is solid phase mono-sulfides, sulfate may also be reduced to a native sulfur or solid phase organic S (Herbert et al., 2000), thereby limiting Fe removal. On the other hand, Fe may accumulate in the barrier as a pyrite-like phase or in a non-sulfide phase, such as siderite ($FeCO_3$) or an iron-carbonate solid solution, thereby increasing Fe-removal. Because this data does not provide insight into the various iron sinks, iron removal estimates will not be discussed further in the results.

The 4-gas model is based on equilibrium batch reactions, and time is not included in the model. In order for removal rates of sulfate to be estimated, residence times from the barrier entry to each specific sampling point were needed. These residence times were determined using Visual MODFLOW (Guiguer et al., 1997) flow and particle-tracking simulations, and modeling was based on flow modeling determined for the PRB by Benner et al. (2002). Rates were determined using the equation:

$$rate = \frac{\Delta C}{t_r} \qquad (3.16),$$

where ΔC is the change in sulfate concentration from the barrier influent to each sampling location, as shown in Table 3.3, and t_r is the residence time to the barrier sampling point from the barrier entry, estimated from flow modeling results. Table 3.4 lists t_r, ΔC, and the rate estimated for each sample location, in addition to estimated residence times from flow modeling through the entire barrier along the flow paths, which include the specific sample locations. These residence times further confirmed that zones of greater degassing (i.e., greater Ar or N_2 depletion), did fall into the slower flow path regime, while zones of limited degassing fell into the fast path regime. Results of the flow and particle-tracking simulations are presented in Figure 3.9. The sulfate reduction and removal rates compare well with the results of Benner et al. (2002) and Herbert et al. (2000), and a comparison is presented in Table 3.5. Consistent with results by Benner et al. (2002) and solid phase sulfur analyses by Herbert et al. (2000), higher rates of sulfate reduction were calculated at the front of the barrier using the 4-gas model (location 29-8 and 29-2).

Due to the many uncertainties, a detailed discussion of the agreement between removal estimates shown in Table 3.5 is not warranted. Sulfate removal rates in this study are based on estimates of sulfate reduced, according to the four-gas analytical model fit to the observed data at locations within the barrier, and residence times to the barrier point from the entry of the barrier using flow modeling. Benner (1999) estimates were developed by taking the lowest input SO_4 concentration to the barrier and comparing that to the highest effluent concentration, and as a result probably reflect the

low end of the rate scale. Herbert et al. (2000) estimates are based on solid phase digestion data, converted to aqueous concentrations. Herbert et al. (2000) found that sulfate species constitute an important S fraction in core samples. Because the current study estimates sulfate removal rates based on expected sulfate reduction according to equation (3.1), sulfate removal as SO_4 (exp., precipitation of gypsum ($CaSO_4 \cdot H_2O$)) is not considered, and removal rates may be underestimated. Table 3.5, however, shows that estimates for this study are higher than those found by Benner (1999) and Herbert et al. (2000). Because removal rates are determined at specific points within the barrier, they could potentially be higher than estimates based on influent-effluent data, as reported by Benner (1999) or average rates over time, estimated by Herbert et al. (2000). If sulfate is depleted along a flow path within the barrier, removal rates based on influent-effluent data may underestimate sulfate reduction rates. In addition, previous estimates were based on seasonal averages, while rates for the current work are for summer conditions, which are more suitable for microbial activity. Benner (2002) determined that seasonal temperature fluctuations cause large variations in sulfate removal rates.

3.6.5 Degassing and Ebullition

The ebullition of gas bubbles was observed above the barrier at a pool of water that had accumulated after rain events at the site. The location of the barrier where the ebullition occurred appeared to be an imperfection in the clay cover, likely the result of coring performed at previous sampling events. The gas was collected and analyzed and mole fractions of the gas revealed that approximately 50.5 percent of the gas was comprised of CO_2, 24.3 percent was CH_4, 23.7 percent was N_2, 0.4 percent consisted of Ar, and 1.1 percent was O_2, while the rate of ebullition from this location was estimated

to be 42 L day^{-1}, based on triplicate measurements. This observation confirms that degassing and ebullition is taking place at the Nickel Rim site. The O_2 observed is likely due to air contamination during sample collection and analysis. After applying a correction, CH_4, CO_2, N_2, and CO_2 gas results change only slightly, with CH_4 accounting for 25.6 percent of the emanating gas. When observed partial pressures of gas concentrations in the groundwater are converted to percentages of total gas, the average gas composition within the barrier is 26.8 percent CH_4, 24.0 percent CO_2, 0.7 percent Ar, 0.1 percent O_2, and 48.4 percent N_2. The composition of the gas bubbles collected above the barrier appears to be more depleted of Ar and N_2, and higher in CO_2, though CH_4 is very similar to the average composition within the groundwater. The degree of depletion of Ar and N_2 within the gas bubbles leaving the barrier is most similar to the depletion of the dissolved gases within the top and bottom portions of the barrier. The average gas composition within the top and bottom portions of the barrier was 46.7 percent CH_4, 28.1 CO_2, 0.4 percent Ar, and 24.8 percent N_2.

3.6.6 Implications of Degassing and Ebullition on PRB Mass Balance

Benner et al. (2002) suggested that H_2S degassing may be an important sink for sulfide, and could possibly solve the sulfide mass balance issue presented. The current work demonstrated low or non-detect observed H_2S concentrations and the lack of ebullition of H_2S, which suggests that degassing and ebullition is an unlikely sink for sulfide. This result indicates that sulfur is almost exclusively removed by precipitation reactions within the PRB, therefore providing the intended sink for Fe (II).

The gas data allows for a crude estimate of CH_2O consumption. The amount of CO_2 and CH_4 produced in moles per litre of groundwater within the barrier can be

estimated, by averaging the results for the four-gas model simulation at each sampling location. Using equations (3.1) and (3.3), this estimate can be converted to CH_2O consumed. Assuming a porosity of 0.4 within the barrier, a groundwater velocity of 16 m a^{-1}, and a cross-sectional area of 45 m^2, the flux of the water through the barrier is 288 m^3 a^{-1} (Benner, 1999). The annual consumption of CH_2O, assuming this flux through the barrier, is 15,900 moles per year. This corresponds to a production of roughly 14,700 mol a^{-1} of CO_2 and 560 mol a^{-1} of CH_4. The barrier contains approximately 1,500,000 moles of carbon, and assuming that a minimum of 10% of the carbon (approximately 150,000 moles) were available at the barrier installation (Benner, 1999), the barrier would be active for 9.4 years at this rate of organic carbon consumption. The annual consumption in this estimate was based on summer rate values, and is therefore an overestimate. Also, the reactivity of organic matter is expected to decrease with time (Westrich and Berner, 1984), therefore, it would be expected that gas production would decrease with time.

Ebullition was observed above the barrier at a single point, and is likely to occur at other locations from the PRB as well. The significance of this process is unknown, but ebullition may need to be considered to accurately complete the mass balance within the PRB. The gas production estimate can be compared to ebullition seen above the barrier at a single location. Assuming the ideal gas law:

$$pV = nRT \tag{3.17}$$

can be applied to the ebullition data described in the previous section, where p is the atmospheric pressure of 1 atm, V is the ebullition volume estimated of 42 L day^{-1}, R is the gas constant (8.206×10^{-5} m^3 atm K^{-1} mol^{-1}), T is temperature in degrees Kelvin (290

degrees) and n are the moles of gas, where n can be estimated as the mass loss due to ebullition per year. Using these parameter values, n is estimated to be 642 mol a^{-1}, which converts to approximate losses of 160 mol a^{-1} of CH_4, 332 mol a^{-1} of CO_2, 154 mol a^{-1} of N_2, and 2 mol a^{-1} of Ar from the barrier using the mole fraction ebullition gas results. For those calculations, it was assumed that ebullition is only occurring at a single location and that the rate of ebullition of 42 L day^{-1} is constant throughout the year. It can be expected that rates of ebullition vary seasonally and diurnally and that ebullition is not restricted to a single location. Though there are a number of uncertainties in the ebullition estimates, these results do indicate that ebullition from the barrier may be significant, and may need to be considered to accurately complete the mass balance within the PRB.

3.6.7 Analysis of Mixing Processes Down Gradient of Barrier

Figures 3.3 and 3.4 shows that CH_4 and CO_2 continues to be elevated down gradient of the barrier, while N_2 and Ar remain depleted. Concentrations of dissolved gases within the groundwater down gradient of the barrier are most similar to groundwater exiting the barrier along the faster flow paths. Because the pore water downgradient of the barrier has attained a gas composition similar to the composition within the barrier, it appears that little physical mixing of treated and untreated groundwater is occurring, and that the pore water composition in Ar and N_2 depleted zones is representative of the composition of treated water.

3.6.8 Reactive Transport Modeling Results

3.6.8.1 Observed and Simulated Data Comparison

Both pore water (Benner et al., 2002) and solid phase data (Herbert et al., 2000) after 23 months of barrier operation were used to quantitatively compare model results to field observations (Mayer et al., submitted). In this study, additional pore water data was provided by the University of Waterloo for several dates exceeding 23 months of operation, and solid phase sulfur data (Daignault, 2002) collected after 71 months (nearly 6 years) of operation were used to calibrate the model. Finally, dissolved gas data collected for this work in July 2003 were included in the calibration process. This data set allowed the simulation of degassing and the long-term modeling of the site.

Table 3.6 provides a summary of the calibrated organic carbon fraction reaction parameters used. The effective rate coefficients for the formation of sulfide and elemental sulfur are slightly different than those used by Mayer et al. (submitted, Table 1), because their fractions assume a barrier porosity of 0.35, while the current simulations assume a barrier porosity of 0.40. In addition to reporting rate coefficients normalized to the bulk volume of the treatment material, effective rate coefficients normalized to the organic carbon fraction are also provided to highlight the range of reactivity (Table 3.6).

The most recent and complete data set for observed concentrations of SO_4, Fe, alkalinity, and pH was collected after 6 years of barrier operation, and is used in this discussion for comparison. Generally, the modeling results achieve a good match to the observed concentration changes within the barrier (compare Figures 3.10 and 3.11) for after 6 years. Simulated sulfate concentration decline to less than 2.4×10^{-2} mol L^{-1}, while the maximum observed concentration at the down-gradient end of the barrier was 2.9 x

10^{-2} mol L^{-1}. Simulated iron concentrations decrease to < 4 x 10^{-3} mol L^{-1}, while observed concentrations do not exceed 1 x 10^{-2} mol L^{-1}. Both simulated and observed sulfide concentrations (observed not shown due to limited data collected) only locally exceed values of 5 × 10^{-4} mol L^{-1} within the barrier. Simulated results indicate the presence of dissolved sulfide downgradient of the barrier, which is not seen in the field data. Mayer et al. (submitted) noted this result for modeling up to 23 months of operation, and suggested that dissolved sulfide exiting the barrier is consumed by reactions with the aquifer minerals, which have not been simulated. Alkalinity ranges between 3 x 10^{-3} and 4 x 10^{-2} eq L^{-1} in both simulated and observed data. Despite the large number of processes that affect pH in this system, the simulated pH range of 6.1-7.1 agrees well with the observed range of 6.1-6.7. A reliable data set for the above parameters was not available for after 8 years of barrier operation, however, the simulated results discussed above are provided in Figure 3.12 for completeness.

Daignault (2002) presented results of solid phase sulfur chemistry for 2001, after nearly 6 years of operation. Model results for 71 months of operation show that precipitation of mackinawite, corresponding to the AVS fraction, represents by far the largest accumulation of mass within the barrier (Figure 3.13). Mackinawite precipitation accounts for a total volume fraction of about 0.11% at the up-gradient side of the barrier, and 0.07% throughout the entire barrier, on average. This is consistent with Mayer et al. (submitted), who estimated that 0.05% of the total volume fraction was due to precipitation of mackinawite after 23 months of operation. Table 3.7 compares the results presented by Daignault (2002) to spatially averaged results from the simulation after 83 months of barrier operation. Daignault (2002) estimated that approximately 75%

of total reduced inorganic S (TRS) is present in the AVS fraction. Spatial averaging of the simulated results indicates that 61% of TRS exists in form of mackinawite (AVS). It should be noted that simulated absolute S-accumulation values depend on the assumed organic carbon density. However, the ratio between the different S-fractions is not affected by the uncertainties regarding organic carbon density.

Similar to Mayer et al. (submitted), the simulated organic-carbon bound S fraction is over-predicted, however, the remaining S-fractions appear to be adequately represented in the simulation. A solid-phase data set was not available for 8 years of barrier operation; however, the simulated results discussed above are provided in Figure 3.14 for completeness.

Most importantly, the modeling results also achieve a good match to the observed gas partial pressure data for July 2003 (compare figures 3.15 and 3.16). The observed trends of greater CO_2 and CH_4 partial pressures at the top and bottom sections of the PRB (i.e., low flow zones) and greater Ar and N_2 depletion in those sections were reproduced. The degassing rate and rates of methanogenesis were calibrated until a reasonable fit to the observed gas data was found. Rates of methanogenesis of 10, 20, and 16 times less than the rate of sulfate reduction were attempted, and similar to the findings of the 4-gas degassing model calculations for the observed data presented in section 3.6.2, a ratio of 16:1 provided the best fit. This supports the 4-gas model degassing results, which indicated that sulfate reduction is the dominant processes leading to the consumption of organic carbon. Simulated CO_2 partial pressures ranged from 0.03 atm to 0.68 atm within the PRB, while the minimum and maximum observed partial pressure were 0.15 atm and 0.41 atm, respectively. Simulated CH_4 partial pressures ranged from 0.01 atm to

0.97 atm within the PRB, while the minimum and maximum observed partial pressure were 0.06 atm and 0.86 atm, respectively. Both the observed and simulated CH_4 maximum values were found at the low flow zone at the bottom of the PRB, near the downgradient side. Downgradient of the PRB, N_2 and Ar partial pressures remain slightly depleted in both simulated and observed results, while CH_4 and CO_2 concentrations remain elevated.

3.6.8.2 Long term trends

Both observed, as well as simulated sulfate reduction rates show a decrease over time (Figure 3.17), and compare well with the data presented by Benner et al. (2002) and the additional data provided by Bain (University of Waterloo). Organic carbon consumption due to methanogenesis was also considered, and the rate of methanogenesis mimics the trend of sulfate reduction (Figure 3.17), though at much slower rates as discussed in the previous section. Though observed methane data was only available for July 2003, the observed rate of methanogenesis obtained using the 4-gas degassing model and the simulated trend shown in Figure 3.17 agree for after 8 years of operation. The decreasing trend has previously been attributed to the presence of various organic carbon fractions (Benner et al., 2002). Sulfate reduction rates are described using the multimodal Monod-expression defined by equation 13. Using this simple model for sulfate reduction and methanogenesis, organic carbon consumption in the low permeability lenses becomes sulfate limited, and rates of organic carbon consumption due to sulfate reduction are less in these areas than in the central portion (i.e., preferred pathway) of the barrier (Figure 3.18). As the "fast" and "intermediate" organic carbon fractions are consumed over time within the preferred pathway, the rates of sulfate

reduction become very low within this region, while the rates appear higher within the low permeability lenses (see Figure 3.18, 8 years). The low permeability lenses correspond to areas of higher rates of methane production (Figure 3.19). After 95 months of barrier operation, 97% of the total organic carbon remains, however only 1.3% of the "intermediate" and 2.0% of the "slow" organic carbon fraction remains in the PRB. The "fast" fraction is almost entirely consumed, with only 0.6% remaining primarily in the low flow zones, which are nearly inaccessible to sulfate. The "slower" fraction is almost untouched (> 98% remain). In Section 3.6.6 an estimate of approximately 1% of the organic carbon is consumed per year. These simulations suggest that 0.36% of the organic carbon is consumed per year, indicating that the barrier lifetime will be approximately 27 years.

This model does not fully describe the complexity of the organic carbon assemblage; however, the general trend of overall reactivity decline is well described. One may expect that the remaining "slower" fraction will have to be further subdivided to predict barrier performance beyond the simulated 8 years.

The simulation results can also be compared to observed solid phase accumulations within the PRB, which are available at 3, 14, 23 (Herbert et al., 2000) and 71 months (Daignault, 2002) (Figure 3.20). As previously mentioned, direct comparison of the simulated and observed solid phase accumulations is hampered by uncertainty regarding the in-situ density of the organic carbon and also barrier porosity. If organic carbon densities would be lower or if the effective porosity would be higher, the simulations would tend to overestimate solid phase sulfur accumulations based on calibrated aqueous sulfate reduction rates.

Observed solid phase accumulations of TRS (sum of mackinawite and S^0 in the model) and corresponding rates emphasize the initial rapid buildup of reduced sulfur phases. The first 3.5 years of the simulated results reproduce the trend presented by Mayer et al. (submitted), however, the different porosities and slightly different organic carbon effective rate coefficients (see Table 3.6) used in this work led to initially higher rates of accumulation. The rates of accumulation from the simulation after 71 months of barrier operation are successful in matching the results presented by Daignault (2002). The simulated results indicate that accumulation rates have slowed to a nearly constant rate, as only the slowest organic carbon fraction remains available. Overall, the simulation is successful in matching the sulfide accumulation after 8 years of barrier operation.

3.6.8.3 Degassing Mass Balance Results

Degassing was considered in the model simulations, and Figure 3.21 provides the degassing rates of Ar, CH_4, CO_2, and N_2 over time. Table 3.1 provided Henry's Law constants for the gases of concern at 17°C. The table shows that N_2 is the least soluble, followed by Ar and CH_4, with CO_2 being the most soluble. In Figure 3.21, initially primarily N_2 is lost to degassing, as it is the least soluble gas, and has the highest partial pressure initially within the groundwater. As CH_4 and CO_2 are produced and accumulate within the barrier, more of each gas contributes to degassing. Over time, N_2 remains the highest contributor to degassing because there is a constant influx of N_2 into the barrier, with approximately equal amounts of CH_4 and CO_2 degassing. Table 3.8 provides a summary of the influx of N_2, Ar and CO_3, CH_4 and CO_3 production within the barrier, and the mass of each parameter lost to degassing over time. This table highlights the

solubility effect of each parameter. Only 68.8 moles of CH_4 is produced within the barrier over 8 years per meter barrier width, and 51% of that CH_4 is lost to degassing, while only 1.4% of the CO_3 is lost to degassing, according to the simulation. These results suggest that in order to properly assess organic carbon consumption due to competing TEAPs sulfate reduction and methanogenesis, degassing must be considered.

MIN3P assumes that gas bubbles leave the saturated zone instantaneously and exit to the atmosphere, but in all likelihood only a portion of the gas bubbles are lost to ebullition, while some gas remains within the porous media. By using the ideal gas law, one can speculate about the potential importance of ebullition in respect to completing the mass balance. By assuming an average pressure, P, over depth of 1.18 atm, an average annual temperature, T, of 283 K, and an average of n = 270 mol a^{-1} lost to degassing (sum of moles lost to degassing, Table 3.8), one can estimate that a volume, V, of 5.3 m^3 of gas within the barrier would be occupied by gas bubbles. The gas bubbles would occupy approximately 6.4% of the pore spaces in one year, or reduce porosity from 0.4 to 0.37. If one assumed that all bubbles remained within the pores, and made the same calculation for the cumulative moles over 8 years (2160 moles), a volume of 42.7 m^3 would be occupied by bubbles, which would take up 50% of the pore space. It is unlikely that is the case, confirming that ebullition from the barrier must be significant. Porosity loss within the barrier due to degassing is likely occurring, though ebullition appears to be relieving some of that loss.

3.6.8.4 Degassing Mass Balance: Four-Gas Model vs. MIN3P

The 4-gas degassing model considers a 1 L batch system, and follows a "parcel" of pore water on a specific flow path as it passes through the barrier, but cannot account

for mixing within the porous media. MIN3P, on the other hand, by considering transport processes represents a stationary volume with an in flux and out flux of water undergoing reactions. When degassing occurs, MIN3P simply disposes of the volume of gas while the 4-gas degassing model considers that the volume of gas remains within the 1 L system.

Estimates of CO_2 and CH_4 produced and lost to degassing were made in section 3.6.6 using the 4-gas degassing model, based on results from specific locations within the barrier. These values can be compared to the mass balance degassing results from the MIN3P simulations, and are summarized in Table 3.9. Overall, the 4-gas degassing model estimates for CO_2 and CH_4 production within the entire barrier are factors of approximately 3-5 times higher than those obtained from the reactive transport simulations. As a result, CH_2O consumption estimates for the barrier are also approximately 3 times higher. Aside from the fundamental difference of a batch versus transport system, there are three primary differences between the assumptions used to obtain the estimates that explain the varying results.

In the MIN3P simulations, temporal fluctuations are considered, and therefore an average rate of CH_2O consumption over the years of operation can be calculated which takes into account slower consumption in the winter and faster consumption in the summer. The 4-gas model calculations were based on data collected during the summer of the 8^{th} year of barrier operation, when rates of sulfate reduction and methanogenesis are likely highest for the year, and therefore will greatly overestimate a yearly average rate. MIN3P simulations show that peak summer rates of sulfate reduction and methanogenesis are 2 to 3 times higher than for other times of the year (Figure 3.17).

Using the same barrier flux for MIN3P simulations and the 4-gas model calculations, this implies that the summer rates determined from the 4-gas model will calculate an average CH_2O consumption rate that is at least 2 to 3 times higher than the average consumption rate determined from MIN3P for the 8^{th} year of operation.

The 4-gas degassing model determined the rates of CH_2O consumption, and CH_4 and CO_2 production at specific points within the barrier, and these rates were then normalized to the entire barrier width, averaged, and assumed to be constant along the remainder of the flow path. Sulfate reduction is considered to be a Monod type reaction, indicating that again, the 4-gas model will overestimate the average rate of CH_2O consumption, because the parcel of water does not reach the end of the barrier flow path before this rate is determined.

The observed data (Figure 3.17) indicates that rates of sulfate reduction (i.e., the dominant consumer of CH_2O), after a rapid decline in removal during the first 2 to 3 years of operation, have been fairly steady for the past 5 to 6 years of operation. Therefore, even though 4-gas model results presented in Table 3.9 were based exclusively on data collected during the summer of the 8^{th} year of barrier operation, it is not too surprising that by not accounting for temporal fluctuations and by normalizing rates determined at specific points within the barrier, they are higher than the MIN3P results.

Despite difference in the calculations, the estimates differ by less than an order of magnitude.

3.7 Summary and Conclusions

Within the barrier, elevated CH_4 and CO_2 concentrations are observed, while N_2 and Ar concentrations are depleted in comparison to atmospheric levels. These results indicate the formation of gas bubbles within the barrier, and degassing was indeed observed above the barrier. H_2S is below detection throughout most of the barrier (i.e., only detected at two sampling locations), indicating that essentially all H_2S in the barrier is removed by precipitation of metal sulfides. Observed CO_2 concentrations could be explained by the TEAPs methanogenesis and sulfate reduction.

The gas distribution within the barrier could be used as a proxy for residence times, confirming earlier findings based on Cl and SO_4 analysis by Benner et al. (2002). Analysis of the data suggests that the average ratio of sulfate reduction to methanogenesis along fast pathways through the barrier is three times that observed along slow pathways. On average, over 90% of the CO_2 is produced by sulfate reduction, while the remaining CO_2 is produced by methanogenesis. While the results of the 4-gas model are not unique, and many assumptions were made in the calculations, the results indicate that sulfate reduction is the main process by far of organic carbon consumption within the barrier along both the fast and slow flow paths.

Dissolved gas data for groundwater downgradient of the PRB indicates that little mixing occurs between groundwater exiting the barrier along the slow paths, and groundwater exiting the barrier along the faster paths.

Reactive transport modeling of the Nickel Rim PRB for 8 years of barrier operation generally provided a good match to observed data. Degassing was incorporated into the simulations and observed dissolved gas trends were therefore well

represented. The simulation results suggest that a simple degassing model may provide a suitable estimate for the process of degassing, although no information on the volume change due to bubble formation or the fate of the trapped gas can be obtained. Rates of methanogenesis and sulfate reduction obtained from the modeling further demonstrated that sulfate reduction is by far the dominant TEAP. Using the ratio of sulfate reduction to methanogenesis of 16:1, the simulations provided a reasonable estimate of organic carbon consumption due to each TEAP, which also match the observed trends (though data was limited for methane). By incorporating methanogenesis and degassing into the model simulations, a more accurate determination of the long-term fate of the organic carbon treatment material could be made.

The dissolved gas data for Nickel Rim provides additional information to delineate rates of microbially mediated sulfate reduction, methods of organic carbon consumption, slow and fast flow zones within the barrier, and mixing down gradient of the barrier. By including the process of degassing into the reactive transport modeling, a more accurate representation of the barrier treatment material consumption was presented.

3.8 References

Amos, R.T., K.U. Mayer, B. A. Bekins, G. N. Delin, R. L. Williams, 2005. Use of dissolved and vapour-phase gases to investigate methanogenic degradation of petroleum hydrocarbon contamination in the subsurface. *Water Resour. Res.*, 41, W02001, doi:10.1029/2004WR003433.

Bain, J. G., D. W. Blowes, and W. D. Robertson, 1995. The hydrogeochemistry of a sand aquifer affected by discharge from the Nickel Rim tailings, Sudbury, Ontario. In: *Proceedings of Sudbury '95-Mining and the Environment*, ed. T.P. Haynes and M.C. Blanchette, 715-723. Ottawa: CANMET.

Bain, J. G. 1996. The physical and chemical hydrogeology of a sand aquifer affected by drainage from the Nickel Rim tailings impoundment, M.Sc. thesis, Dept. of Earth Sciences, University of Waterloo, Waterloo, Ontario.

Benner, S. G., D. W. Blowes, C. J. Ptacek, 1997. A full-scale porous reactive wall for the prevention of acid mine drainage. *Groundwater Monit. Remed.* 17, 99-107.

Benner, S. G., 1999. Hydrogeology, Geochemistry and Microbiology of a Reactive Barrier for Acid Mine Drainage. Ph.D thesis, University of Waterloo, Waterloo, Ontario, Canada.

Benner, S. G., D. W. Blowes, W. D. Gould, R. B. Herbert, Jr., C. J. Ptacek, 1999. Geochemistry of a Permeable Reactive Barrier for Metals and Acid Mine Drainage. *Environ. Sci. Technol.*, 33, 2793-2799.

Benner, S. G., W. D. Gould, D. W. Blowes, 2000. Microbial populations associated with the generation and treatment of acid mine drainage. *Chem. Geol.,* 169, 435-448.

Benner, S. G., D. W. Blowes, C. J. Ptacek, K. U. Mayer, 2002. Rates of sulfate reduction and metal sulfide precipitation in a permeable reactive barrier. *Appl. Geochem.*, 17, 301-320.

Boudreau, B. P., and J. T. Westrich, 1984. The dependence of bacterial sulfate reduction on sulfate concentration in marine sediments. *Geochim. Cosmochim. Acta,* 48:2502–2516.

Boudreau, B.P., and B. R. Ruddick, 1991. On a continuum representation of organic matter diagenesis. *Am. J. Sci.* 291, 507–538.

Cirpka, O. A., and P. K. Kitanidis, 2001. Transport of volatile compounds in porous media in the presence of a trapped gas phase. *J. Contam. Hydrol.*, 49, 263-285.

Daignault, E. C. M., 2002. The solid phase sulphur speciation of metal sulphides in a permeable reactive barrier, Nickel Rim mine, Sudbury, Ontario, B.Sc. thesis, University of Waterloo, Waterloo, ON.

Guiguer, N. and T. Franz. 1997. Visual MODFLOW for Windows v. 2.7.2, Waterloo Hydrogeologic, Inc.Waterloo, Ontario, Canada.

Herbert, R. B., S. G. Benner, D. W. Blowes, 2000. Solid phase iron-sulfur geochemistry of a reactive barrier for the treatment of mine drainage. *Appl. Geochem.*, 15, 1331-1343.

Johnson, R. H. 1993. The physical and chemical hydrogeology of the Nickel Rim mine tailings, Sudbury, Ontario, M.Sc. thesis, University of Waterloo, Waterloo, Ontario.

Lide, D. R., editor-in-chief, 1994. *CRC Handbook of Chemistry and Physics, 75th Edition*; CRC Press, Inc.: Boca Raton, Florida.

Mayer, K. U., S. G. Benner, and D. W. Blowes (submitted). Process-Based Reactive Transport Modeling of a Permeable Reactive Barrier for the Treatment of Mine Drainage, *J. Contam. Hydrol.*

Mayer, K. U., E. O. Frind, and D. W. Blowes, 2002. Multicomponent reactive transport modeling in variably saturated porous media using a generalized formulation for kinetically controlled reactions, *Water Resour. Res.*, 38, doi: 10:1029/2001WR000862.

Mayer K. U., D. W. Blowes, E. O. Frind, 2001. Reactive transport modeling of an in situ reactive barrier for the treatment of hexavalent chromium and trichloroethylene in groundwater, *Water Resour.* , 37, 3091-3103.

Roychoudhury, A.N., E. Viollier, and P. van Cappellen, 1998. A plug flow-through reactor for studying biogeochemical reactions in undisturbed aquatic sediments. *Appl. Geochem.* 13:269–280.

Stumm, W. and J. J. Morgan, 1996. *Aquatic Chemistry, Chemical Equilibria and Rates in Natural Waters, Third Edition*; John Wiley & Sons, Inc.: New York, p 472 and p 474.

Waybrant, K. R., D. W. Blowes, C. J. Ptacek, 1995. Selection of reactive mixtures for the prevention of acid mine drainage using in situ porous reactive walls. Proc. Sudbury '95, Mining and the Environment, CANMET, Ottawa, ON vol. 3, pp. 945-953.

Waybrant, K. R., D.W. Blowes, C. J. Ptacek, 1998. Selection of reactive mixtures for use in permeable reactive walls for treatment of mine drainage. *Environ. Sci. Technol.*, 32 1972-1979.

Westrich, J. T., and Berner, R. A., 1984. The role of sedimentary organic matter in bacterial sulfate reduction: the G model tested. *Limnol. Oceanogr.* 29, 236-249.

Yamamoto, S.; J. B. Alcauskas; T. E. Crozier, 1976. Solubility of methane in distilled and sea water. *J. Chem. Eng. Data*, 21, 78-80.

Tables

Gas	H_2	Ar	O_2	N_2	CH_4	H_2S	CO_2
K_H (M atm^{-1})	8.3×10^{-4}	1.6×10^{-3}	1.5×10^{-3}	7.4×10^{-4}	1.7×10^{-3}	1.2×10^{-1}	4.5×10^{-2}

Table 3.1. Henry's Law Constants used for 4-gas model calculations for T = 290 degrees Kelvin. All Henry's Law constants are from the CRC Handbook of Chemistry and Physics, 75th Edition (1994), except for methane values, which were taken from Yamamoto et al. (1976).

Sampling Location	ratio of sulfate reduction to methanogenesis
29_2	15
29_8	40
30_a	7
30_4	45
30_3	7
30_b	7
31_2	7
31_a	5
31_4	15
31_b	15
Greater degassing zone.	8
Limited degassing zone	24
Overall Average	16

Table 3.2. Final ratios of sulfate reduction to methanogenesis used to fit observed gas partial pressures at each sampling location within the barrier to 4-gas model results.

Sampling Location	Sulfate removed (mmol L^{-1})	Sulfate removed (mg L^{-1})
29_2	8.3	792
29_8	14.0	1344
30_a	13.0	1243
30_4	9.0	864
30_3	9.5	907
30_b	2.8	269
31_2	10.2	974
31_a	16.5	1584
31_4	5.3	504
31_b	9.0	864

Table 3.3. Estimates of sulfate removal, reported in mmol L^{-1} and mg L^{-1}, based on observed gas partial pressures at each sampling location and 4-gas model "step" results.

Sampling Location	Estimated residence time through PRB and sampling location [days]	Estimated residence time from entry point to sampling location (days)	Sulfate removed (mmol L^{-1})	Sulfate reduction rate (mol L^{-1} d^{-1})	Sulfate reduction rate (mmol L^{-1} a^{-1})
29_2	132	20	8.3	4×10^{-4}	151
29_8	73	13	14.0	1×10^{-3}	393
30_a	548	250	13.0	5×10^{-5}	19
30_4	72	42	9.0	2×10^{-4}	78
30_3	128	78	9.5	1×10^{-4}	44
30_b	72	42	2.8	7×10^{-5}	24
31_2	126	108	10.2	9×10^{-5}	34
31_a	226	190	16.5	9×10^{-5}	32
31_4	74	62	5.3	8×10^{-5}	31
31_b	74	62	9.0	1×10^{-4}	53
Slow Path Ave.	232				56
Fast Path Ave.	73				116
Overall Average	153				86

Table 3.4. Residence times, sulfate reduction and reduction rates based on MODFLOW flow and particle tracking simulations and 4-gas model results.

Current Work [a]

Flow Path	Residence Time (Days)	Sulfate reduced (mmol L^{-1})	Sulfate reduced (mg L^{-1})	Rate of Sulfate reduction (mmol L^{-1} a^{-1})
Slow Ave	232	26	2487	56
Fast Ave	73	23	2224	116
Average	153	25	2355	86

Benner (1999) [b]

Flow Path	Residence Time (Days)	Sulfate reduced (mmol L^{-1} pv^{-1})	Sulfate reduced (mg L^{-1} pv^{-1})	Rate of Sulfate reduction (mmol L^{-1} a^{-1})
Slow Ave	160	31	2976	71
Fast Ave	65	5	480	28
Average	90	13	1248	53

Herbert et al. (2000) [c]

Flow Path	Rate of Sulfate reduction (mmol L^{-1} a^{-1})
Slow Ave	25
Fast Ave	36
Average	30.5

a Calculations for this work are based on observed gas data fit to 4-gas analytical model, and estimate residence times.

b Benner (1999) calculations are based on changes in aqueous concentrations (influent-effluent) and estimated residence times.

c Calculations are from Herbert et al. (2000), and are based on solid phase digestions. They were converted to aqueous concentrations in Benner (1999).

Table 3.5. Comparison of removal estimates with previous studies.

Reaction	$\varphi_{initial}$ [-]	[a]Effective rate coefficient [mol dm^{-3} s^{-1}]	[b]Effective rate coefficient [mol dm^{-3} s^{-1}]
CH_2O-H_2S (1)	0.0012	1.8×10^{-9}	1.5×10^{-6}
CH_2O-S (1)		5.4×10^{-10}	4.5×10^{-7}
CH_2O-CH_4 (1)		1.2×10^{-10}	9.8×10^{-8}
CH_2O-H_2S (2)	0.0015	1.3×10^{-9}	8.5×10^{-7}
CH_2O-S (2)		3.8×10^{-10}	2.6×10^{-7}
CH_2O-CH_4 (2)		8.3×10^{-11}	5.5×10^{-8}
CH_2O-H_2S (3)	0.0018	9.3×10^{-10}	5.2×10^{-7}
CH_2O-S (3)		2.8×10^{-10}	1.5×10^{-7}
CH_2O-CH_4 (3)		6.0×10^{-11}	3.4×10^{-8}
CH_2O-H_2S (4)	0.3290	1.0×10^{-9}	3.0×10^{-9}
CH_2O-S (4)		3.0×10^{-10}	9.1×10^{-10}
CH_2O-CH_4 (4)		6.5×10^{-11}	2.0×10^{-10}

[a] normalized to bulk volume of treatment material
[b] normalized to volume of organic carbon fraction

Table 3.6. Initial volume fractions and calibrated effective rate coefficients for organic carbon consumption reactions.

	observed		simulated	
	maximum	average	maximum	average
[a]AVS [b](mackinawite)	74	32	72	39
[a]S^0/pyrite [b](S^0)	29	11	30	25
[a]TRS [b](AVS_S^0/pyrite)	103	43	102	64
[a]Org. S [b](S-sink)	20	9	51	27
[a]SO_4-S [b](gypsum)	15	6	30	5

[a] measured parameter

[b]simulated parameter

Table 3.7. Observed and simulated averaged S-accumulations in solid phase [mol m^{-3}] after 71 months of barrier operation. Observed accumulations as reported by Daignault (2002) using a dry bulk density of 0.2 g organic carbon cm^{-3} treatment material.

Degassing Mass Balance (Simulated 1 m section of PRB)				
Parameter	*Influx over 8 years [moles]*	*Source from Solid Phase over 8 years [moles]*	*Lost to Degassing [moles]*	*Percent Lost to Degassing [%]*
CH_4	0.0	68.8	35.1	51.0
CO_3	228.9	3094.7	46.9	1.4
N_2	132.2	0.0	60.9	46.1
Ar	3.7	0.0	1.1	29.9
Degassing Mass Balance (Total width of PRB (15 m))				
CH_4	0	1033	527	51.0
CO_3	3434	46421	704	1.4
N_2	1983	0	914	46.1
Ar	55	0	17	29.9

Table 3.8. Simulated mass balance of CH_4, CO_3, N_2, and Ar for 8 years of barrier operation within a 1 m wide section of reactive material, and the resulting estimate of degassing through the entire 15 m width of the PRB.

	MIN3P Simulated Results		**4-Gas Degassing Model Results**		**4-Gas Degassing:MIN3P results**
	[mol][1]	[mol a^{-1}]	[mol][1]	[mol a^{-1}]	
CH_2O Consumed	44600	5575	127368	15921	2.9
CO_2 Produced	46421	5803	117576	14697	2.5
CH_4 produced	1033	129	4512	564	4.4

[1] Indicates total moles consumed or produced after 8 years of operation.

Table 3.9. Comparison of MIN3P and 4-Gas Degassing Model 8 year treatment material consumption totals and annual average rates.

Figures

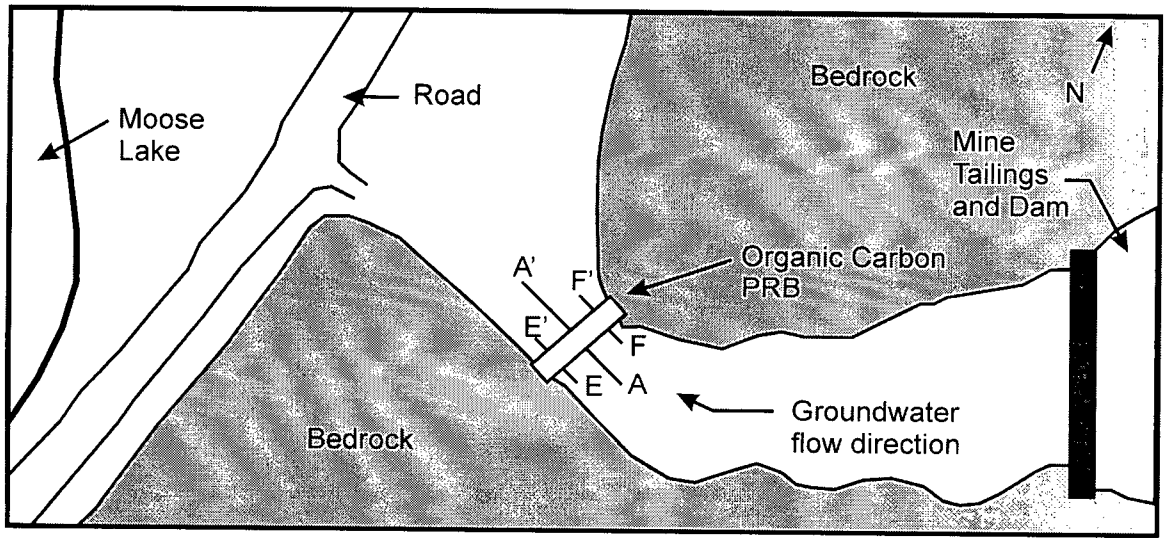

Figure 3.1. Map view of the Nickel Rim PRB installation showing the mine tailings impoundment, groundwater flow path, and the location of the reactive barrier and monitoring well transects. After Benner et al., 1997.

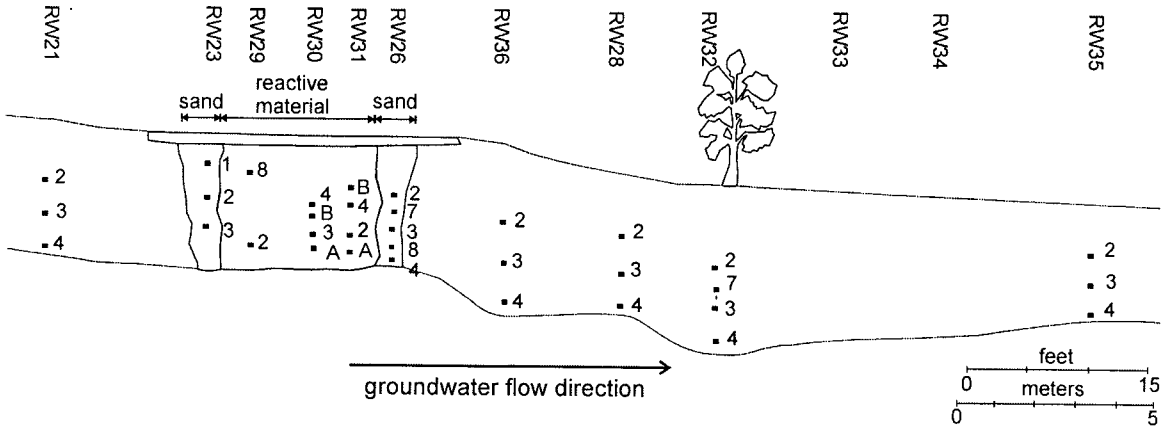

Figure 3.2. Sampling locations for July 2003 along cross-section A-A'. After Benner et al., 1999.

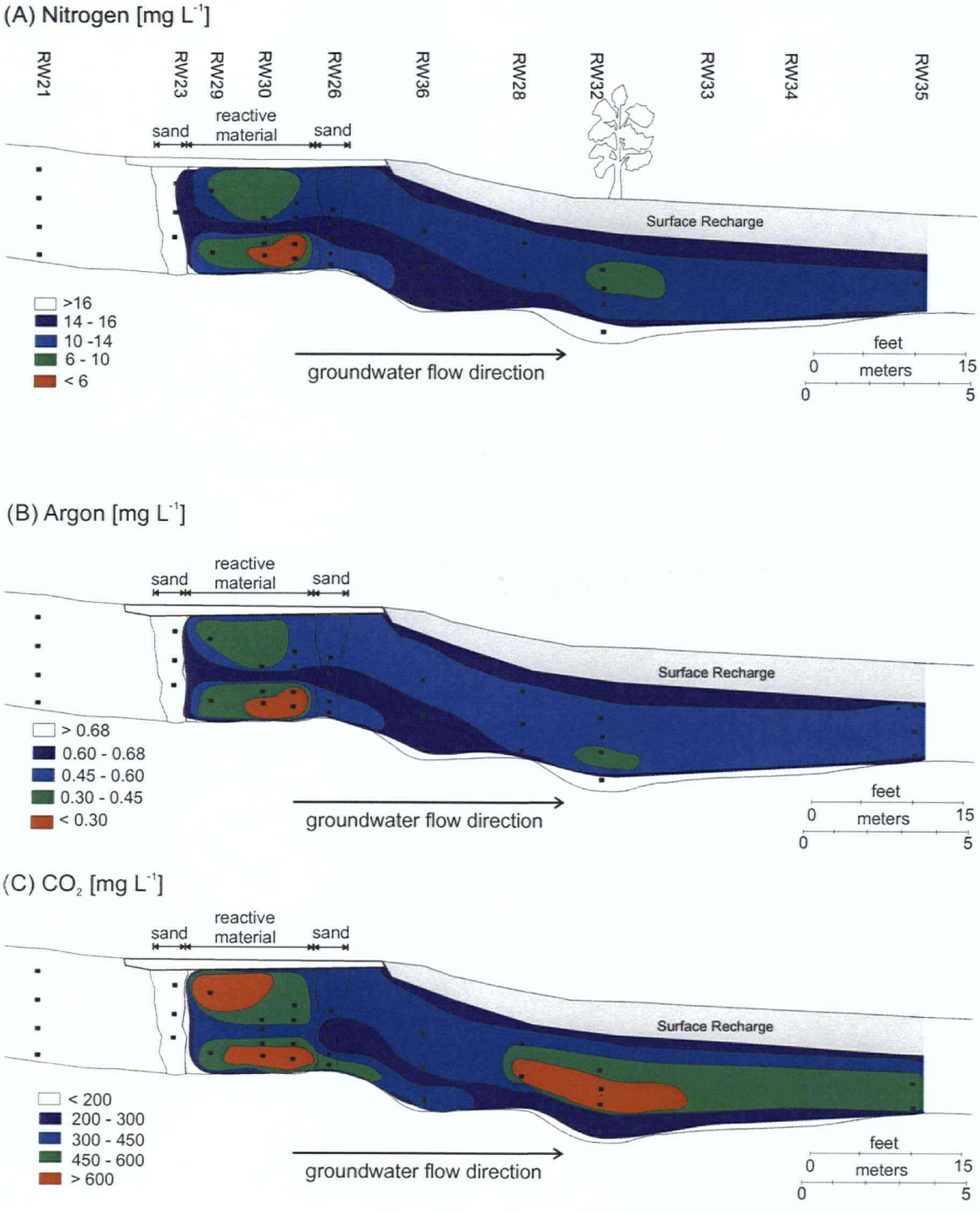

Figure 3.3. Cross-sectional profile along transect A-A' for July 2003: Dissolved (A) Nitrogen, (B) Argon, and (C) CO_2. Concentrations are expressed in mg L^{-1}.

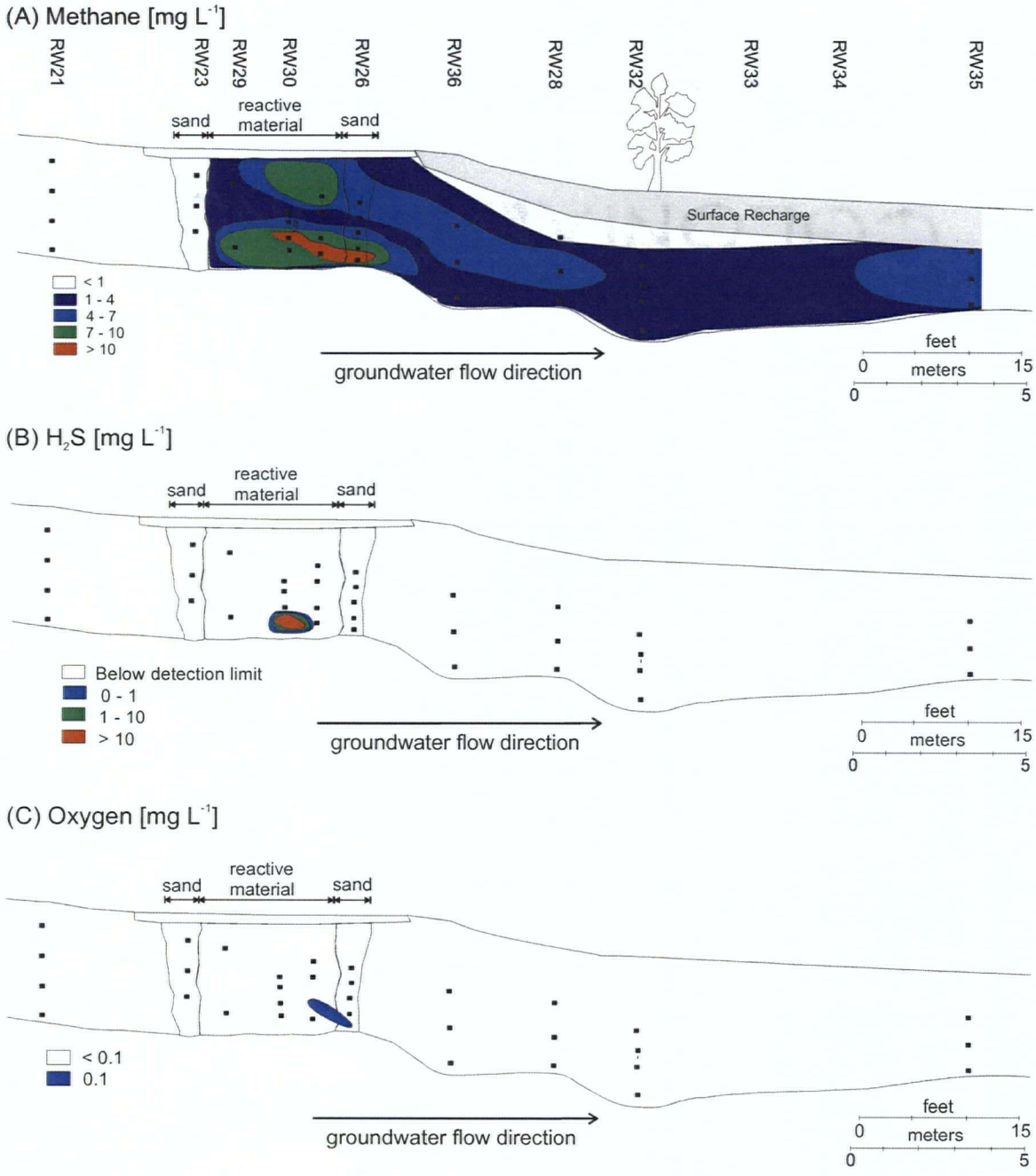

Figure 3.4. Cross-sectional profile along transect A-A' for July 2003: Dissolved (A) CH_4, (B) H_2S, and (C) O_2. Concentrations are expressed in mg L^{-1}.

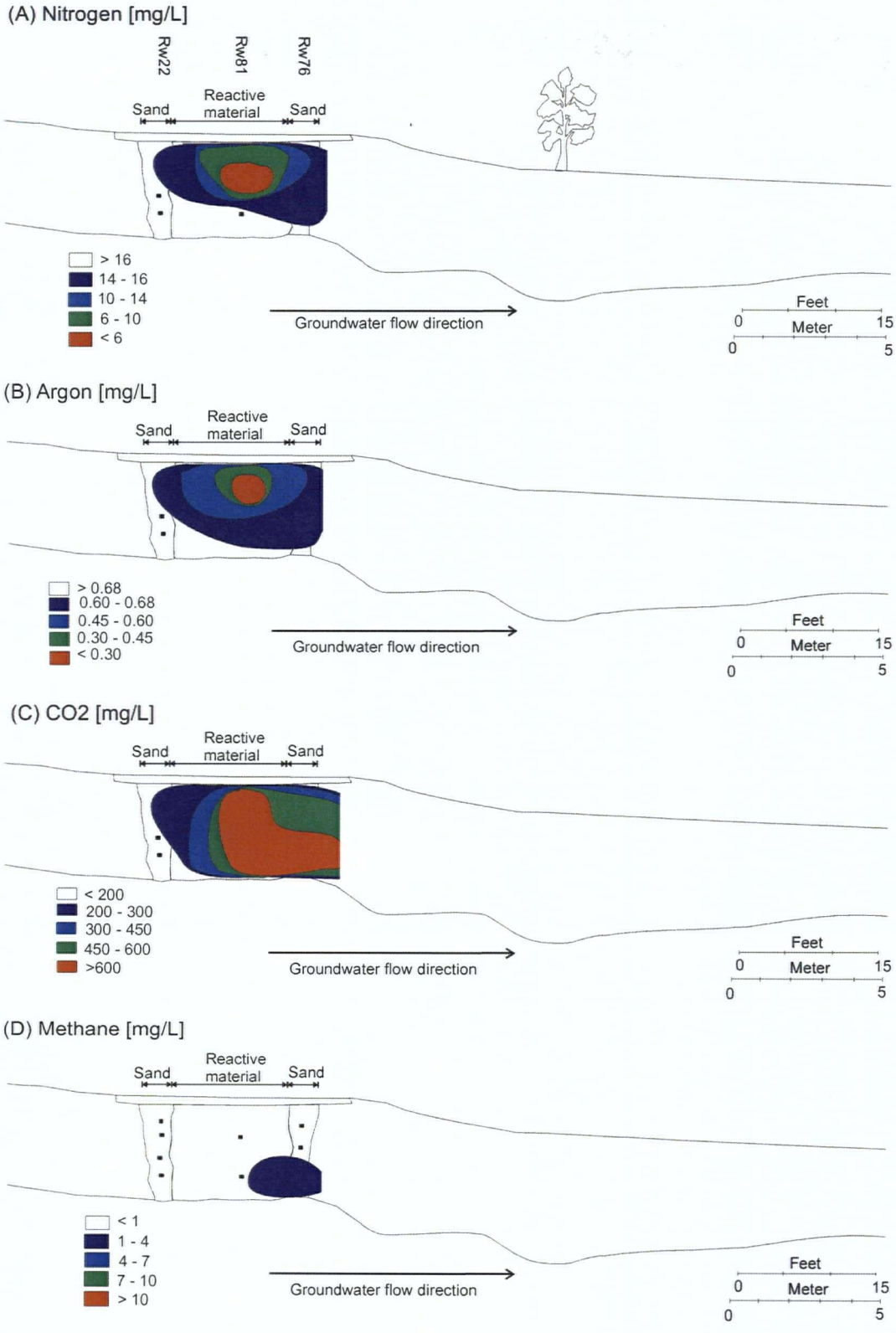

Figure 3.5. Cross-sectional profiles along transect E-E' for July 2003: Dissolved (A) Nitrogen, (B) Argon, (C) CO_2, and (D) CH_4.

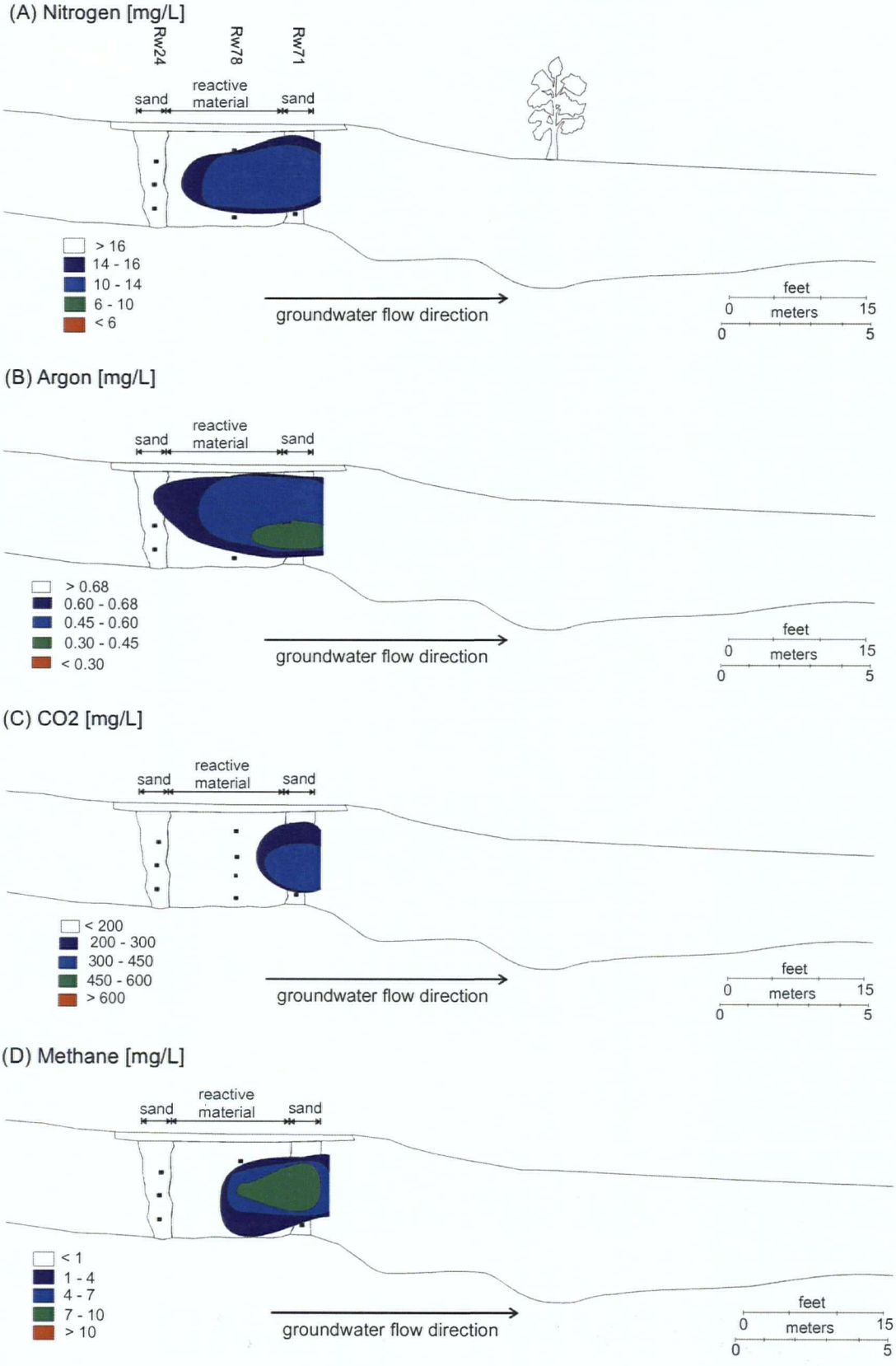

Figure 3.6. Cross-sectional profiles along transect F-F' for July 2003: Dissolved (A) Nitrogen, (B) Argon, (C) CO_2, and (D) CH_4.

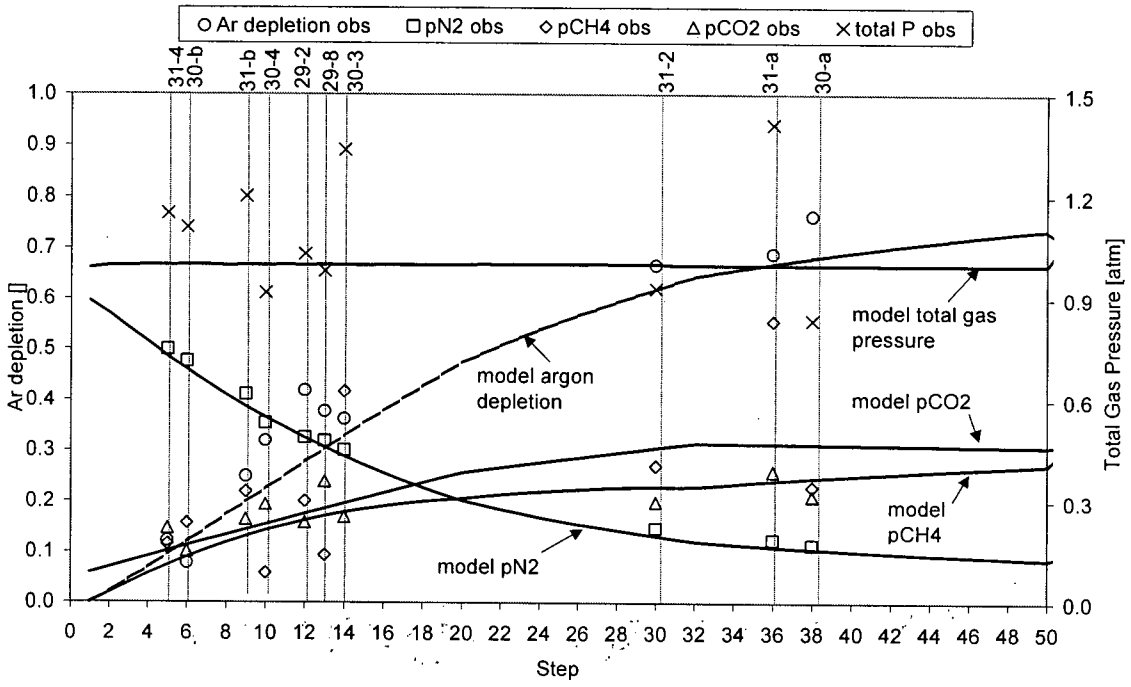

Figure 3.7. Four-gas model results plotted with observed partial and total pressure gas measurements for sampling locations from well nests 29, 30, and 31 along transect A-A'. A sulfate reduction to methanogenesis ratio of 16:1 was in the model.

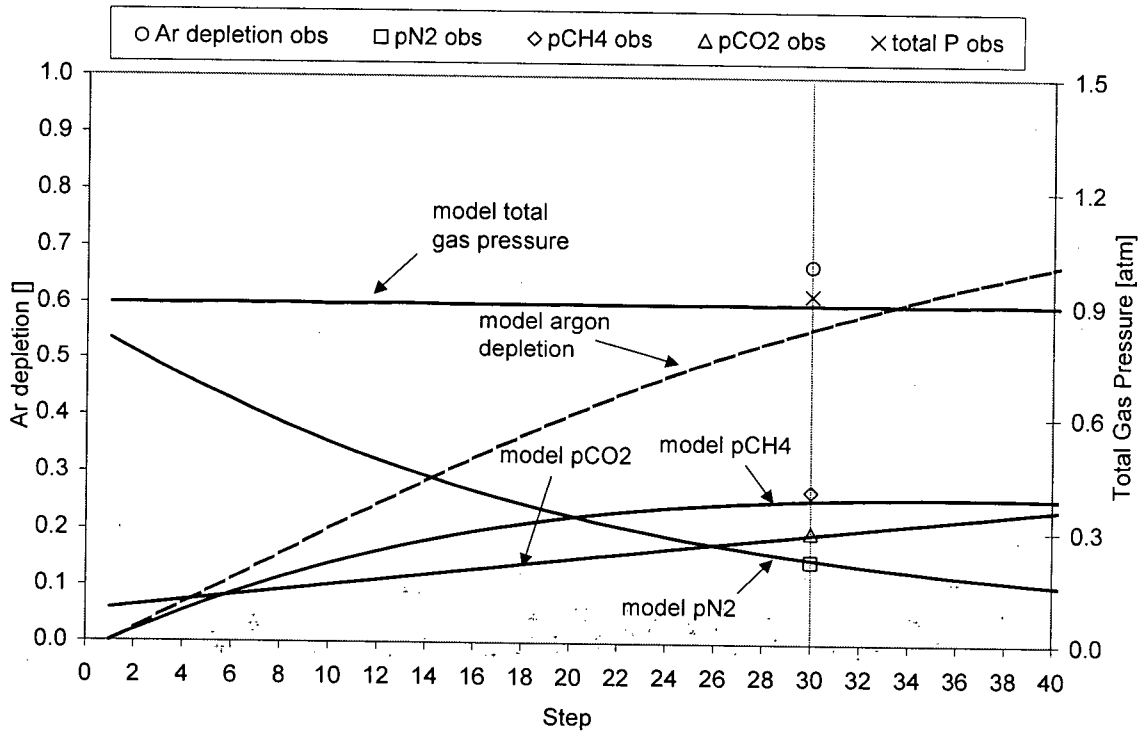

Figure 3.8. Four-gas model results plotted with observed partial and total pressure gas measurements for sampling location 31-2 along transect A-A'. A sulfate reduction to methanogenesis ratio of 7:1 was used in the model.

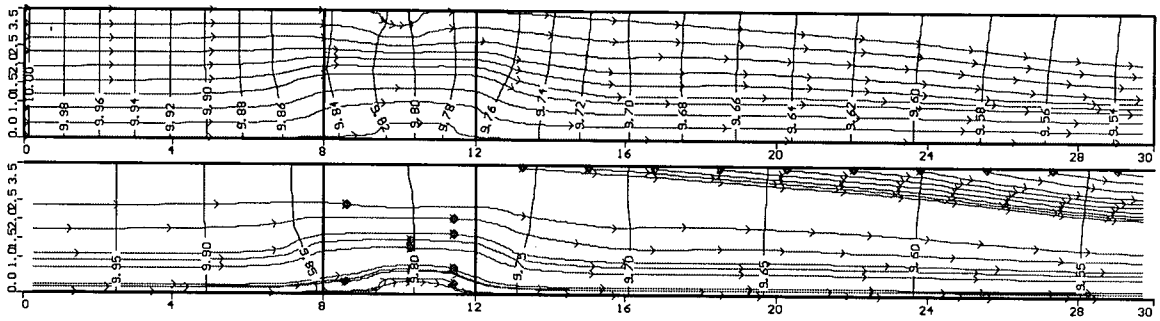

Figure 3.9. Flow conditions and particle tracking from sampling points within the barrier. MODFLOW results using Benner et al., (2002) flow modeling boundary conditions.

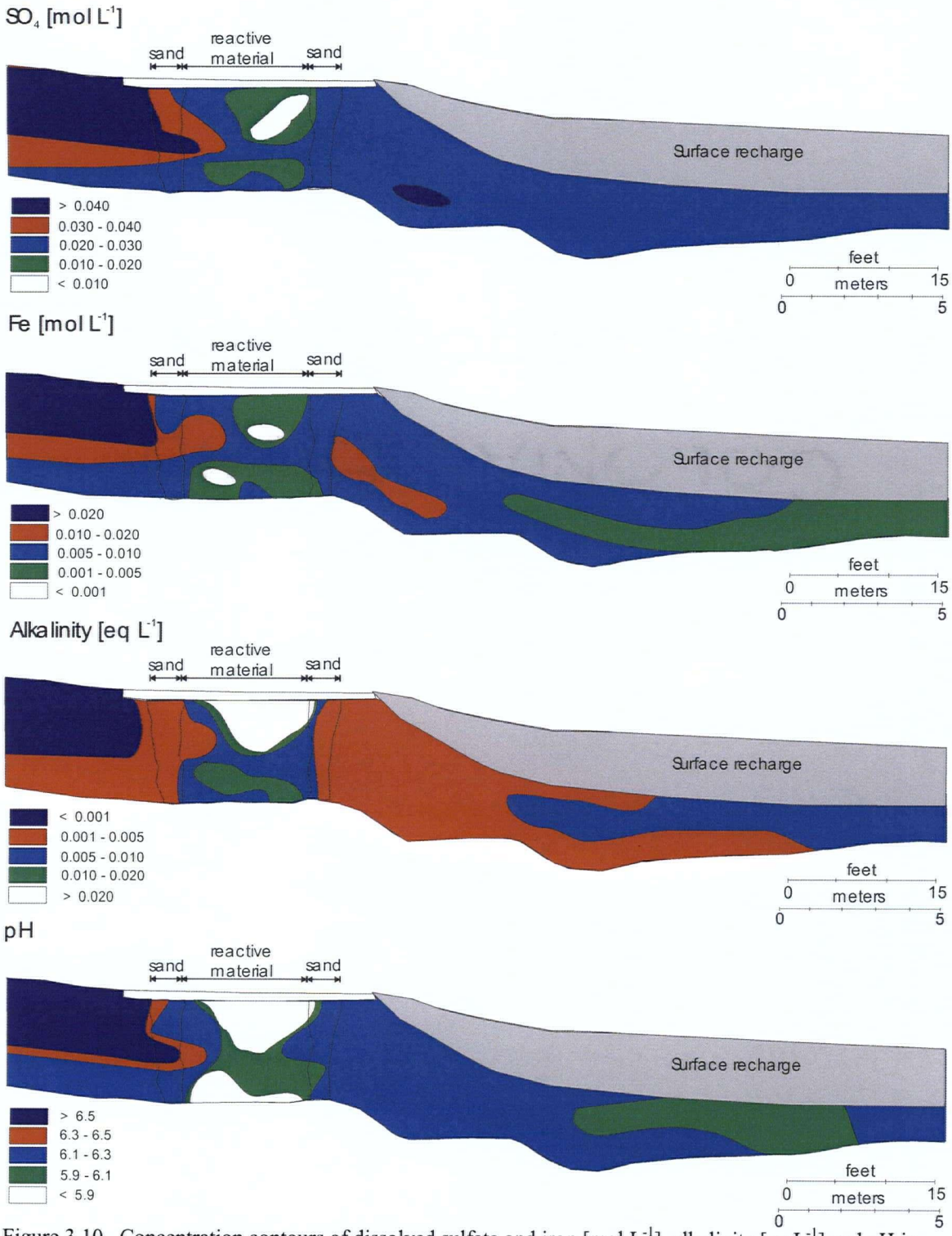

Figure 3.10. Concentration contours of dissolved sulfate and iron [mol L^{-1}], alkalinity [eq L^{-1}] and pH in the Nickel Rim PRB study area for August 2001 (74 months of barrier operation, modified from University of Waterloo data set).

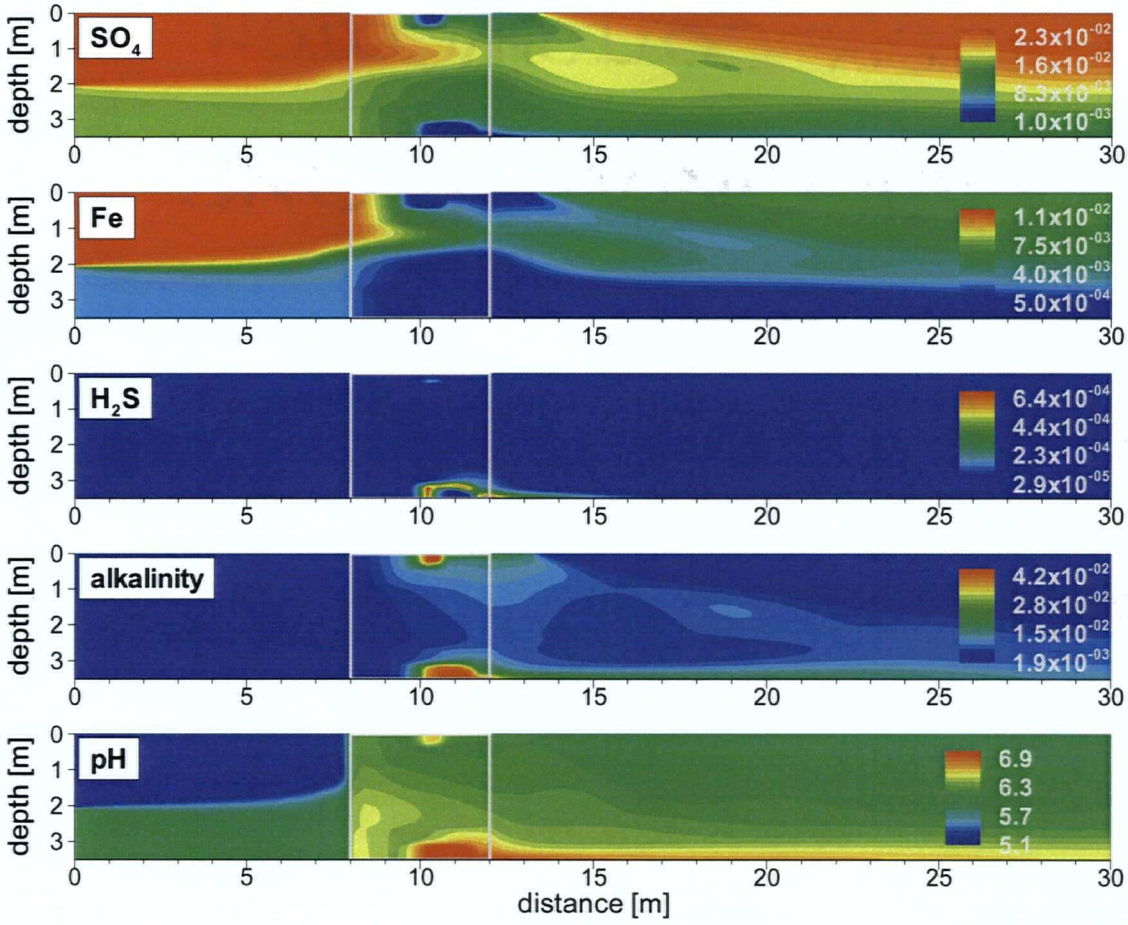

Figure 3.11. Simulated concentration contours for SO_4, Fe, H_2S [mol L^{-1}], alkalinity [eq L^{-1}] and pH after 72 months of operation (August 2001).

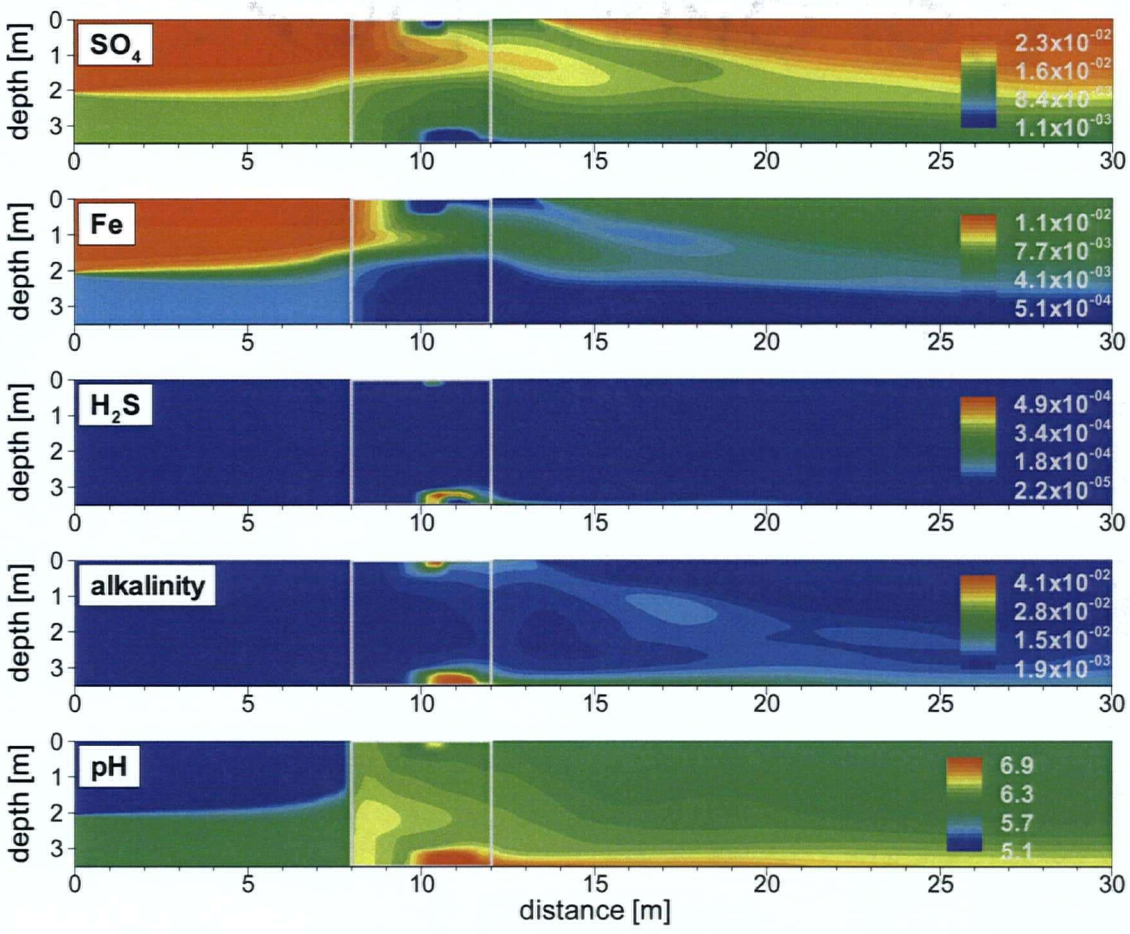

Figure 3.12. Simulated concentration contours for SO_4, Fe, H_2S [mol L^{-1}], alkalinity [eq L^{-1}] and pH after 95 months of operation (July 2003).

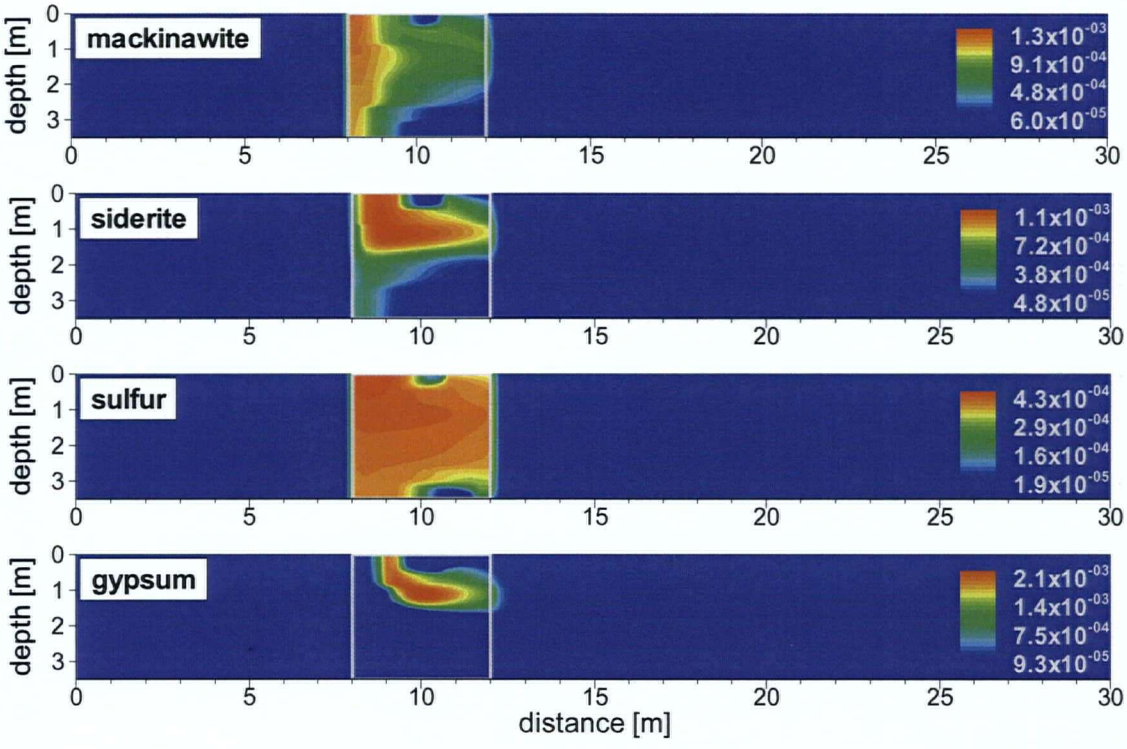

Figure 3.13. Simulated concentration contours of mineral volume fractions [cm^3 mineral cm^{-3} treatment material] for mackinawite, siderite, sulfur, and gypsum after 71 months of operation (July 2001).

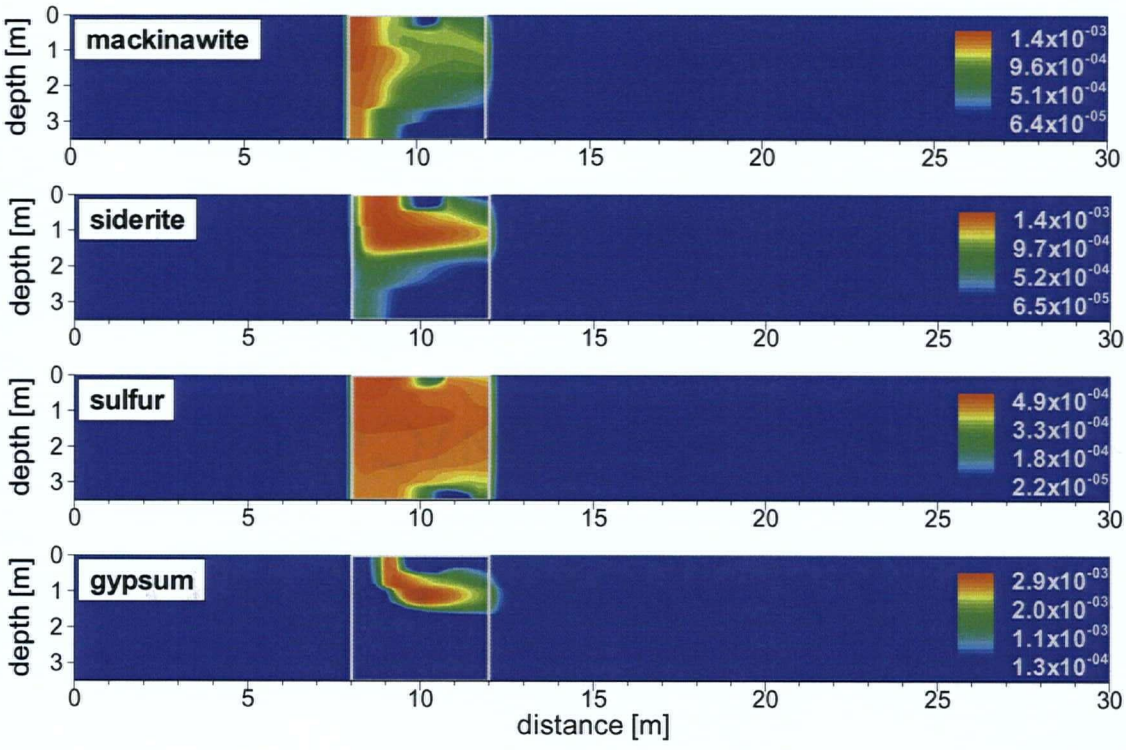

Figure 3.14. Simulated concentration contours of mineral volume fractions [cm^3 mineral cm^{-3} treatment material] for mackinawite, siderite, sulfur, and gypsum after 95 months of operation (July 2003).

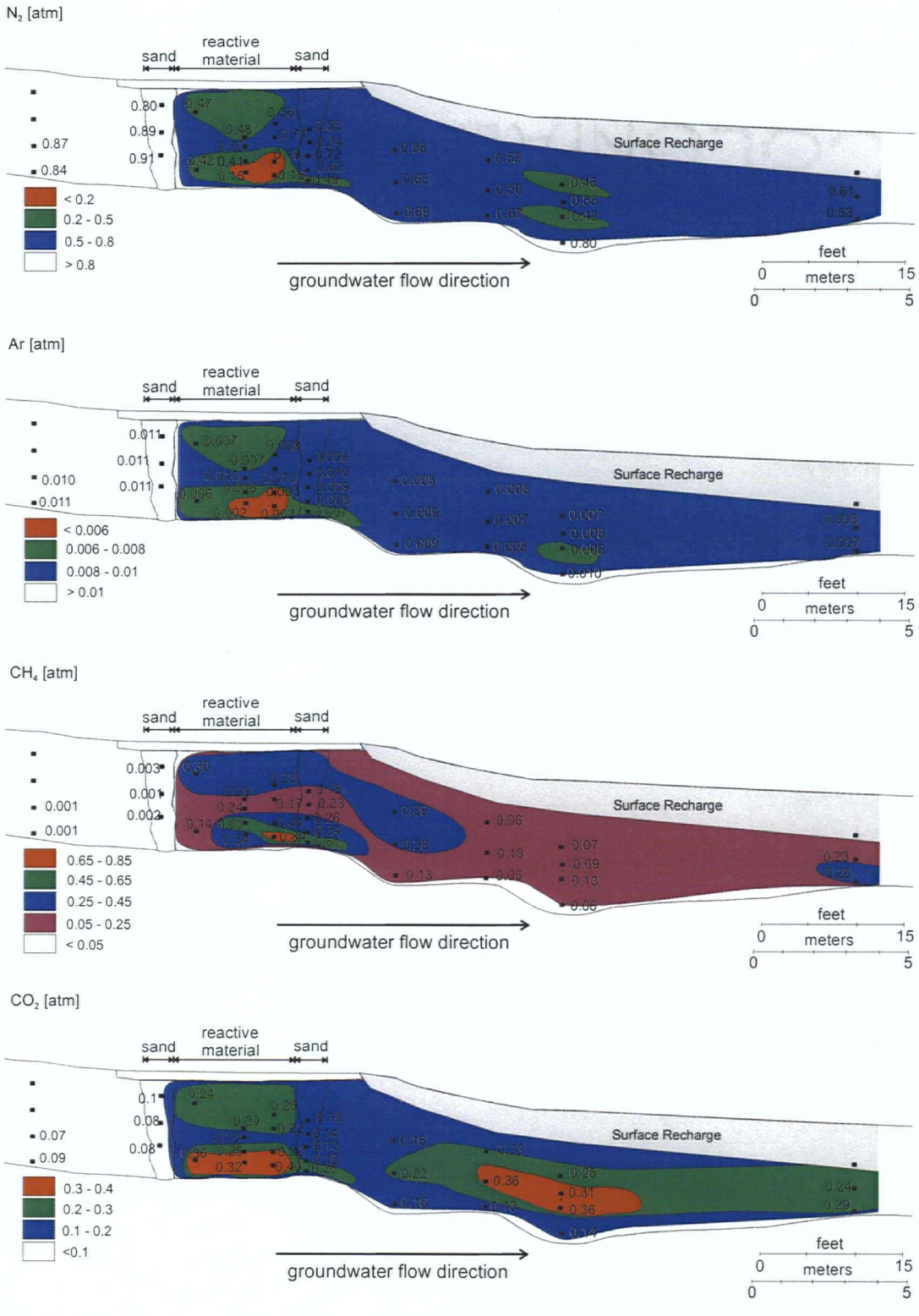

Figure 3.15. Gas partial pressure contours of observed N_2, Ar, CH_4, and CO_2 [atm] in the Nickel Rim PRB study area for July 2003.

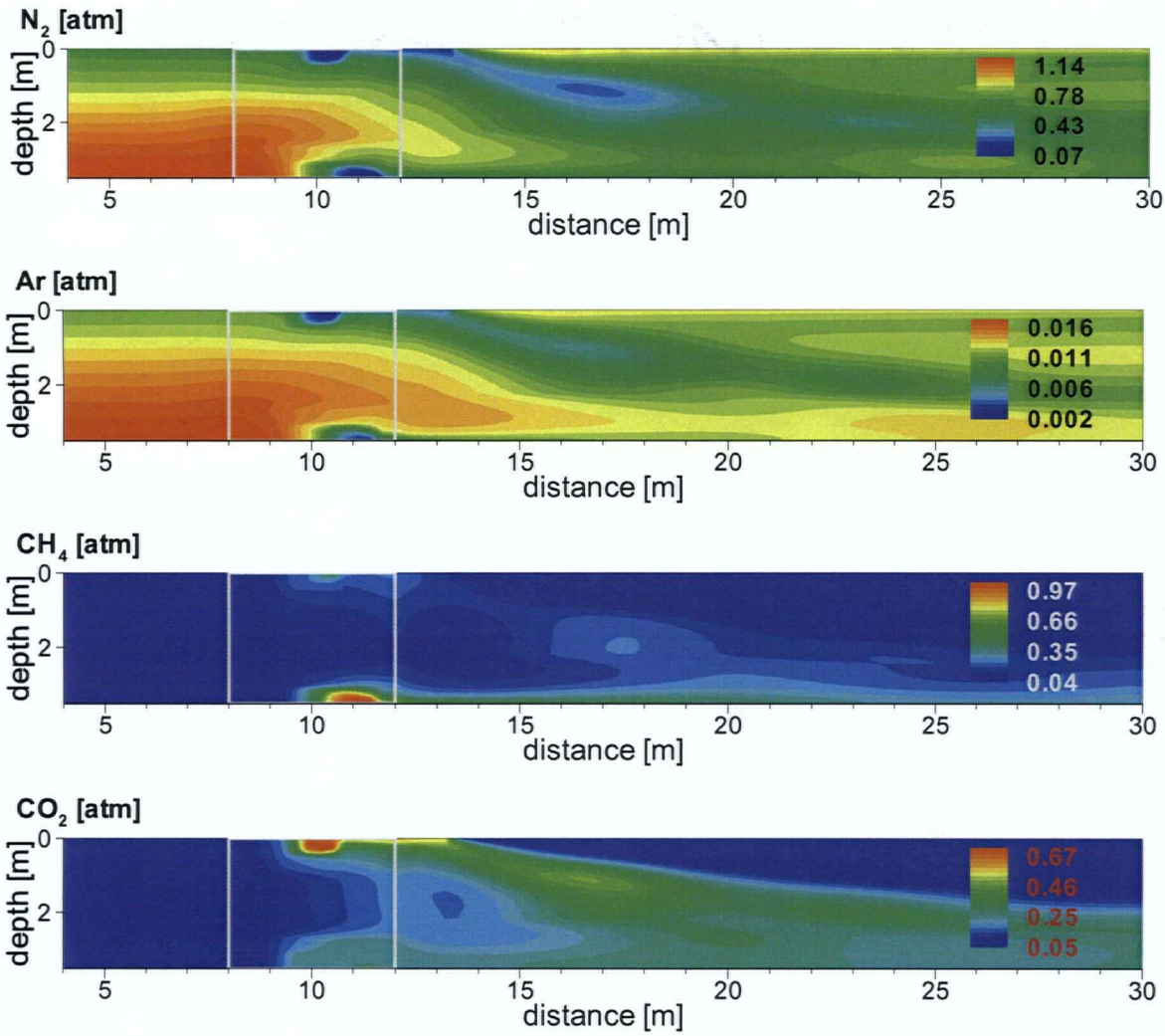

Figure 3.16. Simulated gas partial pressure contours for N_2, Ar, CH_4, and CO_2 [atm] after 95 months of operation (approximately August 2003).

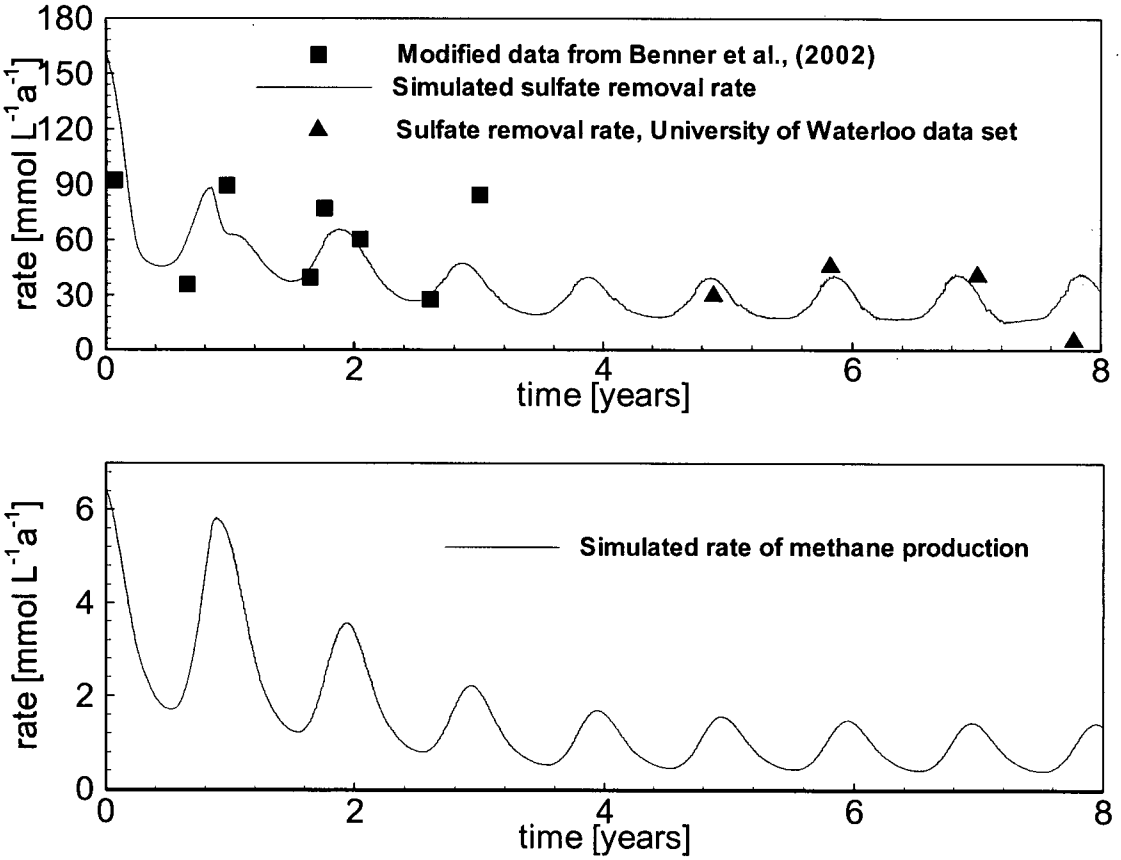

Figure 3.17. Long-term trend of average sulfate reduction rate (simulated and observed) and rate of methanogenesis (simulated).

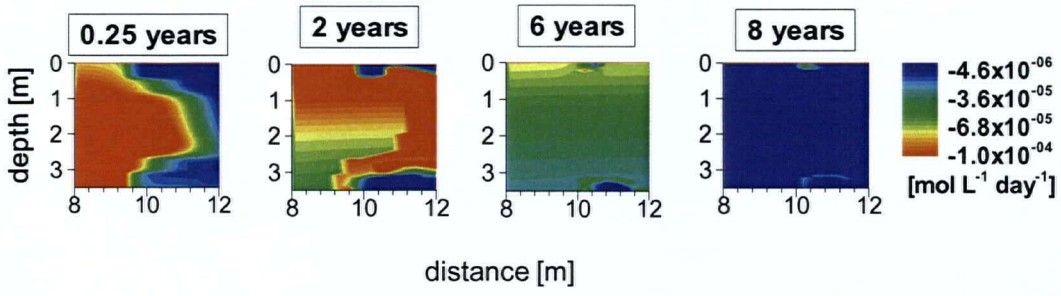

Figure 3.18: Simulated contours of organic carbon consumption rates by sulfate reduction [mol L^{-1} day^{-1}] for 1995 (3 months or 0.25 years of barrier operation), 1997 (23 months or approximately 2 years of barrier operation), 2001(71 months or approximately 6 years of barrier operation) and 2003 (95 months, or approximately 8years of barrier operation.

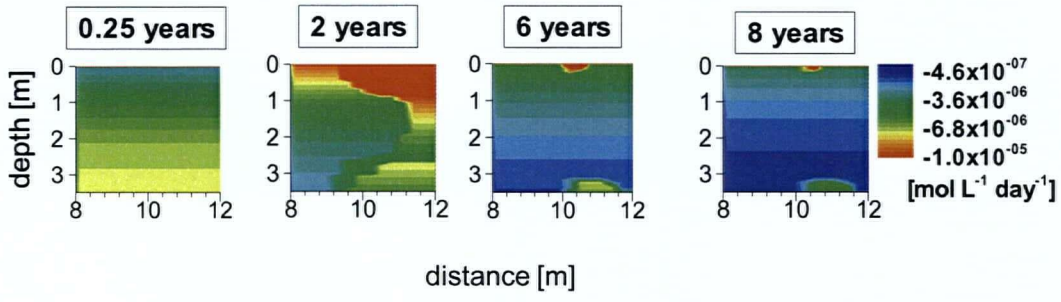

Figure 3.19: Simulated contours of organic carbon consumption rates by methanogenesis [mol L^{-1} day^{-1}] for 1995 (3 months or 0.25 years of barrier operation), 1997 (23 months or approximately 2 years of barrier operation), 2001(71 months or approximately 6 years of barrier operation) and 2003 (95 months, or approximately 8years of barrier operation.

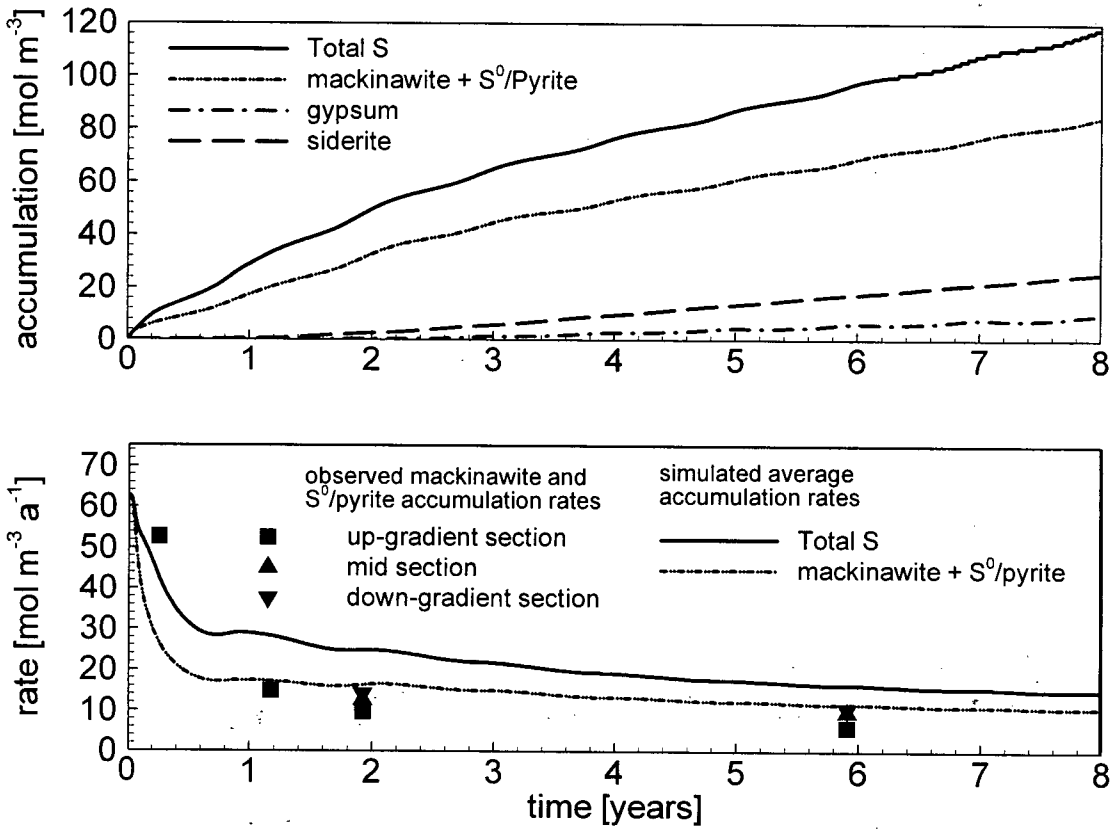

Figure 3.20. Solid phase sulfur accumulation and accumulation rates. Observed accumulation rates reported by Daignault (2002) were obtained using a dry bulk density of 0.2 g organic carbon cm^{-3} treatment material.

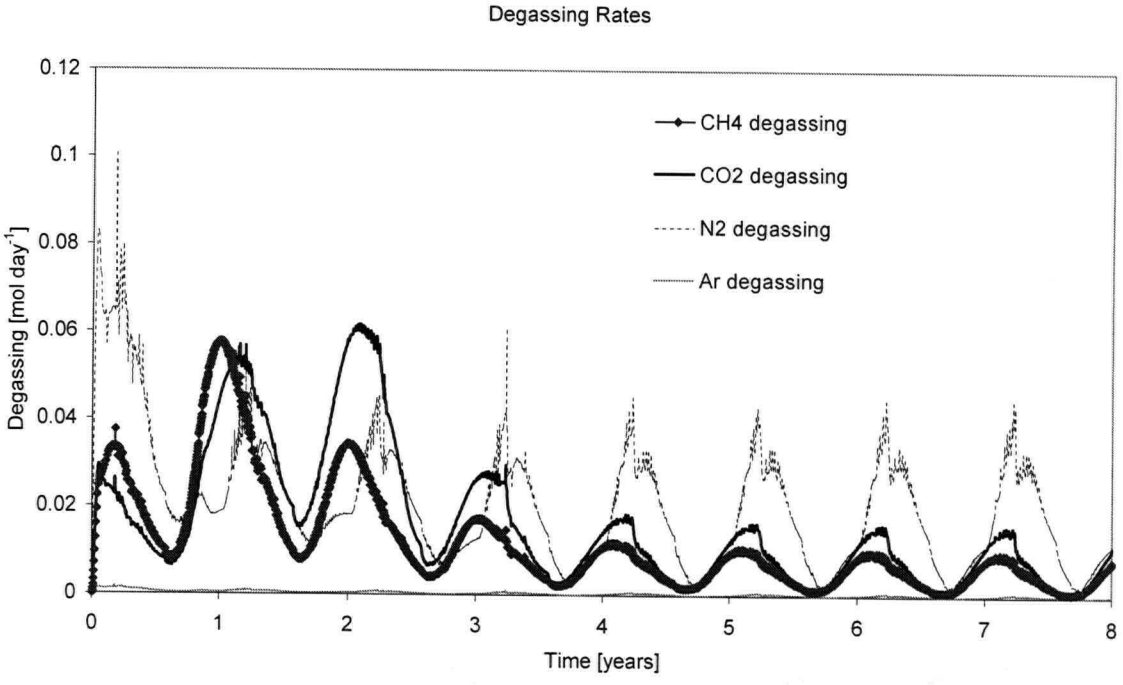

Figure 3.21. Simulated degassing rates over time for CH_4, CO_2, N_2, and Ar [mol day^{-1}].

Chapter IV:

Using dissolved gas analysis for investigating the performance of a zero-valent iron/organic carbon permeable reactive barrier for the treatment of acid mine drainage

4.1 Introduction

The present study was conducted at a zero-valent iron (Fe^0)/organic carbon mixed PRB test cell at the Campbell Mine in Balmertown, Ontario, which was designed to treat acid mine drainage high in arsenic (As) and sulfate (SO_4).

The reducing conditions within the PRB promote the microbially mediated reduction of sulfate (Benner et al., 1997):

$$SO_4^{2-} + 2CH_2O + 2H^+ \rightarrow H_2S + 2CO_{2(g)} + 2H_2O \qquad (4.1)$$

and dissolved metals rapidly react with hydrogen to form metal sulfides within the barrier. Though the reduction of sulfate is generally considered a biological process, Fe^0 may also contribute to the reduction of sulfate via (Blowes et al., 2000):

$$4Fe^0 + SO_4^{2-} + 9H^+ \rightarrow 4Fe^{2+} + HS^- + 4H_2O \qquad (4.2)$$

Effective removal of arsenic using zero-valent iron has been demonstrated in field, laboratory, and modeling studies (Su and Puls, 2001; Nikolaidis et al., 2003). Arsenic, in the form of Arsenite(III), forms surface precipitates with reduced sulfur within the zero-valent iron media (Nikolaidis et al., 2003), suggesting conditions are favourable within the PRB for the precipitation of orpiment (As_2S_3).

Another naturally occurring reaction within the barrier, though not a part of the treatment process, is the decomposition of the organic carbon coupled with methanogenesis (Stumm and Morgan, 1996):

$$2CH_2O \rightarrow CO_{2(g)} + CH_{4(g)} \quad (4.3)$$

Equations 4.1 through 4.3 describe the primary overall reactions occurring within the PRB. Intermediate reactions that occur within the PRB may be evident as well, though are less important. For instance, unlike the Nickel Rim PRB, as the anoxic groundwater enters the PRB, anaerobic corrosion of Fe^0 occurs by the oxidative action of water (Reardon, 1995):

$$Fe_{(s)} + 2H_2O_{(l)} \rightarrow Fe^{2+} + 2OH^- + H_{2(g)} \quad (4.4)$$

This reaction will increase pH, and the generation of $H_{2(g)}$ creates reducing conditions within the PRB. Previous studies have shown that aerobic (Su and Puls, 2001 and 2003) and anaerobic corrosion (Manning et al., 2002) of Fe^0 produces an efficient sorbent for both As(III) and As(V) composed of iron hydroxides and green rusts.

Hydrogen, which is produced by reaction 4.4 in a Fe^0 environment, is an important substrate for many anaerobic bacteria. Sulfate-reducing microorganisms utilize hydrogen following the equation (Chapelle, 2001):

$$SO_4^{2-} + 4H_2 + H^+ \rightarrow HS^- + 4H_2O \quad (4.5)$$

Methanogens also use H_2 according to the equation (Chapelle, 2001):

$$HCO_3^- + 4H_2 + H^+ \rightarrow CH_4 + 3H_2O \quad (4.6)$$

The abundance of methane produced by methanogenesis can be modified by microbial methane oxidation. Anaerobic methane oxidation:

$$CH_4 + SO_4^{2-} + 2H^+ \rightarrow H_2S + CO_2 + 2H_2O \quad (4.7)$$

has been reported in environments where denitrification or sulfate reduction occurs (Reedburgh 1980; Zhang et al. 1998; Grossman et al. 2002), and could potentially occur within the PRB. [Intermediate reactions, described by Equations 5 through 7 could

potentially take place at Nickel Rim PRB as well, however, the conditions are less reducing (i.e., less H_2), and therefore they are less significant to that system and are left out of the discussion in Chapter 3].

Methane may also be subject to aerobic oxidation when it diffuses across an anoxic-oxic interface (Megonigal et al. 2004):

$$CH_4 + 2O_2 \rightarrow CO_2 + 2H_2O \qquad (4.8)$$

Equations (4.2) and (4.4) lead to the consumption of the Fe^0 treatment material, while equations (4.1) and (4.3) lead to consumption of the organic carbon treatment material. Equations (4.1) and (4.2) describe overall reactions which lead to sulfate reduction and will promote metal sulfide precipitation. All equations involve the consumption or production of gases, with a net production of gases such as H_2 (Reardon, 1995), CH_4, possibly H_2S (Machemer, et al., 1993), and CO_2.

As outlined in the introductory chapter, a significant amount of gas production may induce degassing and possibly ebullition, which may also affect dissolved gas composition. In this case, groundwater entering the PRB is already anoxic with depleted levels of N_2 and Ar, and high levels of CH_4. These conditions indicate that methane production in the groundwater outside of the PRB has already caused degassing. In addition, H_2 and CH_4 gases are produced within the PRB, as a result of anaerobic corrosion of iron and methanogenesis, thus increasing the total gas pressure in the system.

4.2 Site Description

Dissolved gas data was collected at a zero-valent iron/organic carbon mixed PRB test cell located at a mine in Ontario during June 2004. The test cell was designed as a

pilot study to investigate the performance of the materials for the removal of arsenic from the groundwater prior to installing a large scale PRB at the site, and the installation was completed in August 2002. The test cell is bound by concrete below, unsealed sheet pile on all four sides, and approximately a 10 cm bentonite clay cap above, overlain by approximately 1.8 m of sand. The reactive material consists of 40% Fe^0, 30% organic carbon (i.e., compost), and 30% gravel. The test cell draws water from two boreholes (BH2002-2 and BH2002-3) located within the mine tailings. BH2002-2 contains high As(III) with concentrations up to 60 mg L^{-1}, while groundwater originating from BH2002-3 contains As(III) below detection (< 1 mg L^{-1}). Water from BH2002-2 and BH2002-3 are combined at a mixing cell adjacent to the PRB at a ratio of approximately 1: 2, resulting in influent groundwater with As(III) concentrations of approximately 20 mg L^{-1}. Groundwater is pumped into the influent gravel end of the 4.5 m long, 2 m wide, 1.5 m deep test cell (Figure 4.1) at rates typically of 300- to- 400 L day^{-1} from mid April until the end of December each year. Assuming a barrier porosity of 0.5, residence time within the reactive material is approximately 15 days. The intention during operation is to keep the reactive material fully saturated while pumping, however, the water level fluctuates often and during the time of this study it was approximately 0.35 m below the clay layer, leaving a small unsaturated zone within the reactive material of the PRB test cell. The site ground elevation is 366 m (0.935 atm).

4.3 Methods

4.3.1 Dissolved Gas Sampling Locations

The sampling conducted took place within the Fe^0/organic carbon mixed PRB test cell June 7 through June 12, 2003. Monitoring points were sampled at well nests 1

through 8 and 10 through 17 within the PRB (Figure 4.1), at piezometers 9 and 18, and at the influent and effluent lines of the test cell. A shallow monitoring well (25b) located within the aquifer, 1.5 m north of the test cell was sampled as well. Monitoring points located within the nests were constructed of 2 cm PVC pipes with a porous tip in place of a screen, and each well nest had 3 sampling intervals (A, shallow; B, intermediate; C, deep) (Bain, personal communication, September 2004). Piezometers 9 and 18 were 2 cm PVC pipes screened throughout the reactive material zone. Monitoring well 25b was a 2 cm diameter stainless steel pipe, screened 3 m bgs (Bain, personal communication, 2004).

4.3.2 Vapour Phase Sampling Locations

Four vapour sampling wells (P2, P4, P5, and P6) were constructed of 2 cm OD stainless steel tubing with a porous tip. Vapour wells were driven to a depth just below the clay cap, within the narrow unsaturated zone of the reactive mixture zone (Figure 3.1).

4.4 Results and Discussion

4.4.1 Spatial Distribution of Dissolved Gases

Cross sections of the dissolved gas data collected in the saturated zone in June 2004 along the north and south transects parallel to the groundwater flow through the PRB test cell are shown in Figures 4.2 through 4.8 for N_2, Ar, CH_4, H_2, and CO_2, respectively. Vapour phase data collected in the unsaturated zone are shown in Figures 4.2 through 4.5 for N_2 and Ar. Dissolved concentrations of SO_4 (data by Bain, U. of Waterloo, Waterloo, Ontario, June 2004) are presented in Figure 4.9. Influent dissolved

concentrations of N_2, Ar, CH_4, H_2, CO_2 and SO_4 are provided in the heading of the corresponding figure for comparison.

N_2 and Ar data (Figures 4.2 and 4.3), expressed as fractions of the average background N_2 and Ar (i.e., influent N_2 and Ar), show that both gases are slightly depleted within the intermediate and deep intervals of the north transect (as low as 0.72 of background N_2 and 0.82 of background Ar at 15b), while they are only slightly depleted within the center of the south transect at the intermediate and deep intervals. Influent N_2 and Ar (0.65 atm and 0.0081 atm, respectively) partial pressures are already depleted relative to atmospheric values (0.78 atm and 0.009 atm). N_2 and Ar appear to be enriched at the shallow depths along both transects. Overall, changes in both N_2 and Ar along the flow path appear to be insignificant. N_2 and Ar data are expressed as mg L^{-1} concentrations in Figures 4.4 and 4.5 for completeness, and mimic the results presented in Figures 4.2 and 4.3.

Influent concentrations of CH_4 are high (12.6 mg L^{-1}), indicating that the water comes from a reducing environment. This is not surprising, because the water originates from tailings that are deposited on peat (Ross, 1998). CH_4 concentrations (Figure 4.6) increase slightly from influent to effluent along the flow path at the deep interval for the north transect, and increase within the centre of the flow path for the deep interval along the south transect. These observations indicate that some methanogenesis is occurring along the deeper flow path. In general, methane concentrations change very little along the deep flow path, suggesting that residence times are short in comparison to methane production rates. Concentrations of CH_4 appear to decrease with shallower depths for

both the north and south transects. Overall, concentrations do not change significantly along the flow path from well nest 1 and 10 to wells 9 and 18, respectively.

H_2 concentrations (Figure 4.7) are elevated within the intermediate and shallow depths of both the north and south transect, though H_2 is present in the south transect throughout the entire depth between well nests 4 and 7. CO_2 concentrations decrease from the influent concentration of 31.5 mg L^{-1} to values ranging from less than 0.01 mg L^{-1} to 0.1 mg L^{-1} along most of the south transect, and decrease to values on the order of 0.01 to 1 mg L^{-1} along most of the north transect; a result of the increase in pH due to Fe^0 oxidation. The pH of the influent groundwater to the PRB had a value of 7.4, while the effluent groundwater had a pH of 9.1. The pH values within the PRB test cell generally ranged from 8.1 to 10.4 (data not shown), however, values of approximately 7.3 to 7.6 were found at the A wells from nests 5 to 7 in the south transect, and a pH of 7.6 was measured in the A well at nest 16 of the north transect. Sulfate concentrations (Figure 4.9) are much less than the influent concentration within the PRB test cell at shallow and intermediate depths, though sulfate concentrations remain high along the flow path of the deep interval for both transects. DO concentrations (not shown) were very low, averaging 0.2 mg L^{-1} throughout both the south and north transects of the PRB test cell.

Because concentration contours for the transects do not allow a conclusive statement of gas composition trends along the flow path, gas partial pressures have been vertically averaged and are presented in Figures 4.10 and 4.11 for the south transect wells and the north transect wells, respectively. However, vertically averaged results only confirm that over all, N_2 and Ar partial pressures do not change significantly along the flow path through the test cell for both the south and north transect in comparison to

influent partial pressures. CH_4 partial pressures and total pressures also remain relatively constant along the flow path. Only CO_2 decreases from influent partial pressures for both transects, but then remains constant throughout both profiles. H_2 shows a significant increase in partial pressures in both the south transect from well nests 4 to 7, and in the north transect from well nests 13 to 16. This trend may indicate that H_2 production exceeds consumption where H_2 partial pressures are high. Low H_2 partial pressures may be due to short residence times.

4.4.2 Vapour Phase Gas Distribution

Cross sections of the vapour phase gas data collected in the unsaturated zone above the PRB in June 2004 along the transect parallel to the groundwater flow through the PRB test cell are shown in Figures 4.2 through 4.5 for N_2 and Ar, respectively. All data for the four vapour wells (P2, P4, P5, and P6) are presented in Table 4.1. Figures 4.2 and 4.3 indicate that the unsaturated zone has become enriched with N_2 and Ar to above atmospheric levels. Table 4.1 shows that oxygen has been nearly depleted from the unsaturated zone. The presence of H_2 and CH_4 within the unsaturated zone indicates that degassing and ebullition from the saturated zone may be taking place, however, because Fe^0 and organic carbon are present within the unsaturated zone, H_2 and CH_4 may also be the result of local production of these gases. The percentage of H_2 and CH_4 increase slightly along the flow path through the test cell, while the percentage of CO_2 within the vapour phase decreases slightly. N_2 and Ar enrichment within the unsaturated zone appears to be near constant along the flow path.

4.4.3 *Preferential Flow Paths and Relative Residence Times*

The lack of significant depletion of N_2 and Ar at intermediate and deep intervals indicates that residence times are very short in comparison to gas production rates along these flow paths. Influent CH_4 (Figure 4.6) concentrations are high, and remain high and fairly constant throughout the intermediate and deep portions of the barrier, supporting this observation, and indicating that this is the preferred pathway through the barrier. If residence times were relatively long in comparison to the time scale of gas production, one would expect that significant CH_4 production would occur within the PRB, however, this is not the case. SO_4 concentrations also remain similar to the influent SO_4 concentrations along the deep and intermediate flow path.

As stated previously, H_2 (Figure 4.7) is generally not detected at deeper intervals, while it is present at shallow depths. H_2 concentrations seem to support that residence times are shorter at the deeper intervals than at shallow depths. H_2 is likely produced throughout the PRB by anaerobic corrosion of Fe^0, and it is likely that what H_2 is present is utilized along the flow paths where sulfate is present (equations 6 and 7), while it accumulates in the zones that are sulfate limited (Figure 4.9). High sulfate concentrations do correspond to low H_2 concentrations.

Dissolved gas data strongly suggests that most of the injected water is passing through the barrier at deep and intermediate levels. These results suggest that dissolved gas analysis can be useful in determining relative residence times and overall flow patterns within this PRB. The signature of the water at shallow depths is very different from the signature of water within the intermediate and deep intervals of the PRB, indicating that little exchange occurs between these zones. It is possible that the shallow

portion of the PRB is nearly hydraulically excluded from the deeper portions of the barrier, and that this narrow shallow zone may experience residence times that are much longer than the majority of the PRB.

4.4.4 Origin of Pore Water in PRB Shallow Zone

A conclusive explanation for the enrichment of N_2 and Ar at shallow depths for both the south and north transects (Figures 4.2 and 4.3) cannot be determined. Possible explanations include leakage of relatively pristine precipitation water from the ground surface into the test cell. In addition, gaps between the clay layer and the unsealed sheet piling may provide a conduit for precipitation to enter the reactive material zone. Dissolved gas sampling results for the aquifer monitoring point 25b outside of the test cell are shown in Table 4.2 for comparison, and show that the aquifer contains N_2 and Ar concentrations very close to the influent concentrations to the test cell, suggesting that the aquifer groundwater is not causing the enrichment of N_2 and Ar at shallow depths. An alternative explanation for the enrichment of Ar and N_2 at shallow depths is gas diffusion from the unsaturated zone back into the water table, which will be discussed in more detail.

CH_4 data supports the theory that outside water is leaking into the test cell, because at shallow depths within the PRB CH_4 concentrations are much lower than the CH_4 concentrations in the influent water (as low as 0.3 mg L^{-1} at well 6b). Lower methane concentrations are seen in the surrounding aquifer (4.7 mg L^{-1} at well 25b), however these concentrations do not explain the even lower concentrations at shallow depths within the test cell. Precipitation water leakage is most likely the cause of the low methane concentrations. An additional possible explanation for low methane

concentrations at shallow depths may be due to aerobic methane oxidation (equation 8), the fluctuating water table and diffusive exchange.

Sulfate within the aquifer was reported to be high (greater than 1,000 mg L^{-1} at monitoring well 25b), indicating that this water is not leaking into the test cell causing the low concentrations, which are observed at shallow depths. Explanations for low SO_4 concentrations include very long residence times, and/or relatively pristine precipitation water (recharge) leaking into the test cell from above.

Though N_2 and Ar enrichment at the water table, as well as low CH_4 and SO_4 concentrations could be explained by precipitation water leaking into the test cell, gas diffusion from the unsaturated zone was also considered. The unsaturated zone is enriched in N_2 and Ar, and therefore N_2 diffusion into the water table was simulated using the reactive transport code MIN3P (Mayer et al., 2002) for the 2 years of test cell operation, and model parameters and initial and boundary conditions are shown in Table 4.3. The 1-D simulation was over a 1.5 m fully saturated vertical domain, with an initial N_2 partial pressure of 0.65 atm. At time t=0, the N_2 at the boundary was allowed to diffuse into the saturated domain. The diffusion modeling shows that N_2 diffusion would be very limited at the water table after 2 years, however, the minor gas diffusion, in addition to the water table fluctuations observed at the site, could create the effect of enriched N_2 and Ar at the shallow depths within the test cell.

Atmospheric exchange (discussed further in section 4.4.5) may occur in the shallow zone across the unsaturated clay, and it is likely that the water table will pick up that signature. CH_4 concentrations are also low at the water table. Oxygenation of anoxic waters in a fluctuating water table system has been described by others (Williams

et al., 2000), while Kettunen et al. (1999) demonstrated that methane oxidation potentials could be maintained despite water table fluctuations. Gas diffusion, in addition to the water table fluctuations may cause O_2 to enter the shallow portion of the test cell, which could then rapidly be consumed by CH_4 oxidation (equation 4.8).

The dissolved gas data set provides evidence for both the argument that precipitation water may be leaking into the test cell from above, and that the shallow gas data is explained by gas diffusion and water table fluctuations. However, the data set does not provide enough evidence to prove or disprove either hypothesis.

4.4.5 Degassing and Ebullition

Vapour phase gas results show that argon and nitrogen are generally enriched above atmospheric levels within the unsaturated zone, suggesting that air is advectively moving into the region (ingress of air through the clay cap), driven by consumption of O_2 within the unsaturated zone. The presence of methane (as much as 0.32 percent) and hydrogen gas (as much as 1.13 percent) within the unsaturated zone suggests that degassing and ebullition may also be occurring, though it is equally likely that methanogenesis and aerobic corrosion of Fe^0 are taking place within the unsaturated zone and causing the production of these gases. Typically, one would expect N_2 and Ar depletion at the water table if significant degassing and ebullition were occurring; however, this trend is not observed. For this reason, degassing and ebullition do not appear to be important factors in this PRB system.

4.4.6 PRB Treatment

Little can be determined regarding the reaction rates and treatment success of the Fe^0/organic carbon mixed PRB using the dissolved gas data set alone. Unlike the Nickel

Rim data analysis described in Chapter 3, short residence times relative to reaction rates inhibit gas accumulation and degassing. These conditions do not justify data interpretation using the 4-gas degassing model developed and described in Chapter 3 for the current data set. Even if the actual residence times within the PRB were known, gas production rates and treatment rates could not be determined due to the lack of a significant trend of Ar, N_2, and CH_4 along the flow path.

Based on the dissolved gas signature of the water, the shallow portion of the PRB appears to be less reactive in the overall treatment of the system, due to the very long residence times, or because it contains different water entering the PRB, while the intermediate and deep portions of the PRB seem to actively treat the groundwater.

4.5 Summary and Conclusions

Overall, dissolved gas concentrations within the PRB do not change significantly from influent to effluent, though they may vary along the flow path through the PRB. Minor depletion of N_2 and Ar along the transect flow paths at the intermediate and deep intervals indicate that some degassing is occurring locally, while the presence of CH_4 and H_2 within the unsaturated zone indicates that ebullition from the saturated zone or production of these gases within the unsaturated zone may be occurring as well. Enrichment of N_2 and Ar above atmospheric levels within the unsaturated zone suggests advective ingress of air across the clay cap, driven by O_2 consumption. The limited variation in N_2 and Ar concentrations from influent to effluent indicate that residence times within the PRB are very short in comparison to gas production rates. Enrichment of N_2 and Ar at shallow depths of the saturated zone, in addition to low methane concentrations indicates that leakage of recharge through the clay cap and into the PRB

may be occurring, though these observations may also be explained by gas diffusion and water table fluctuations.

The lack of variation in CH_4 concentrations from influent to effluent along the deep interval confirms that this is the faster pathway through the PRB. The absence of H_2 gas at the deep interval also supports the idea that this is the faster (i.e., preferred) flow path within the PRB, as it would be consumed more readily in these areas. Low concentrations of SO_4, CH_4, and accumulation of H_2 at the shallow interval indicates that this is the slow pathway within the PRB.

Due to relatively short residence times and a lack of concentration trends, little can be determined regarding the reaction rates and treatment success of the Fe^0/organic carbon mixed PRB using the dissolved gas data set alone.

4.6 References

Benner, S. G., D. W. Blowes, C. J. Ptacek, 1997. A full-scale porous reactive wall for the prevention of acid mine drainage. *Groundwater Monit. Remed.* 17, 99-107.

Blowes, D. W., C. J. Ptacek, S. G. Benner, C. McRae, T. A. Bennett, and R.W. Puls, 2000. Treatment of inorganic contaminants using permeable reactive barriers. *J. Contam. Hydrol.*, 45, 123-137.

Chapelle, F. H., 2001. Groundwater microbiology and Geochemistry, 2nd edition. John Wiley & Sons, Inc., New York, NY.

Grossman, E. L.; L. A. Cifuentes; I. M. Cozzarelli, 2002. Anaerobic methane oxidation in a landfill-leachate plume. *Environ. Sci. Technol.*, 36, 2436-2442.

Kettunen, A., V. Kaitala, A. Lehtinen, A. Lohila, J. Alm, J. Silvola, P. J. Martikainen, 1999. Methane production and oxidation potentials in relation to water table fluctuations in two boreal mires. *Soil Biol. Biochem.*, 31, 1741 – 1749.

Machemer, S. D., J. S. Reynolds, L. S. Laudon, T. R. Wildeman, 1993. Balance of S in a constructed wetland built to treat acid mine drainage, Idaho Springs, Colorado, U.S.A. *Appl. Geochem.*, 8, 587-603.

Manning, B. A., M. L. Hunt, C. Amrhein, J. A. Yarmoff, 2002. Arsenic(III) and arsenic(V) reactions with zerovalent iron corrosion products. *Environ. Sci. Technol.*, 36, 5455-5461.

Mayer, K. U., E. O. Frind, and D. W. Blowes, 2002. Multicomponent reactive transport modeling in variably saturated porous media using a generalized formulation for kinetically controlled reactions. *Water Resour. Res.*, 38, doi: 10:1029/2001WR000862.

Megonigal, J. P., M. E. Hines, P. T. Visscher, 2004. Anaerobic metabolism: linkages to trace gases and aerobic processes, from *Treatise on Geochemistry,* 8, 317-424.

Nikolaidis, N. P., G. M. Dobbs, J. A. Lackovic, 2003. Arsenic removal by zero-valent iron: field, laboratory and modeling studies. *Water Res.*, 37, 1417-1425.

Reardon, E. J., 1995. Anaerobic corrosion of granular iron: measurement and interpretation of hydrogen evolution rates. *Environ. Sci. Technol.*, 29, 2936-2945.

Reedburgh, W. S., 1980. Anaerobic methane oxidation: rate depth distributions in Skan Bay sediments. *Earth Planet. Sci. Letters*, 47, 345-352.

Ross, C.S., 1998. A hydrogeological and geochemical study of a gold mine tailings-derived plume, Campbell Mine, Balmertown, Ontario. M.Sc. Thesis, Dept of Earth Sciences, University of Waterloo.

Stumm, W. and J. J. Morgan, 1996. *Aquatic Chemistry, Chemical Equilibria and Rates in Natural Waters, Third Edition*; John Wiley & Sons, Inc.: New York, p 472 and p 474.

Su, C. and R. W. Puls, 2001. Arsenate and Arsenite removal by zerovalent iron: kinetics, redox, transformation, and implications for in situ groundwater remediation. *Environ. Sci. Technol.*, 35, 1487-1492.

Su, C. and R. W. Puls, 2003. In situ remediation of arsenic in simulated groundwater using zero-valent iron: laboratory and column tests on combined effects of phosphate and silicate. *Environ. Sci. Technol.*, 37, 2582-2587.

Williams, M. D, and M. Oostrom, 2000. Oxygenation of anoxic water in a fluctuating water table system: an experimental and numerical study. *J. Hydrol.*, 230, 70 – 85.

Zhang, C., E. L. Grossman, J. W. Ammerman, 1998. Factors influencing methane distribution in Texas groundwater. *Ground Water*, 36, 58-66.

Tables

Vapour Well	CH_4	CO_2	H_2	Ar	O_2	N_2	Total
			Percent of Total Vapour Measured				
P2	0.10	0.01	0.56	1.22	0.14	97.96	100.00
P4	0.24	0.01	0.77	1.22	0.16	97.60	100.00
P5	0.31	0.01	1.05	1.15	2.97	94.51	100.00
P6	0.32	0.00	1.13	1.21	0.10	97.24	100.00
			Fraction of Atmospheric				
		CO2		Ar	O2	N2	
P2		0.44		1.36	0.01	1.26	
P4		0.30		1.35	0.01	1.25	
P5		0.24		1.28	0.14	1.21	
P6		0.12		1.35	0.00	1.25	

Table 4.1. Vapour phase data for June 2004.

Monitoring Well	CH_4	CO_2	H_2	Ar	O_2	N_2	Total
	dissolved gas concentrations (mg L^{-1})						
25b	4.74	105.12	0.00	0.67	0.30	16.28	NA
	partial pressures (atm)						
	0.152	0.044	0.000	0.009	0.005	0.685	0.895

NA = not applicable.

Table 4.2. Dissolved gas concentrations and gas partial pressures for monitoring well 25b, located within the aquifer, and just adjacent to the PRB.

Parameter	Units	Value
Gaseous Effective Diffusion Coefficient (D_{eff_g})	[m^2s^{-1}]	7.9×10^{-6}
Porosity (ϕ)	[]	0.5
N2 Partial Pressure		
Initial Condition	[atm]	0.65
Boundary Condition	[atm]	0.97

Table 4.3. Gas diffusion modeling parameters, using the reactive transport code MIN3P, for a 1-D model simulation of diffusion only, in a 1.5 m domain.

Figures

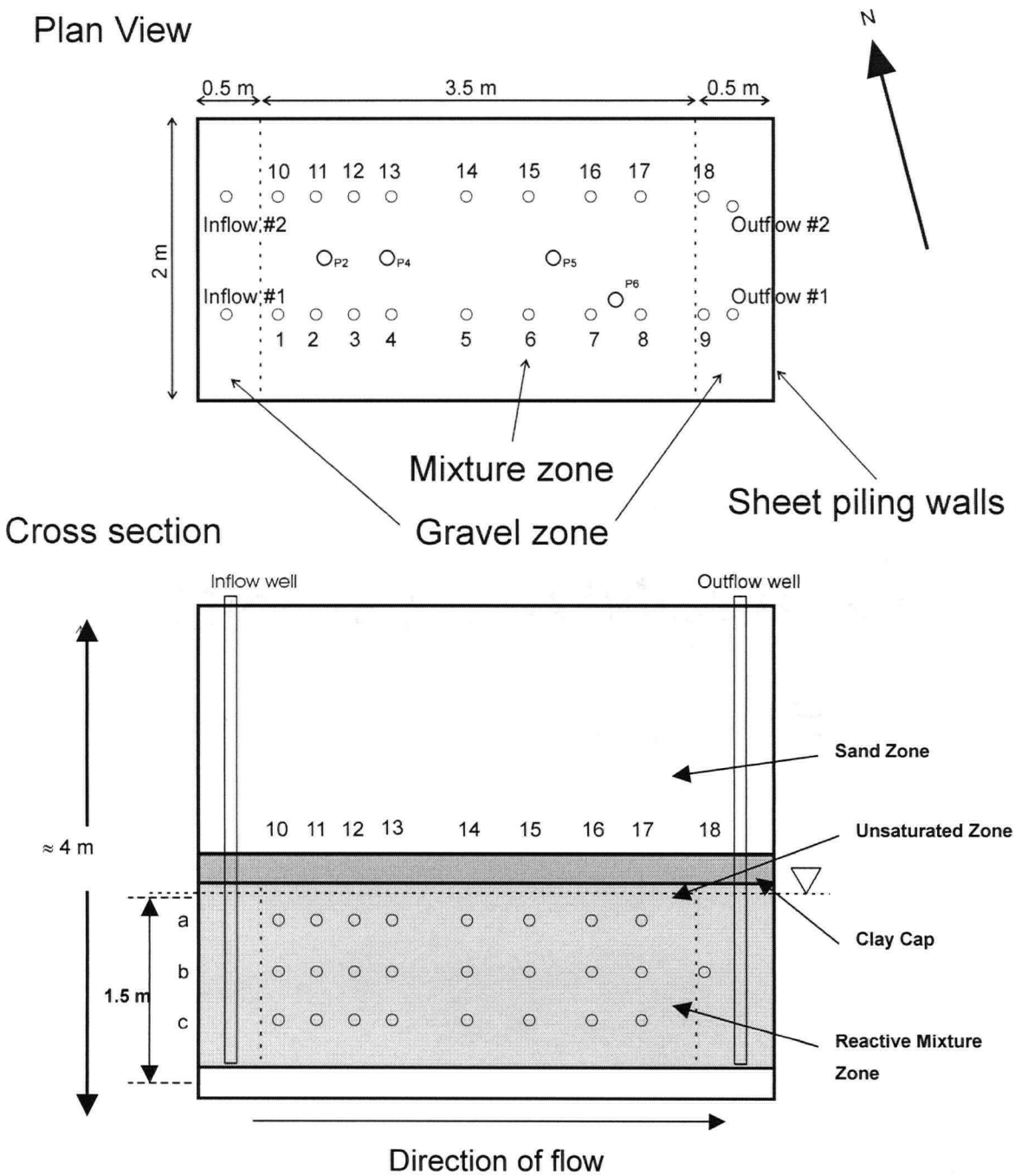

Figure 4.1. Plan view and cross-sectional profile of the Fe^0/organic carbon mixed PRB test cell (After Bain, personal communication, April 15, 2004).

(A) South

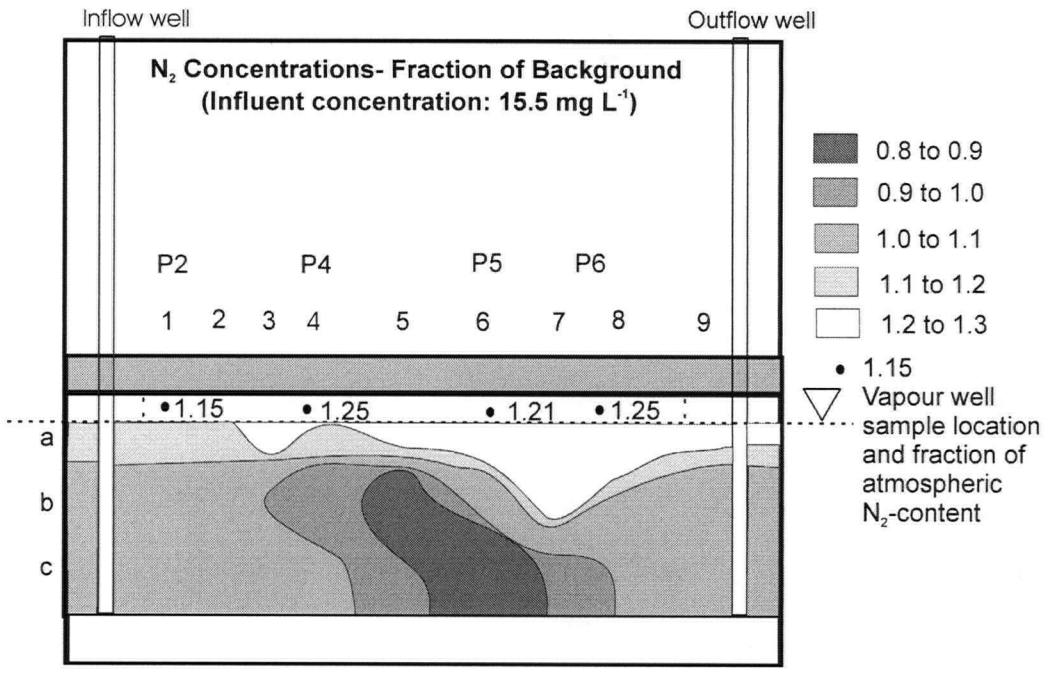

(B) North

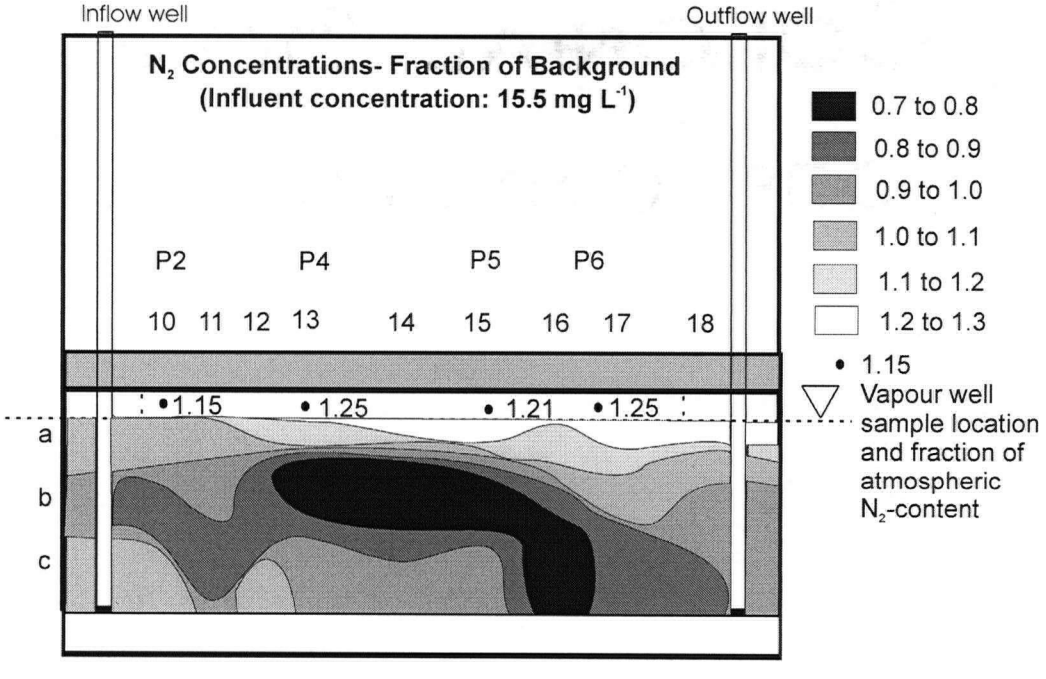

Figure 4.2. Cross-sectional profiles of dissolved and vapour phase N_2 fractions along (A) south (well nests 1-9) and (B) north (well nests 10-18) transects for June 2004. Aqueous phase data are expressed as fractions of the average background dissolved N_2, while vapour phase data are shown as fractions of atmospheric N_2-content for vapour wells P2, P4, P5, and P6.

(A) South

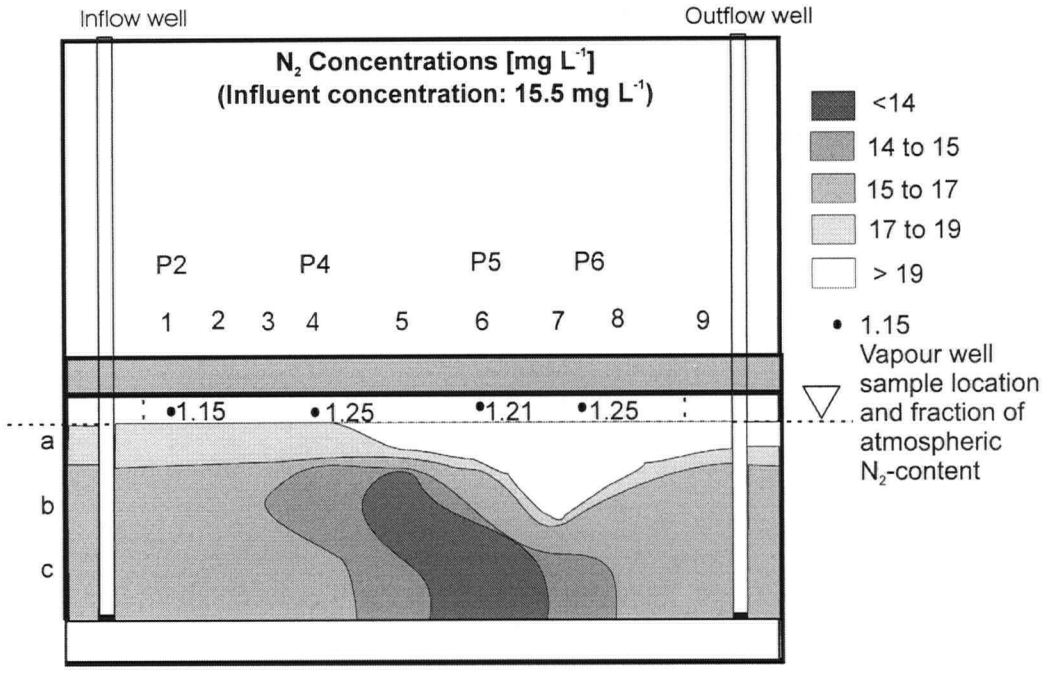

(B) North

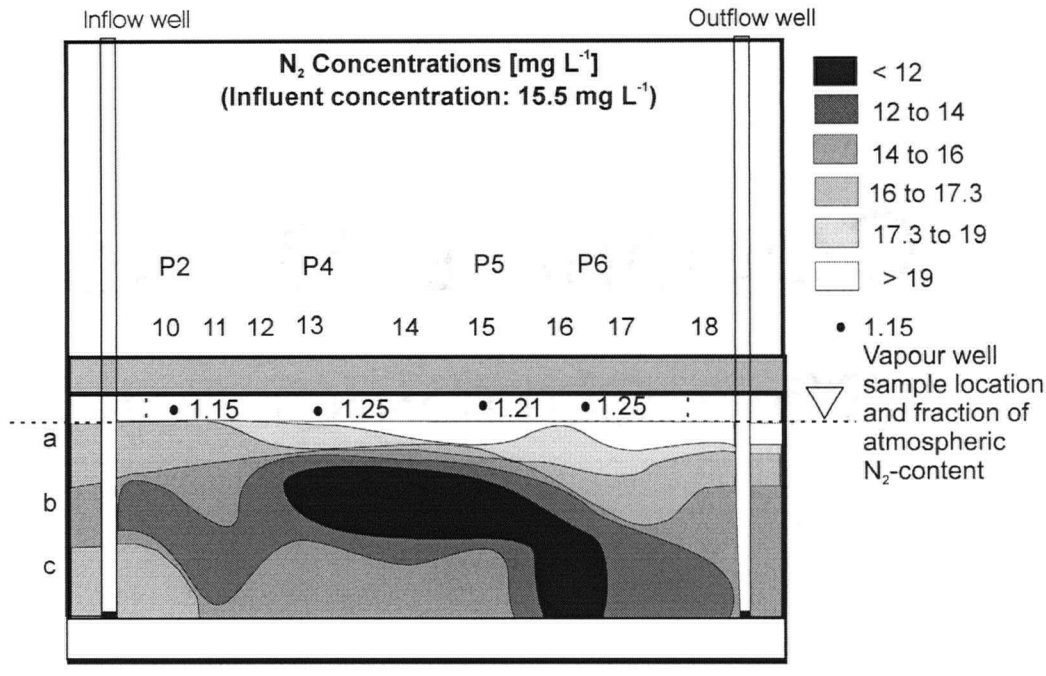

Figure 4.3. Cross-sectional profiles of dissolved and vapour phase N_2 concentrations along (A) south (well nests 1-9) and (B) north (well nests 10-18) transects for June 2004. Aqueous phase data are expressed in mg L^{-1}, while vapour phase data are shown as fractions of atmospheric N_2-content for vapour wells P2, P4, P5, and P6.

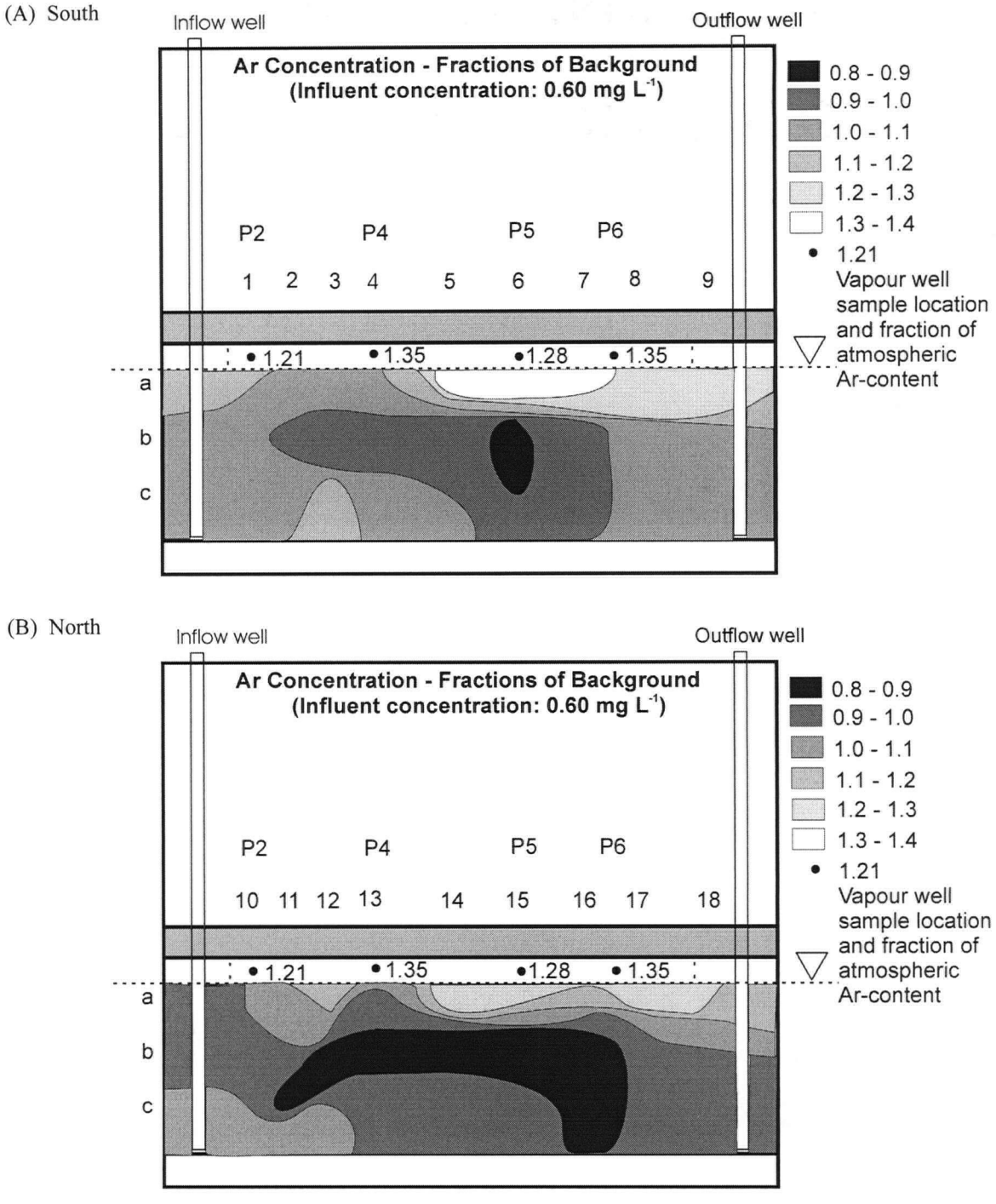

Figure 4.4. Cross-sectional profiles of dissolved and vapour phase Ar fractions along (A) south (well nests 1-9) and (B) north (well nests 10-18) transects for June 2004. Aqueous phase data are expressed as fractions of the average background dissolved Ar, while vapour phase data are shown as fractions of atmospheric Ar-content for vapour wells P2, P4, P5, and P6.

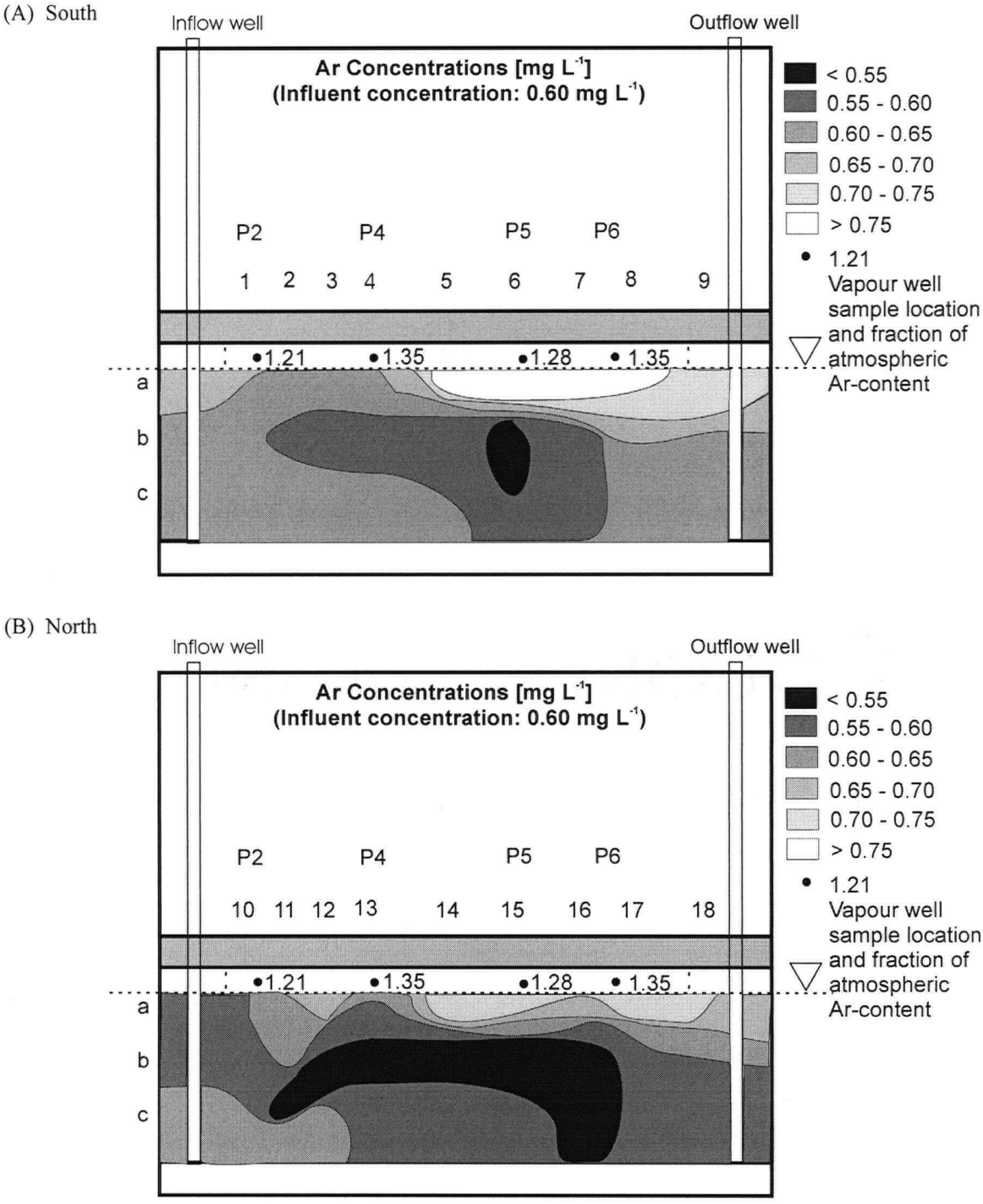

Figure 4.5. Cross-sectional profiles of dissolved and vapour phase Ar concentrations along (A) south (well nests 1-9) and (B) north (well nests 10-18) transects for June 2004. Aqueous phase data are expressed in mg L^{-1}, while vapour phase data are shown as fractions of atmospheric Ar-content for vapour wells P2, P4, P5, and P6.

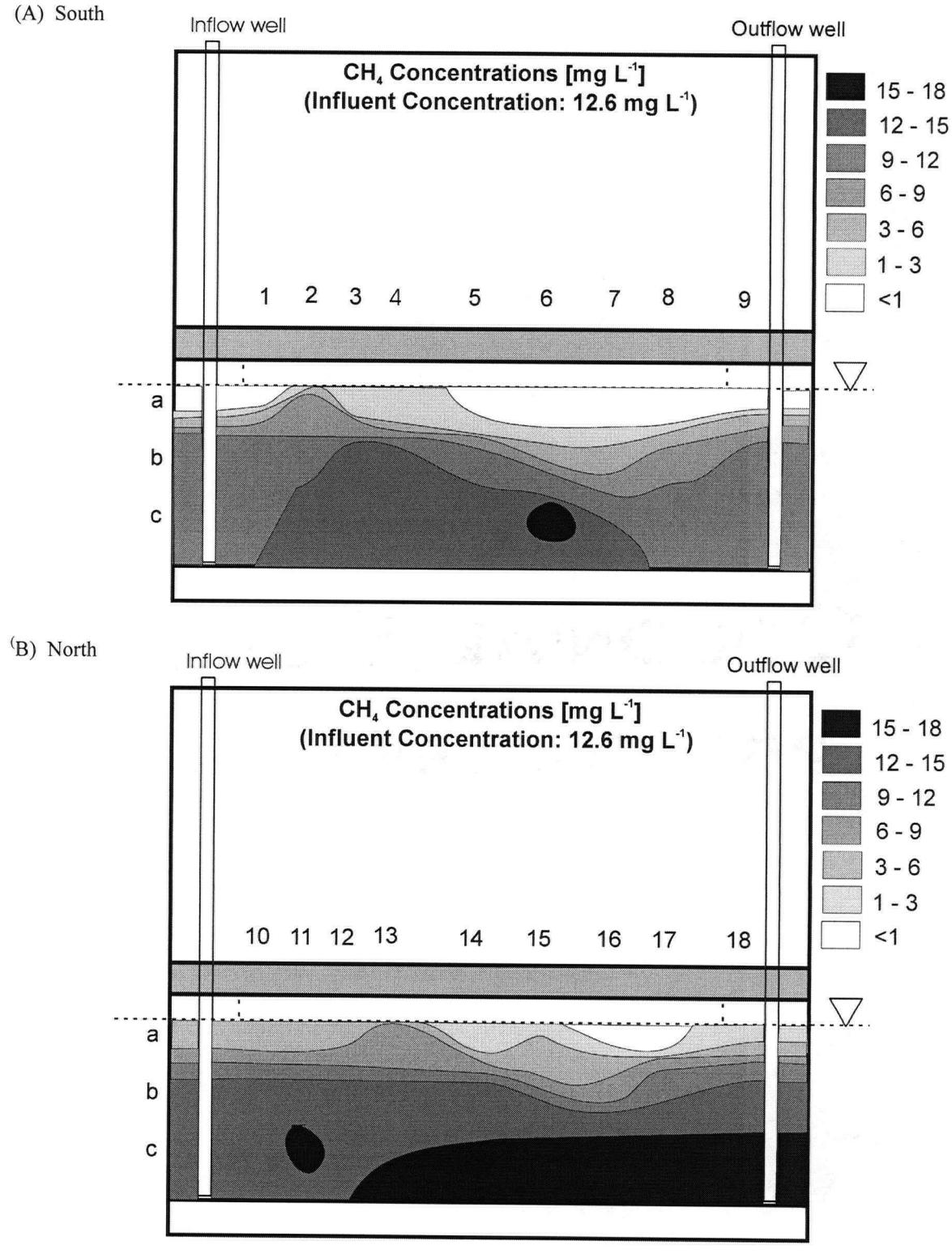

Figure 4.6. Cross-sectional profiles of dissolved CH_4 concentrations along (A) south (well nests 1-9) and (B) north (well nests 10-18) transects for June 2004. Concentrations are expressed in mg L^{-1}.

(A) South

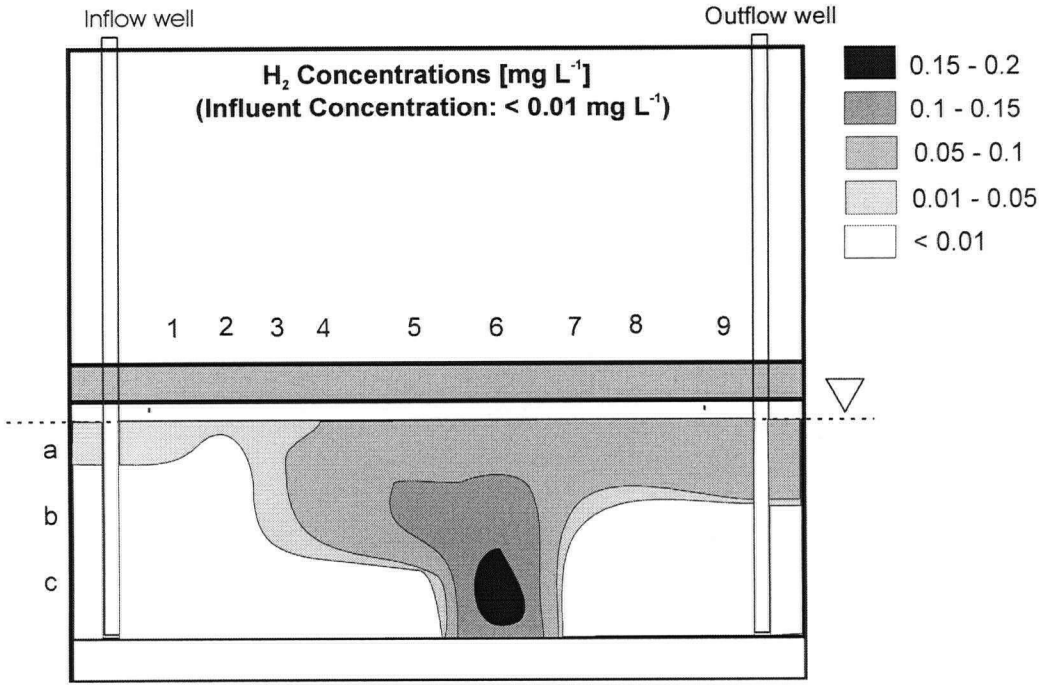

(B) North

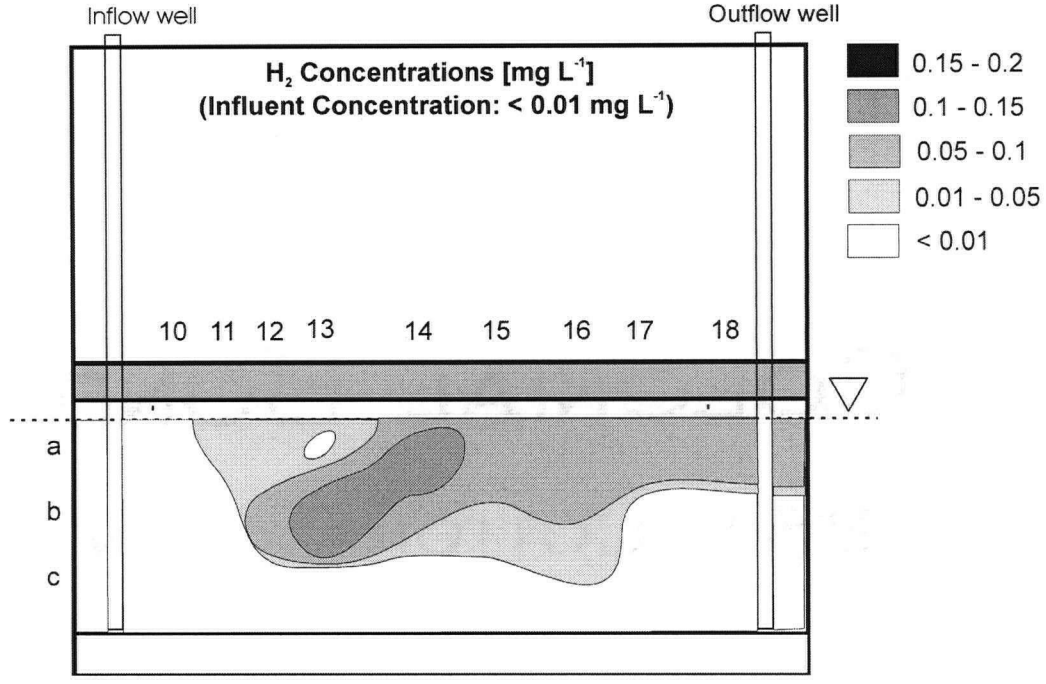

Figure 4.7. Cross-sectional profiles of dissolved H_2 concentrations along (A) south (well nests 1-9) and (B) north (well nests 10-18) transects for June 2004. Concentrations are expressed in mg L^{-1}.

A) South

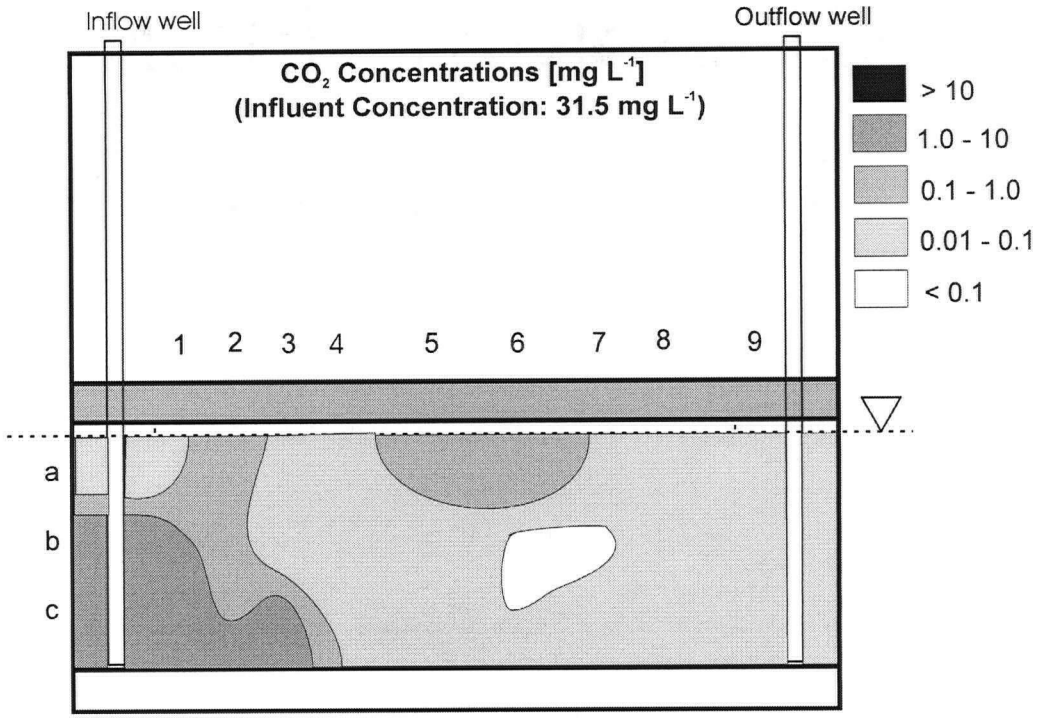

B) North

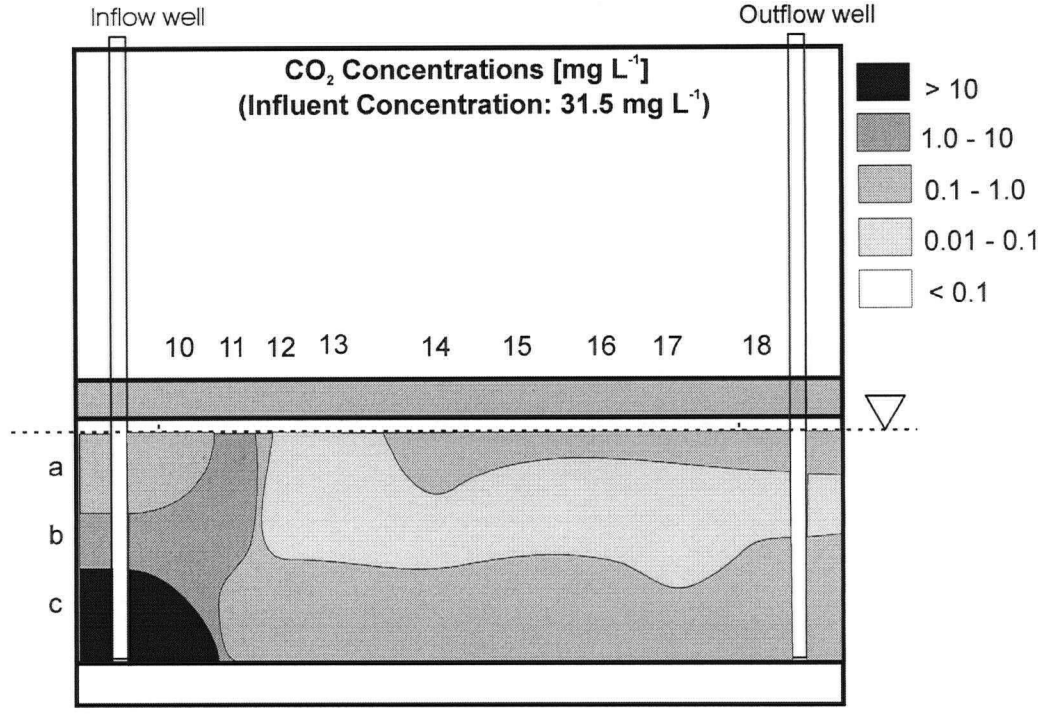

Figure 4.8. Cross-sectional profiles of dissolved CO_2 concentrations along (A) south (well nests 1-9) and (B) north (well nests 10-18) transects for June 2004. Concentrations are expressed in mg L^{-1}.

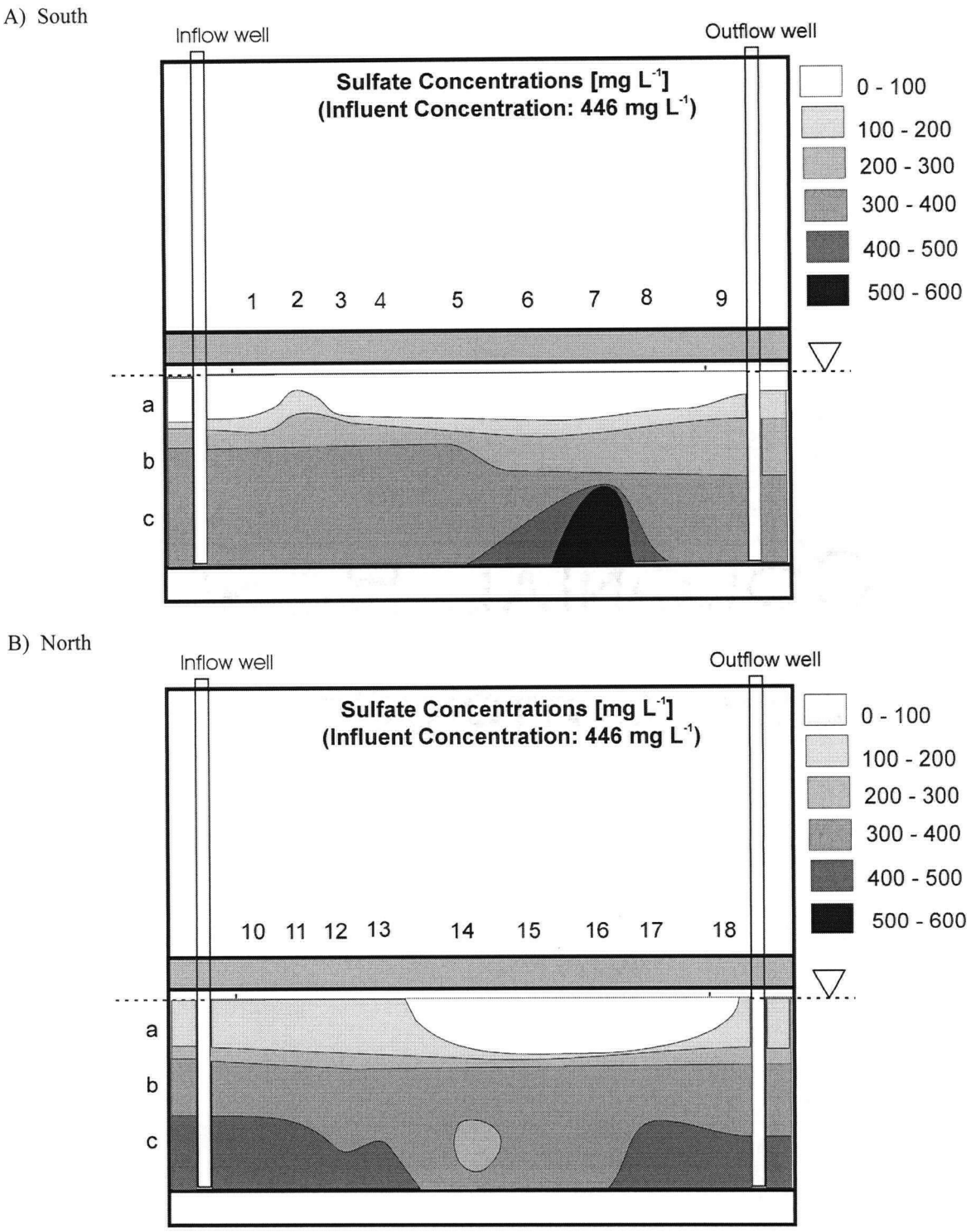

Figure 4.9. Cross-sectional profiles of dissolved SO_4 concentrations along (A) south (well nests 1-9) and (B) north (well nests 10-18) transects for June 2004. Concentrations are expressed in mg L^{-1}.

A)

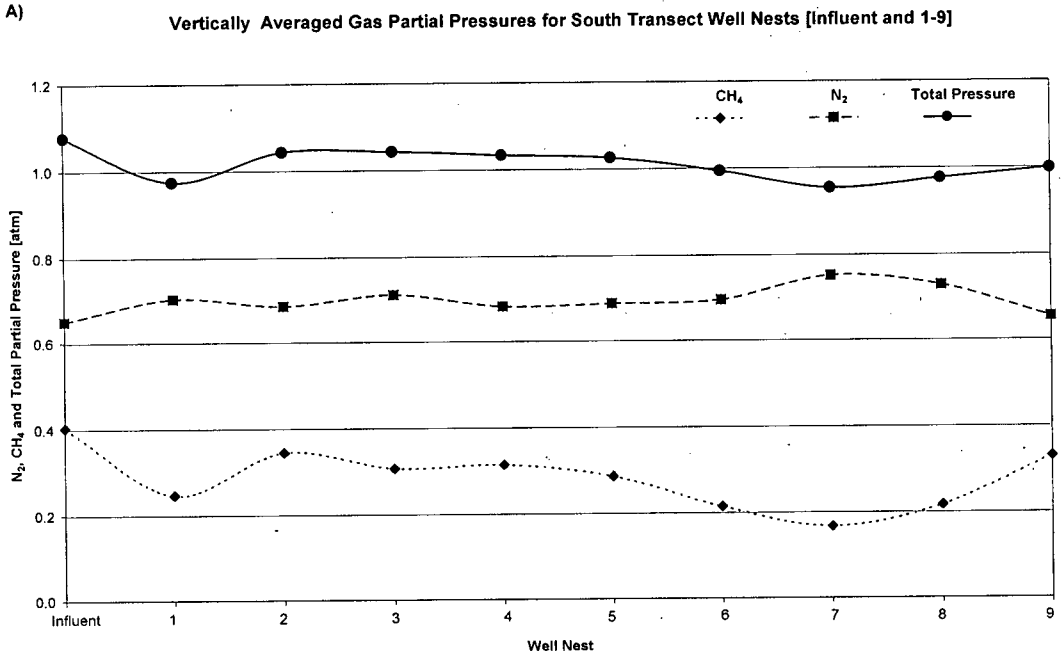

B)

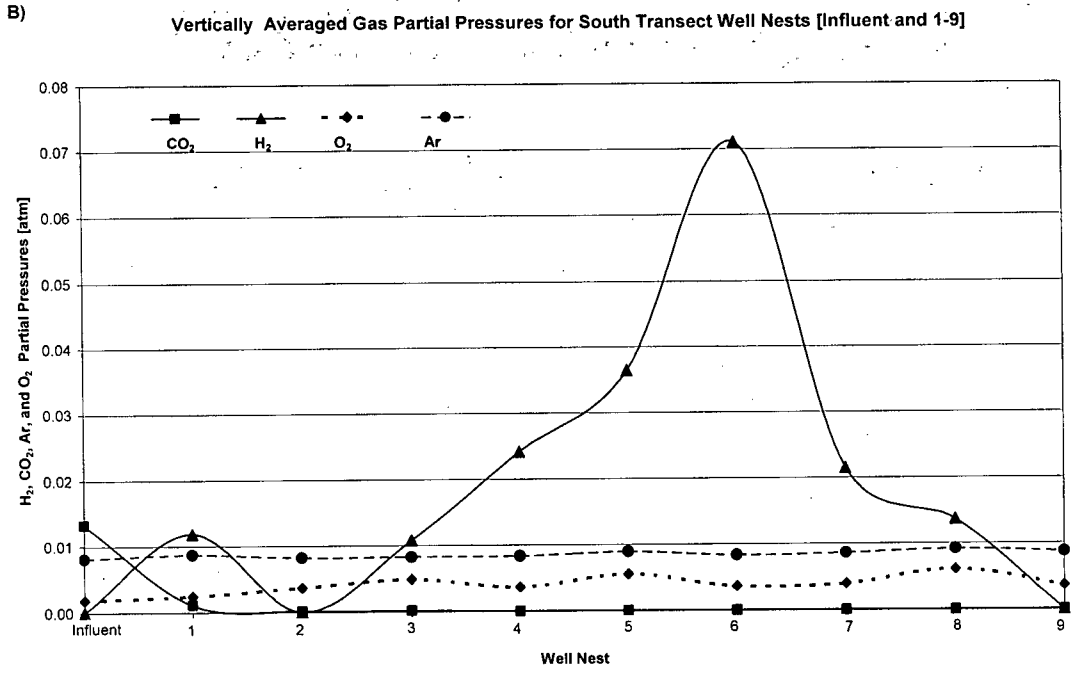

Figure 4.10. Vertically averaged gas partial pressures for A) CH_4, N_2, and Total Pressure, and B) CO_2, H_2, Ar, and O_2 along the south transect (influent, well nests 1 through 8 and well 9).

A)

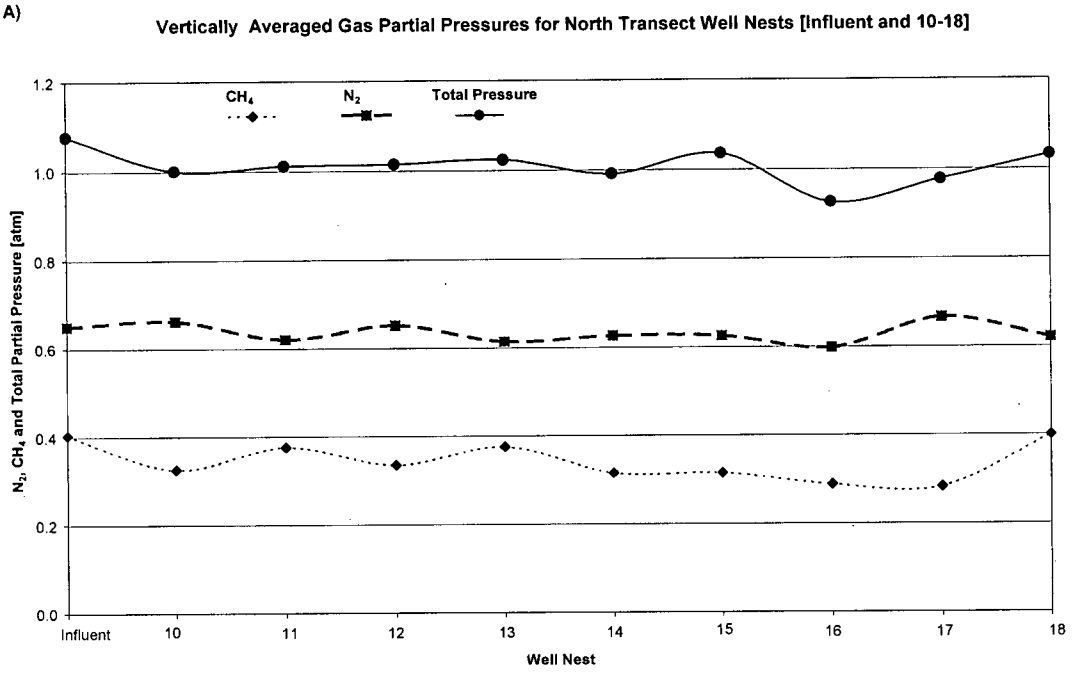

B)

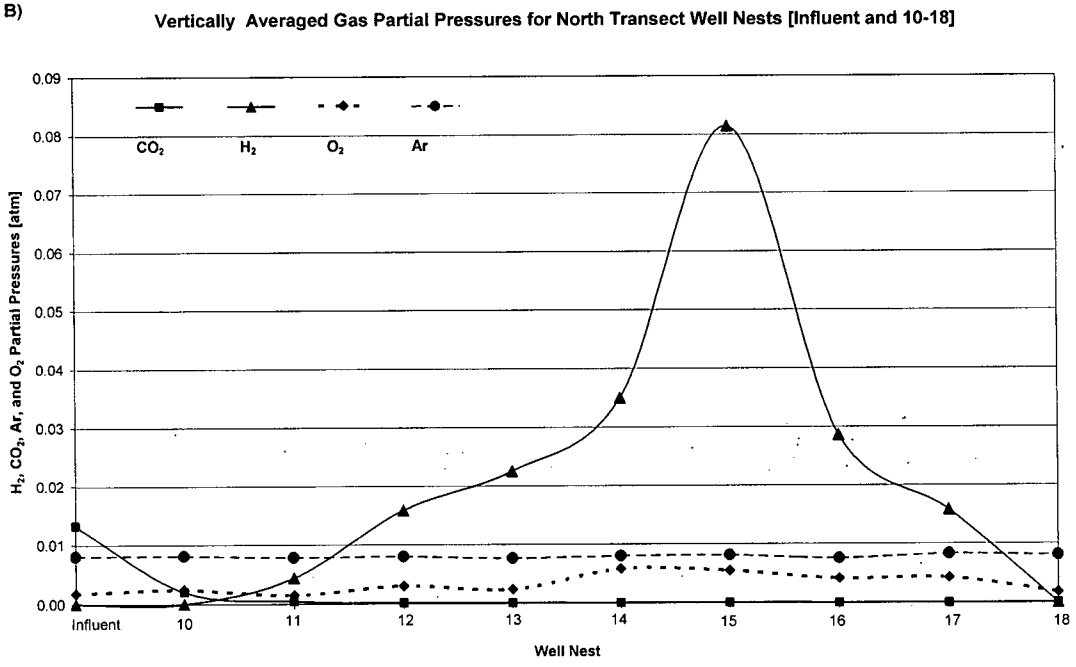

Figure 4.11. Vertically averaged gas partial pressures for A) CH_4, N_2, and Total Pressure, and B) CO_2, H_2, Ar, and O_2 along the south transect (influent, well nests 10 through 17 and well 18).

Chapter V:

Using dissolved gas analysis for investigating the performance of a zero-valent iron/organic carbon permeable reactive barrier at an industrial site

5.1 Introduction

The present study was conducted at a zero-valent iron (Fe^0)/organic carbon pilot PRB at the Columbia Nitrogen site in Charleston, S.C. The contamination scenario at the Columbia Nitrogen site is essentially an acid rock drainage problem. Pyrite and elemental sulfur, which were used at the former phosphate fertilizer plant in the on-site production of sulfuric acid, are present in the subsurface fill material at the site. The pyrite and elemental sulfur undergo a slow but steady oxidation process resulting in the long-term production and release of sulfuric acid. As sulfuric acid is produced, heavy metals (lead, zinc, etc.) and arsenic associated with the pyrite and/or native soils are mobilized. The production of acid and mobilization of metals may conceivably continue for many years at the site. The groundwater has also been reported to have high nitrate (NO_3) levels (4,000 mg L^{-1}) at several sampling locations in the past.

Due to the similarity between the contaminants and PRB treatment materials of the Campbell Mine PRB and the current study, the reactions that have the potential to take place within this PRB can be summarized by section 4.1, equations 1 through 8. Additional metals are targeted for removal in this PRB, and laboratory studies indicate that many metals, including Ag, Cd, Co, Cu, Fe, Ni, Pb, and Zn, are treatable by indirect precipitation resulting from the reduction of sulfate (Waybrant et al., 1995, 1998) (i.e., as a result of equation 1, section 4.1).

In addition to the equations described in section 4.1, if nitrates are present in the groundwater, microbially mediated nitrate reduction may occur within the PRB, and N_2 may be produced by (Robertson et al., 2000):

$$5CH_2O + 4NO_3^- \rightarrow 2N_2 + 5CO_2 + 3H_2O + 4OH^- \quad (5.1)$$

However, chemical reduction of nitrate by Fe^0 is a spontaneous process under acidic conditions (Su and Puls, 2004):

$$NO_3^- + 4Fe^0 + 9H^+ \leftrightarrow NH_3 + 4Fe^{2+} + 3H_2O \quad (5.2),$$

and produces ammonia.

Fe^0 also provides a source of hydrogen for autotrophic denitrification to take place, which is also thermodynamically favourable and may occur by the following reaction (Till et al., 1998):

$$2NO_3^- + 5H_2 \rightarrow N_2 + 4H_2O + 2OH^- \quad (5.3)$$

And by combining reactions 4.4 and 5.3, the following overall process can be described as biological denitrification (Till et al., 1998; Choe et al., 2000):

$$2NO_3^- + 5Fe^0 + 6H_2O \rightarrow N_2 + 5Fe^{2+} + 12OH^- \quad (5.4)$$

Most studies concerning nitrate removal using Fe^0 report ammonia as the final product with few reporting nitrite as an intermediate product (Till et al., 1998; Devlin et al., 2000; Kielemoes et al., 2000). Though N_2 gas formation by equation (5.4) has been suggested as a product of nitrate removal by denitrification, significant measurements of N_2 formation have not been observed (Till et al., 1998; Devlin et al., 2000; Kielemoes et al., 2000).

All reactions described in section 4.1 and this section may lead to the production of gases within the PRB. A significant amount of gas production may induce degassing

and possibly ebullition, which may also affect dissolved gas composition, as described in the previous chapters.

The specific objectives of the current work are outlined in Chapter 1.

5.2 Site Description

Dissolved gas data was collected at the zero-valent iron/organic carbon mixed PRB located at the Columbia Nitrogen site in Charleston, SC (Figure 5.1) in October 2004. This pilot PRB was installed in September 2002 and is monitored by the United States Environmental Protection Agency (EPA). The site is located at a former phosphate fertilizer plant that operated over several decades. The impacted groundwater is currently entering a tidal marsh located immediately down gradient of the site, and adjacent to the Ashley River. The site contains fill material to depths of 12 feet, underlain by native sediments. The fill material is characterized as containing large quantities of fine-grained pyrite cinders. The hydraulic conductivity of the fill material is said to decrease significantly with depth down to 12 ft, presumably reflecting a greater pyrite cinder content with depth. Embedded within the fill material are bricks, chunks of wood, and rocks (e.g. perhaps unspent pyrite) (Ralph Ludwig, personal communication January 7, 2005).

This barrier was constructed to test the performance of the reactive materials for the removal of arsenic and lead, as well as other metals, SO_4, NO_3, and to investigate the acid neutralization potential of the materials. Groundwater is characterized by low pH conditions at much of the site, and in some areas pH values were reported as low as 2. The PRB media consists of 20% zero-valent iron (ZVI) in the form of iron filings, 30% compost derived from leaves and tree clippings, 45% granite pea gravel, and 5%

limestone gravel. Ideally, the PRB would have been constructed down gradient of the source area at the edge of the tidal marsh, but poor accessibility to this area and the significant costs that would result prohibited installation of the pilot PRB at this location (David Smyth, personal communication, 2004). Instead, the PRB was installed directly within the source area to minimize costs, making it difficult to evaluate down-gradient discharge water quality from the PRB.

The PRB dimensions are approximately 26 ft in length, 12 ft in depth and 6 ft in width. Depth to groundwater at the location of the PRB is approximately 4.5 ft. (www.epa.gov/ada/research/waste/research_01.pdf). Two transects (A and B) consisting of eight bundle wells are located perpendicular to the PRB in the direction of groundwater flow (see Figure 4.2), with three of those bundle wells per transect installed within the PRB. Groundwater sampling of the well bundles at the site was conducted for the present study. Each well bundle consists of five intervals of 1/4-inch tubing labelled A, B, C, D, and E, respectively, centered on a 1/2-inch PVC stalk which is open ended at a depth of 12.5 ft bgs and serves as sampling point F (David Smyth, personal communication September 14, 2004).

Groundwater flow at the site has been difficult to determine, due to the relatively flat horizontal hydraulic gradient. The site elevation is sea level (1 atm).

5.3 Dissolved Gas Sampling

The sampling conducted took place within the Fe^0/organic carbon mixed PRB October 4 through October 7, 2004. Monitoring points were sampled at well bundles 1-18 (Figure 5.2). Each well bundle interval was attempted, and samples were collected at only those intervals that yielded water (typically intervals B through F). The A interval

(i.e., most shallow interval) appeared to be dry at most well bundles, and therefore, samples could not be collected. Also, several monitoring points did not yield water at a rate of at least 25 ml min^{-1}, so samples were not collected at these points due to a lack of such low pumping rate capabilities. The 250 ml amber glass sample collection bottles were flushed for 15 to 45 minutes, depending on the flow rate achieved at the well. Samples were collected at low flow rates (30 ml min^{-1} to 150 ml min^{-1}), and typically, the sampling rate was the maximum that the location could yield for the necessary flushing, while preventing bubbles from appearing in the sample line. After each bottle had been sufficiently flushed and capped with a septum cap, the bottle was kept cool and dark until analysis could be conducted 2- to- 3 weeks following collection at UBC.

5.4 Results and Discussion

5.4.1 Spatial Distribution of Dissolved Gases

Cross sections of the dissolved gas data collected in the saturated zone in October 2004 along transects A and B through the PRB test cell are shown in Figures 5.3 – 5.6 for N_2, Ar, CH_4, and CO_2, respectively, and are expressed as aqueous concentrations in mg L^{-1}. N_2 concentrations are near atmospheric at the water table, and become depleted with depth in both transects A and B. Nitrogen depletion is only slightly greater within the PRB at depth along transect B than in the surrounding aquifer, but in general, N_2 concentrations do not change in the horizontal direction, but only vary noticeably in the vertical direction. Ar concentrations mimic the pattern observed and discussed regarding the N_2 concentrations. Again, Ar concentrations are only slightly lower within the PRB than in the surrounding aquifer at depth. The lack of N_2 enrichment within the PRB suggests that, if NO_3 is still a contaminant of concern at the site, the reduction of NO_3

occurs by chemical reduction (equation 5.2), which results in the generation of ammonia (NH_3), which has a high solubility (i.e., Henry's Law constant ($K_{H_{NH_3}}$) $10^{1.77}$ M atm^{-1}; USGS, 1991) and is not expected to cause degassing.

CH_4 concentrations are limited primarily to within and below the PRB in both transects A and B (Figure 5.5), and concentrations as high as 23- to- 24 mg L^{-1} are observed. Methane concentrations appear to increase with depth within the PRB along both transects, and elevated concentrations do not appear down gradient of the PRB past well nests 13 (transect A) or 14 (transect B).

Dissolved CO_2 concentrations (Figure 5.6) are very low within the PRB (generally less than 10 mg L^{-1}), while concentrations up and downgradient of the PRB are very high in both transects, with concentrations ranging from 100- to- 1,000 mg L^{-1} in the shallow portion of the aquifer (upper 3- to 5- feet of the aquifer) and concentrations exceeding 1,000 mg L^{-1} at depth. Though a detailed description of the fill material has not been provided, the high dissolved CO_2 outside of the PRB can likely be attributed mainly to carbonate dissolution due to the acidic conditions at the site. Within the PRB, the Fe^0 has created a very reducing, high pH environment, as will be discussed in section 5.4.2, and therefore CO_2 takes the form of bicarbonate and is not detected.

H_2 concentrations were not detected in any of the samples analyzed, but are probably the most sensitive to sample storage and are therefore unreliable. Detectable H_2 concentrations would be expected in a Fe^0 barrier, due to the corrosive action of water, however it is also likely that H_2 is rapidly consumed within the barrier by microbial processes, such as denitrification, sulfate reduction, and methanogenesis, which are likely to take place within the PRB. During storage H_2 could have been consumed within the

samples by microbial processes or may have reacted with oxygen as a result of atmospheric contamination. Dissolved oxygen concentrations using CHEMets kits (not shown) are very low, and average approximately 0.3 mg L^{-1} throughout the site, with a maximum concentration of 1 mg L^{-1} at a few locations (7B and 16E). Higher dissolved oxygen concentrations were reported using the GC, likely as a result of atmospheric contamination due to the duration of sample storage, as explained in Chapter 2. Ar and N_2 data suggests that this atmospheric contamination was not of great magnitude, as Ar and N_2 are still observed with significant depletion at depth.

5.4.2 Spatial Distribution of Data Provided by the EPA

Sulfate (SO_4), Ammonia-N (NH_4-N), Nitrate-Nitrite-N (NO_3-NO_2-N), and Chloride concentrations, were collected October 6, 2004 and analyzed by the EPA. Data for alkalinity and pH were also collected by the EPA and provided to this study to aid in interpreting the dissolved gas data.

SO_4 concentrations, shown in Figure 5.7, are very high at the site both up and downgradient of the PRB, with concentrations up to 69,900 mg L^{-1} (well 16F) along transect B and 62,700 mg L^{-1} (well 11F) along transect A. Similar to other parameters, SO_4 concentrations are much greater at depth within the aquifer (greater than 5 feet below the water table), and are an order of magnitude lower at shallow depths. Within the PRB, SO_4 concentrations are lower than the surrounding aquifer, with concentrations of less than 100 mg L^{-1} in the shallow portion of the PRB along both transects.

NH_4-N concentrations, shown in Figure 5.8, increase with depth along both transects, with concentrations less than 10 mg L^{-1} at shallow depths and concentrations at depths greater than approximately 10 feet exceeding 100 mg L^{-1}. NH_4-N concentrations

do not change significantly in the horizontal direction at the site. NH_4-N, as explained in the introduction, is a product of the chemical reduction of nitrate by Fe^0 (equation 5.2), however, this data set shows that NH_4 is distributed fairly evenly throughout the aquifer and barrier in the horizontal direction. Further information is not available that could explain the NH_4 presence and trend. Because it is not only found within the PRB, it may have been an original contaminant created during fertilizer production, in which case it will not be affected by the PRB due to its reduced state.

The EPA provided additional data, including Nitrate-Nitrite-N (NO_3-NO_2-N) data and chloride data, however they are not shown here. NO_3-NO_2-N data was generally below the detection limit of 0.1 mg L^{-1}, and had a maximum concentration of 5 mg L^{-1} at well 18F. Nitrate had been reported as a contaminant in the past at this site, but appears to no longer be a concern, as it is generally non-detectable. Denitrification products were not detected either. Because historical NO_3 data was not provided for this study, more discussion cannot be made regarding this contaminant. Chloride data follows a similar trend to that of NH_4, with lower concentrations near the surface (up to 100 mg L^{-1} in shallow wells) and higher concentrations at depth (1,000 to 2,000 mg L^{-1}). Chloride is present as a result of the site location being adjacent to tidal marsh. Unfortunately, tidal and saline wedge influences have not been well characterized at this site, so the effects on the flow field are uncertain. Chloride concentrations are fresh to slightly brackish to depths reported for this study (i.e., 12 feet).

The pH distributions (Figure 5.9) show that pH levels range from 2- to- 4 both up and downgradient of the PRB, while pH levels within the PRB range from 4 to 10 along both transects. Alkalinity data (not shown) shows the opposite trend to that of dissolved

CO_2 concentrations (Figure 5.6) with high alkalinity values within the PRB ranging from 260 to 5,800 mg L^{-1} (as $CaCO_3$), and low values both up and downgradient of the PRB. Because hydroxyl ions are likely to form a large portion of the alkalinity generated within a Fe^0 PRB, bicarbonate values were obtained to further investigate the reactions occurring within the barrier.

By combining the CO_2 concentrations with the pH data provided, estimates of HCO_3^- and CO_3^{2-} could be made using the following thermodynamic equations (Stumm and Morgan, 1996):

$$CO_{2(aq)} + H_2O = H^+ + HCO_3^- \qquad \log K = -6.347 \qquad (5.5),$$

and

$$HCO_3^- = H^+ + CO_3^{2-} \qquad \log K = -10.321 \qquad (5.6)$$

assuming an approximate groundwater temperature of 299 K for determining the equilibrium constant (K value). When comparing the mol L^{-1} of CO_2 outside of the barrier to the mol L^{-1} concentrations calculated for HCO_3 and CO_3 within the barrier (data not shown), it appears that no significant increase in molar carbonate concentrations are found within the barrier relative to outside the barrier. Additional bicarbonate generated within the PRB during SO_4 reduction (equations 4.1) and methanogenesis would likely precipitate within the barrier as calcite or siderite, however, the lack of higher molar concentrations of carbonate within the PRB may indicate the barrier is primarily reducing sulfate by reaction 4.2, or abiotically. Microbial data, or a more complete data set of the cation chemistry would be required for further discussion.

5.4.3 *Flow Paths and Relative Residence Times*

The horizontal gradient at the Columbia Nitrogen site has been reported as very small, and the dissolved gas data seems to support the idea that horizontal flow towards the tidal marsh is not significant. The presence of high CH_4 concentrations (near the solubility limit) limited to the PRB suggests that residence times are long. One would expect some methane to be transported downgradient of the PRB if flow was significant in the horizontal direction; however, this is not the case. However, reoxidation of CH_4 (reactions 4.7 and 4.8, section 4.1) on the tidal marsh side of the PRB could also explain its absence. Oxygen is not present in the groundwater, but SO_4 is present in significant amounts, suggesting this could be the oxidizing agent. The high pH and low CO_2 concentrations are found within the PRB only, also suggesting flow towards the downgradient side of the PRB is insignificant. However, the PRB was placed in the source zone, indicating acidic conditions may continue to persist downgradient, and complicating data interpretation. A number of reactions may be taking place immediately downgradient of the PRB in this setting. Likely, desorption of H^+ ions (i.e., deprotonation) from the fill material is causing the pH to return to low levels, and therefore increasing the CO_2. One would, however, expect this low pH front to be displaced downgradient of the PRB after 2 years of operation, if significant flow were occurring.

5.4.4 *Degassing and Ebullition*

N_2 and Ar concentrations appear near atmospheric at the surface and decrease with depth throughout the site. N_2 and Ar depletion, and therefore degassing are evident at the site, though the process is not limited to the PRB. Outside of the PRB the very low

pH conditions and generation of CO_2 gas may result in degassing and depletion of N_2 and Ar in the aquifer. The lack of depletion at the watertable is likely due to recent recharge entering the aquifer and atmospheric exchange at the water table surface. N_2 and Ar concentrations do not vary in the horizontal direction, and are thus similar within and outside (i.e., both up and down gradient) of the PRB. This indicates that degassing is not significantly induced by reactions within the PRB, although high CH_4 is observed there. Instead, it appears that the high CO_2 within the aquifer takes the form of bicarbonate within the PRB, due to the high pH values (up to 9.8 within the PRB; data collected by EPA, 2004) measured. The net effect of the CH_4 production and bicarbonate formation does not increase the total pressure of the system, and therefore does not lead to degassing and ebullition at the site. Average partial and total pressures for wells inside and outside the PRB are summarized in table 5.1, and support this idea. The increase in the average CH_4 partial pressure from 0.11 atm outside of the PRB to 0.76 atm within the PRB is approximately equal to the decrease in the average CO_2 partial pressure from 0.52 atm outside of the PRB to 0.02 atm within the PRB. The average N_2 partial pressure within the PRB (0.36 atm) is only slightly depleted from the average partial pressure outside of the PRB (0.53 atm).

5.4.5 PRB Treatment

Based on the dissolved gas signature of the water, the PRB does not appear to have significant horizontal flow. CH_4 concentrations are high (but not high enough to induce degassing and ebullition), indicating that transport may be limiting removal of SO_4 within the PRB. Therefore, precipitation of metals and reduction of other contaminants of concern (i.e., SO_4) are likely limited by long residence times within the

barrier. Supporting data other than what was reported from the EPA to aid in interpreting the dissolved gas data is not available. Information regarding the flow field and tidal effects; historical data of cations, anions, and pH; and the fill material and native sediments would certainly provide a better background for interpretation, however, such data was not made available for this work. The data is inconclusive and does not allow the determination of reaction rates and treatment success.

5.5 Summary and Conclusions

N_2 and Ar concentrations appear near atmospheric at the surface, and decrease with depth throughout the upgradient and downgradient aquifer/fill material and PRB. N_2 and Ar depletion, and therefore degassing are evident at the site, but the process is not significantly induced by reactions occurring within the PRB. Despite the lack of N_2 and Ar depletion attributed to PRB, the dissolved gas data set suggests that residence times are long within the (Fe0)/organic carbon pilot PRB. The long residence times and limited flow have allowed for suitable conditions for methanogensis to develop throughout the PRB. The net effect of the CH_4 production and CO_2 partitioning to bicarbonate within the PRB does not increase the total pressure of the system, and therefore does not lead to degassing and ebullition. The lack of degassing and ebullition from the PRB may also suggest that CH_4 production is limited, or that CH_4 is consumed by sulfate reduction. Sulfate concentrations are still quite high within the PRB, making this a possibility. Overall, the lack of available background information at this site limited the dissolved gas data interpretation.

5.6 References

Choe, S., Y. Chang, K. Hwang, J. Khim, 2000. Kinetics of reductive denitrification ny nanoscale zero-valent iron. *Chemosphere*, 41, 1307-1311.

Devlin, J. F., R. Eedy, B. J. Butler 2000. The effects of electron donor and granular iron on nitrate transformation rates in sediments from a municipal water supply aquifer. *J. Contam. Hydrol.*, 46,-81-97.

Kielemoes, J., P. De Boever, W. Verstraete, 2000. Influence of denitrification on the corrosion of iron and stainless stell powder. *Environ. Sci. Technol.*, 34, 663-671.

Robertson, W. D., D. W. Blowes, C. J. Ptacek, and J. A. Cherry, 2000. Long-term performance of in situ reactive barriers for nitrate remediation. *Ground Water*, 38, 689-695.

Stumm, W. and J. J. Morgan, 1996. *Aquatic Chemistry, Chemical Equilibria and Rates in Natural Waters, Third Edition*; John Wiley & Sons, Inc.: New York, p 472 and p 474.

Su, C. and R. W. Puls, 2004. Nitrate reduction by zerovalent iron: Effects on Formate, oxalate, citrate, chloride, sulfate, borate, and phosphate. *Environ. Sci. Technol.*, 38, 2715-2720.

Till, B. A., L. J. Weathers, P. J. Alvarez, 1998. Fe(0)-Supported autotrophic denitrification. *Environ. Sci. Technol.*, 32, 634-639.

USGS, 1991. User's Manual for WATEQ4F, with revised thermodynamic database and test cases for calculating speciation of major, trace and redox elements in natural waters, Open-File Report 91-183, 189 pp. plus diskette

Waybrant, K. R., D. W. Blowes, C. J. Ptacek, 1995. Selection of reactive mixtures for the prevention of acid mine drainage using in situ porous reactive walls. Proc. Sudbury '95, Mining and the Environment, CANMET, Ottawa, ON vol. 3, pp. 945-953.

Waybrant, K. R., D. W. Blowes, C. J. Ptacek, 1998. Selection of reactive mixtures for use in permeable reactive walls for treatment of mine drainage. *Environ. Sci. Technol.*, 32 1972-1979.

Tables

Wells	Average Concentration in Water					
	Partial Pressure CH_4	*Partial Pressure CO_2*	*Partial Pressure Ar*	*Partial Pressure O_2*	*Partial Pressure N_2*	*Total Pressure*
Barrier Wells	0.760	0.025	0.004	0.024	0.360	1.17
Outside Wells	0.106	0.520	0.007	0.007	0.536	1.18
All Wells	0.346	0.290	0.006	0.030	0.492	1.16

Table 5.1. Average partial and total pressure of gases measured within and outside of the barrier, and of all wells (i.e., barrier and outside barrier wells).

Figures

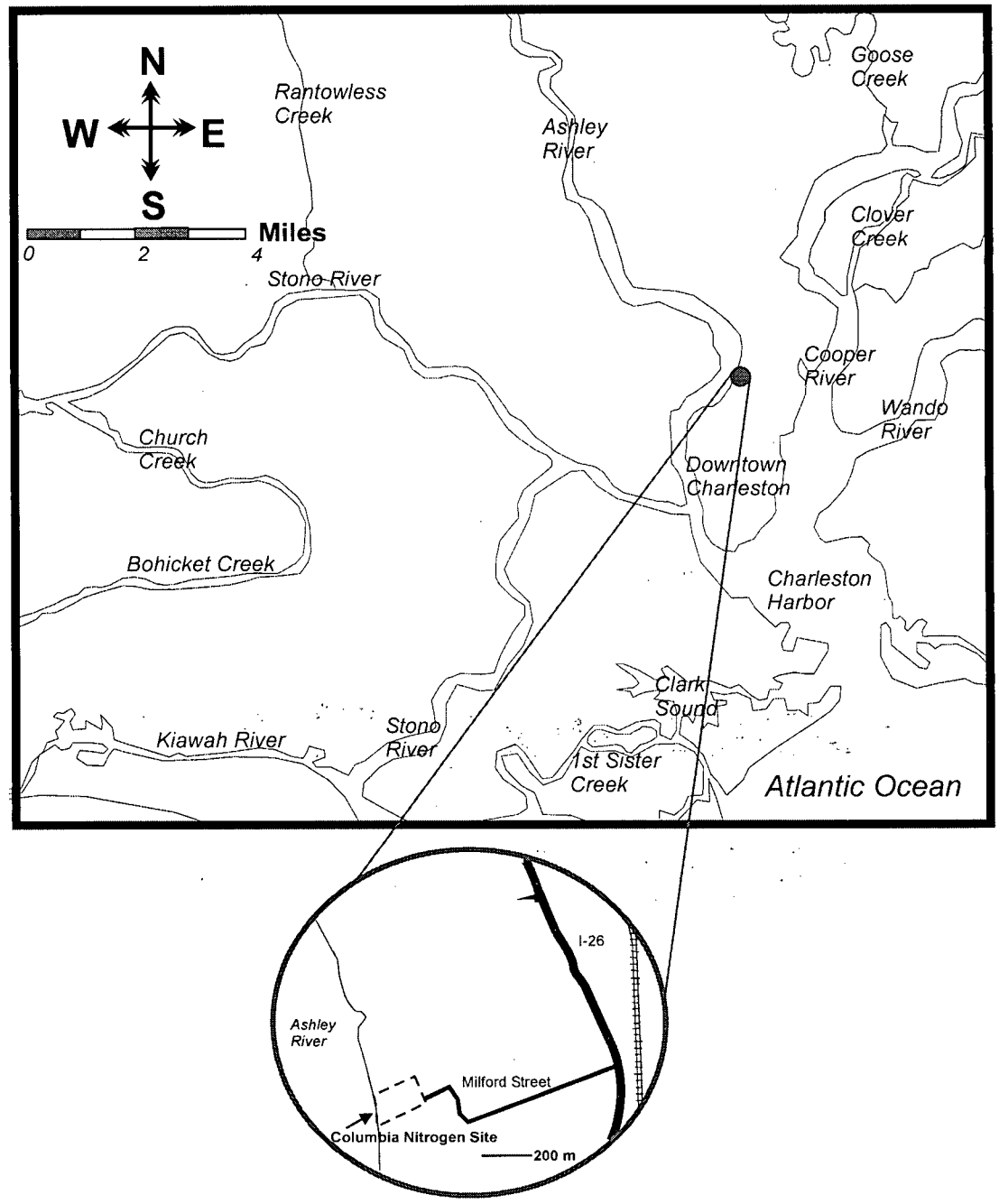

Figure 5.1. Map of region surrounding Charleston, S.C., and blow up of the Columbia Nitrogen Site, just north of Downtown Charleston.

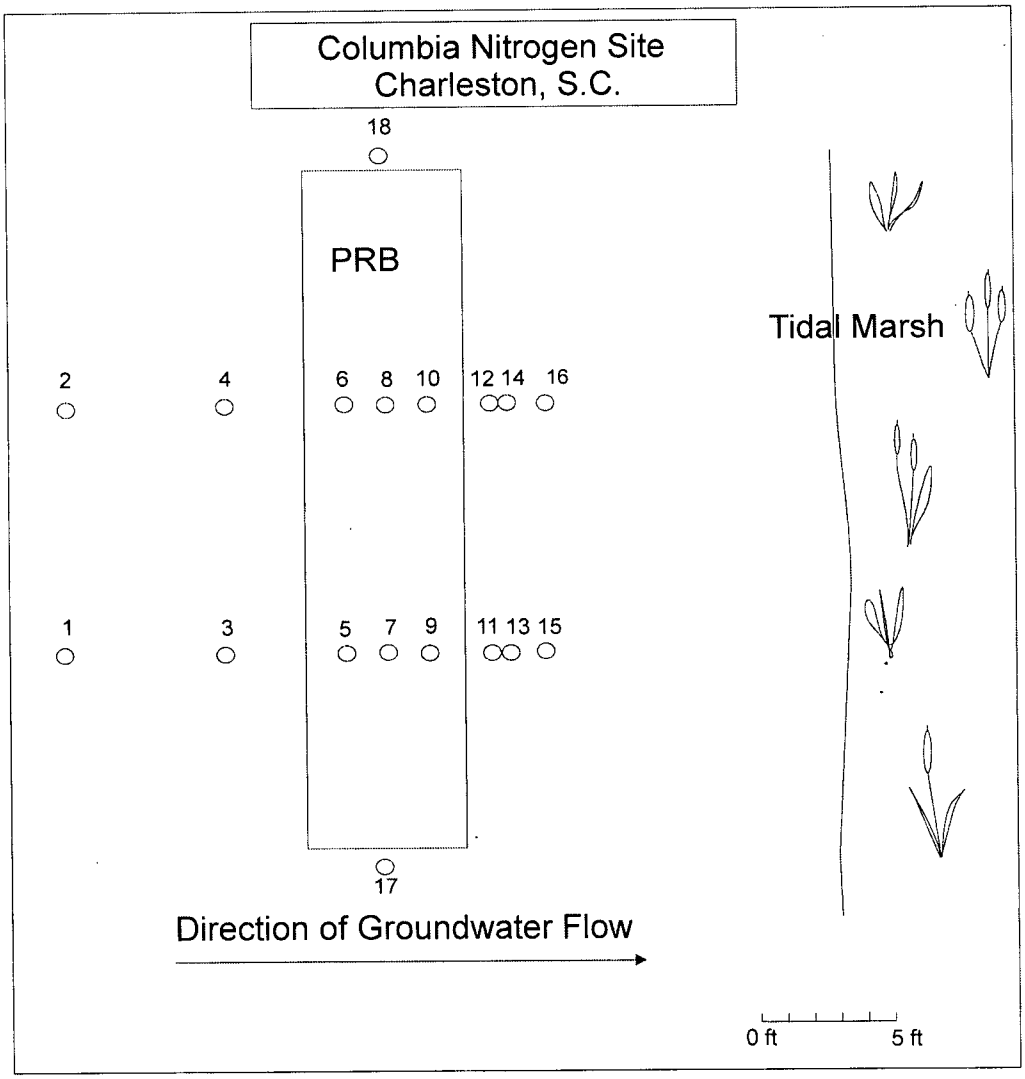

Figure 5.2. Plan view of the Columbia Nitrogen Site in Charleston, S.C.

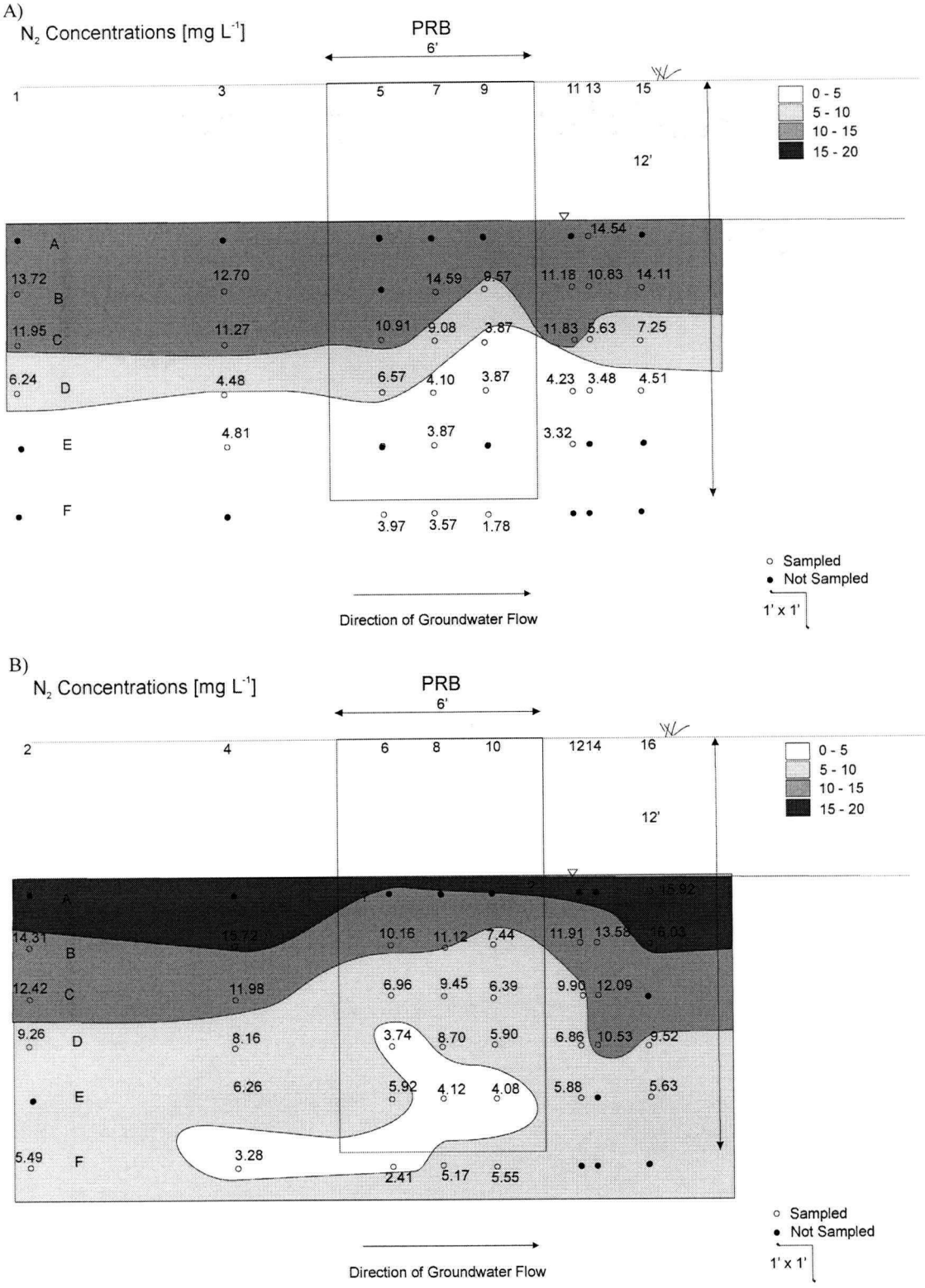

Figure 5.3. Cross-section of dissolved N_2 concentrations along transects A) A (odd well nests 1 through 15) and B) B (even well nests 2 through 16). Data are expressed in mg L^{-1}.

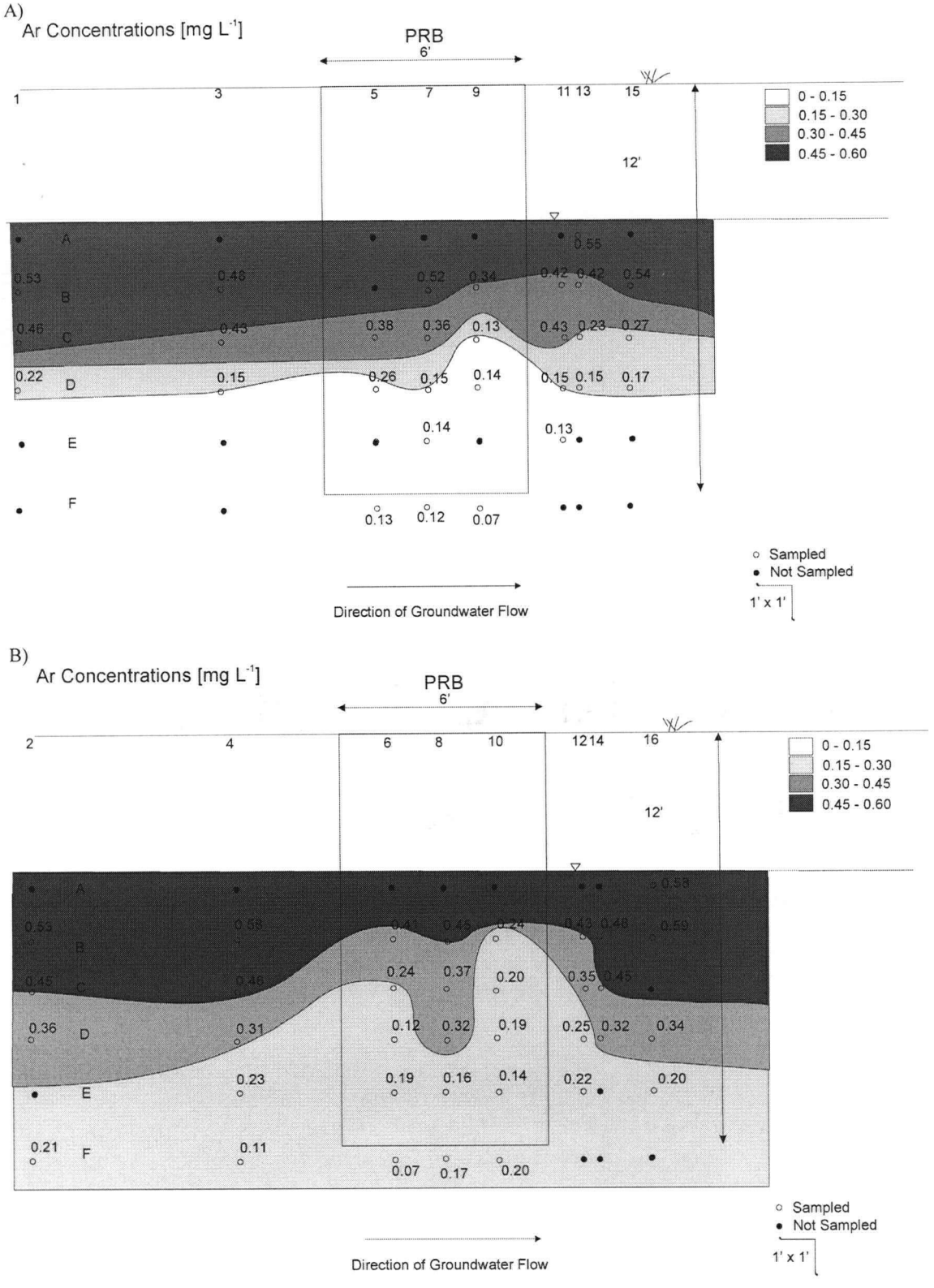

Figure 5.4. Cross-section of dissolved Ar concentrations along transects A) A (odd well nests 1 through 15) and B) B (even well nests 2 through 16). Data are expressed in mg L^{-1}.

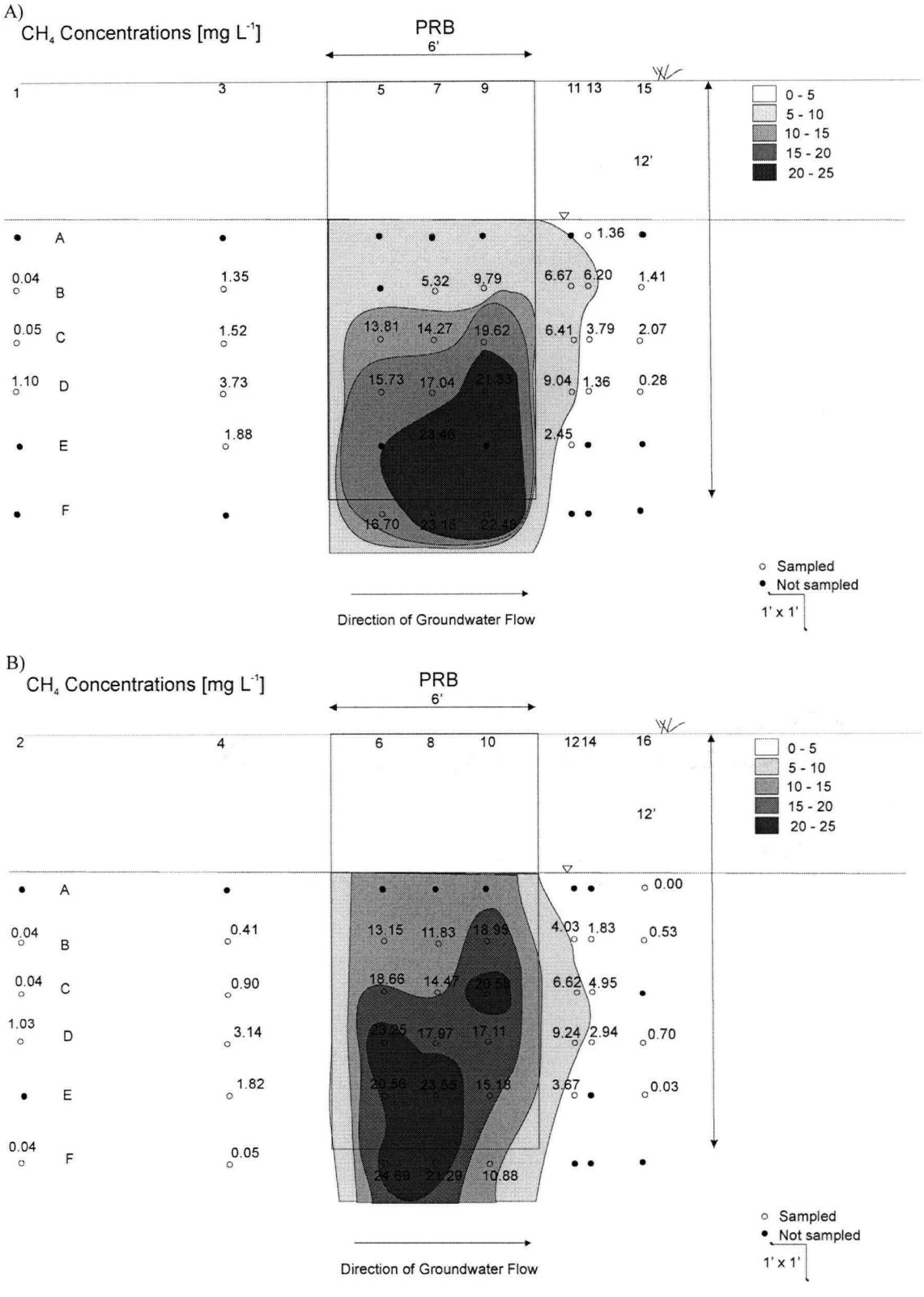

Figure 5.5. Cross-section of dissolved CH_4 concentrations along transects A) A (odd well nests 1 through 15) and B) B (even well nests 2 through 16). Data are expressed in mg L^{-1}.

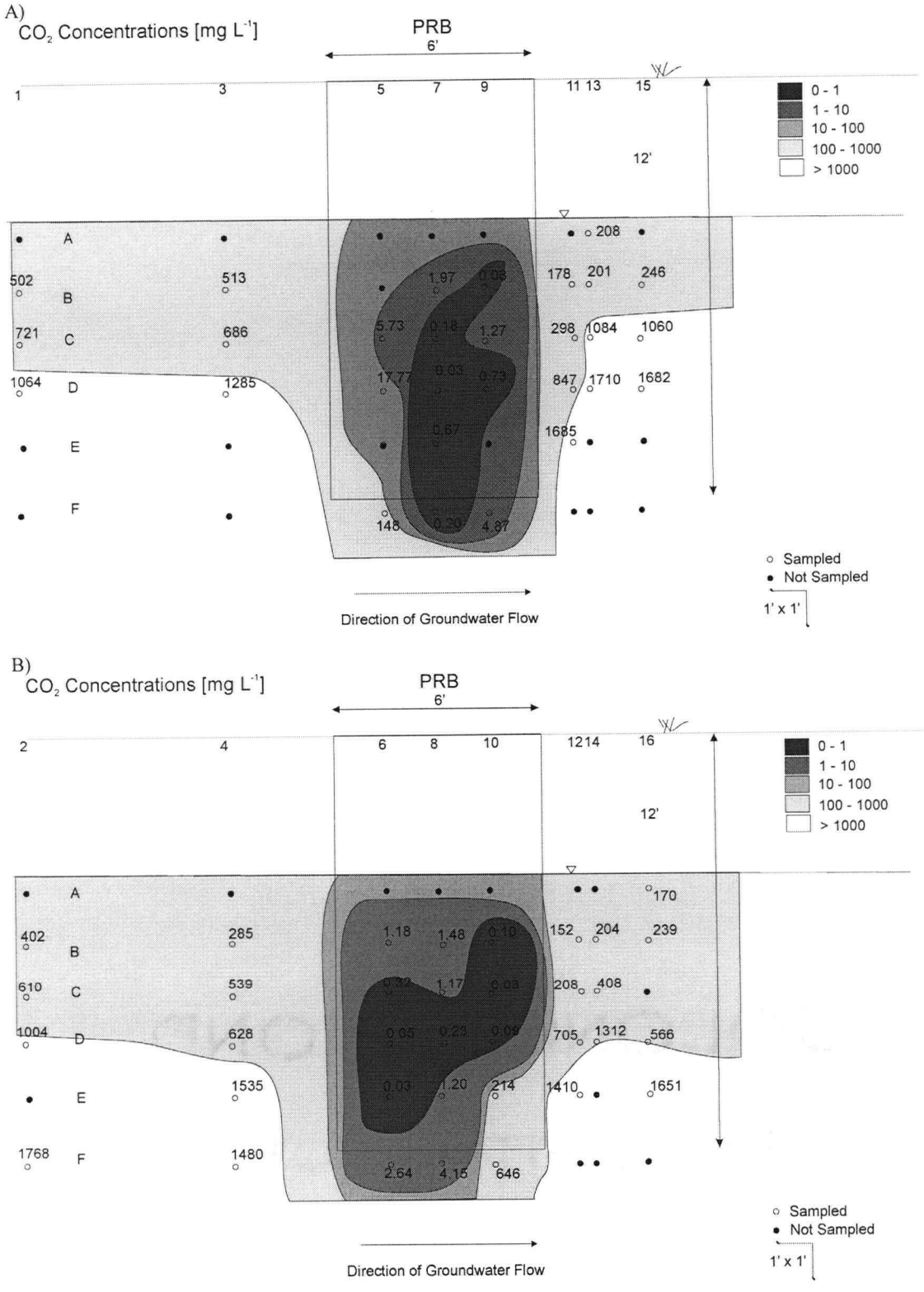

Figure 5.6. Cross-section of dissolved CO_2 concentrations along transects A) A (odd well nests 1 through 15) and B) B (even well nests 2 through 16). Data are expressed in mg L^{-1}.

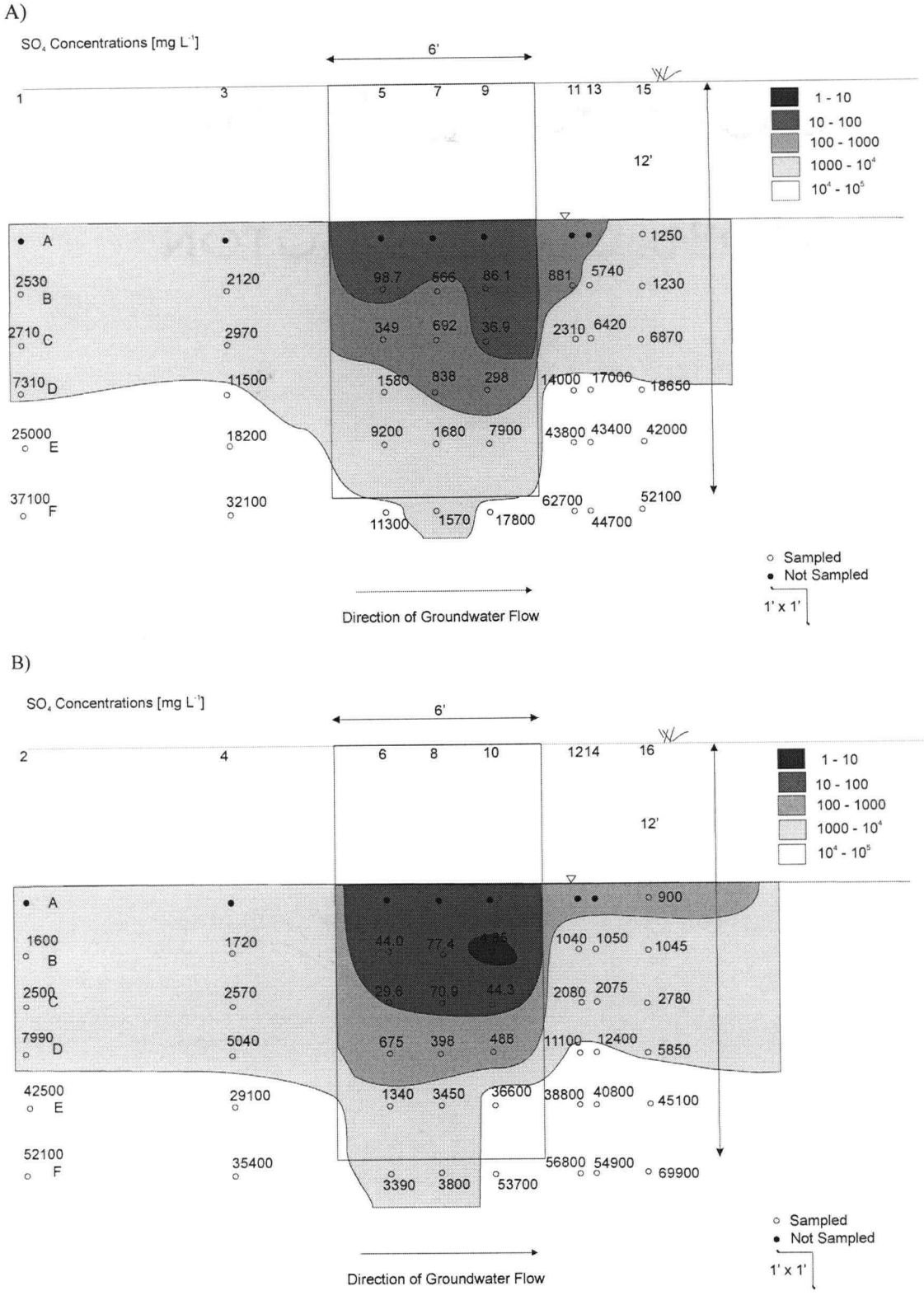

Figure 5.7. Cross-section of dissolved SO_4 concentrations along transects A) A (odd well nests 1 through 15) and B) B (even well nests 2 through 16). Data are expressed in mg L^{-1} (Data are provided by EPA, 2004).

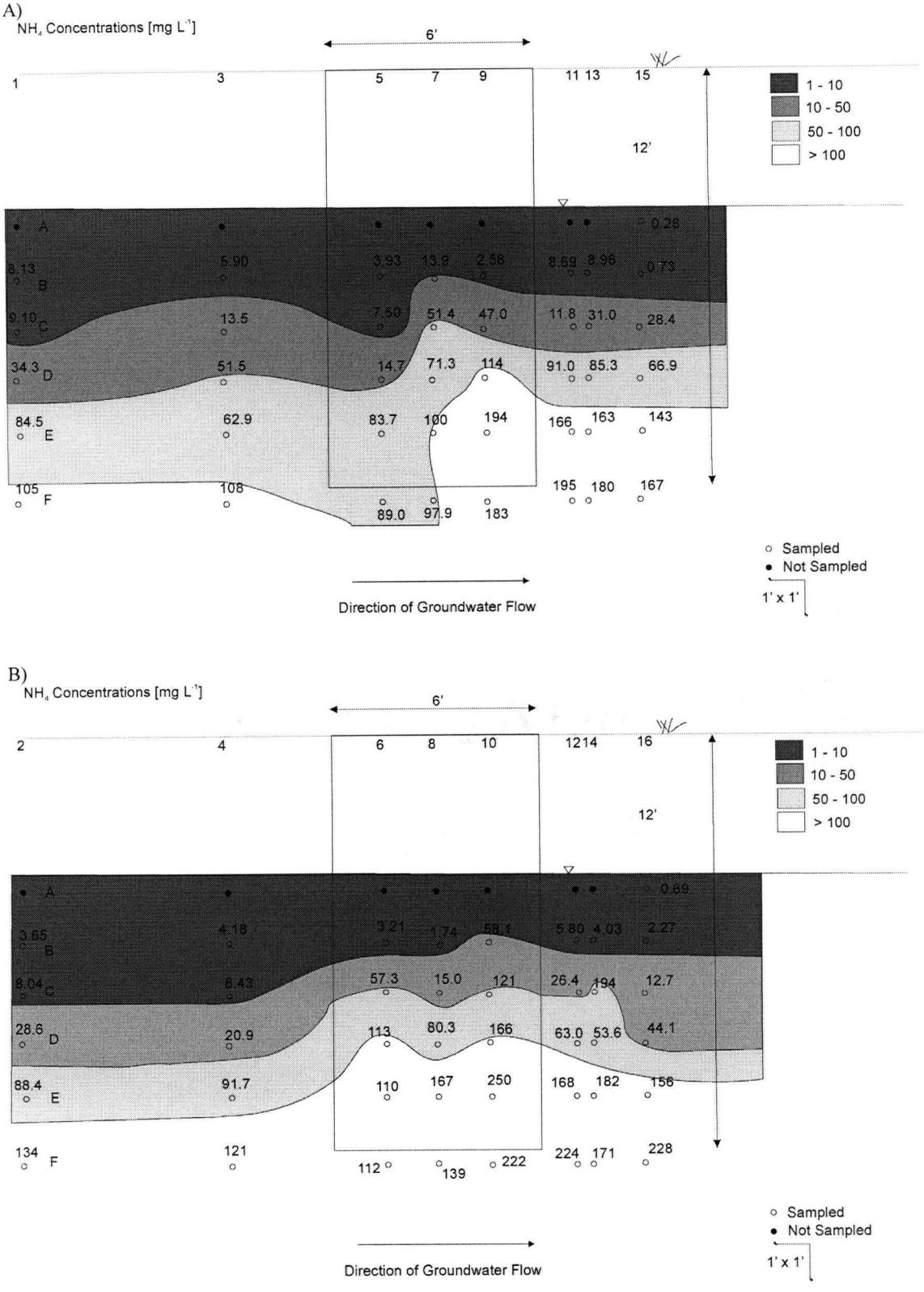

Figure 5.8. Cross-section of dissolved NH_4-N concentrations along transects A) A (odd well nests 1 through 15) and B) B (even well nests 2 through 16). Data are expressed in mg L^{-1}. (Data provided by the EPA, 2004).

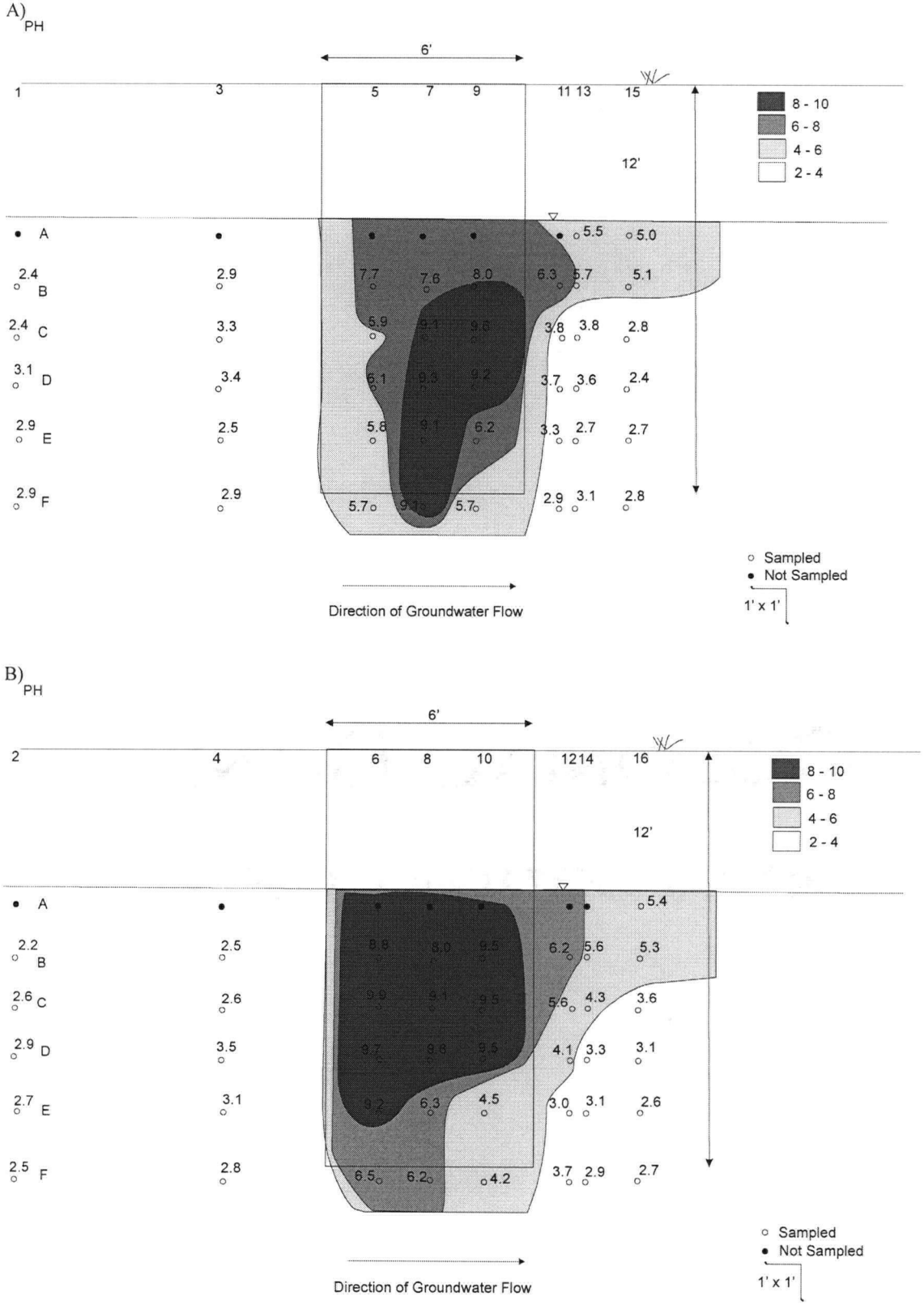

Figure 5.9. Cross-section of pH levels measured along transects A) A (odd well nests 1 through 15) and B) B (even well nests 2 through 16). (Data provided by the EPA, 2004).

Chapter VI: Conclusions

Dissolved gas sampling and analysis were conducted at three PRB sites designed for the treatment of acid mine drainage: the Nickel Rim Mine Organic Carbon PRB (Site I), the Campbell Mine Zero-Valent Iron (Fe^0)/ Organic Carbon Test Cell PRB (Site II), and the Columbia Nitrogen Fe^0/ Organic Carbon Mixed PRB (Site III). The objectives of this work include the use of dissolved gas analysis to investigate the performance of permeable reactive barriers, specifically, to test if the gas composition can be used to investigate, confirm and possibly quantify chemical and physical processes occurring within PRB systems.

Site I was unique in that the physical setting was well understood, and there was an extensive monitoring network with over 8 years of data provided to aid in understanding the dissolved gas data set. The residence times within the PRB at Site I had been determined previously, and the flow field was well understood. The PRB at Site II was installed during August 2002, and most of the PRB was thought to have very short residence times. The Columbia Nitrogen Fe^0/ Organic Carbon Mixed PRB at Site III was installed September 2002, and the flow field there was initially not well understood. Residence times were thought to be quite long, but had not previously been determined. Though the three sites considered in this study were all PRBs with similar contaminants, the physical setting and background chemistry differed greatly, causing the outcome and benefit of the analysis to be very different for each situation.

Dissolved gas data is particularly useful if residence times in the PRB are sufficiently long to allow gas production and degassing. The data set from Site I demonstrates that degassing does occur and that reaction processes can significantly alter

the gas composition of the pore water while passing through the barrier. In this case dissolved gases provide information on both reaction and transport processes. Dissolved gas data allowed us to estimate the ratio of organic carbon consumption by the dominant TEAPs and proved that methanogenesis is insignificant in comparison to sulfate reduction. In addition, it was possible to delineate zones of preferential flow, confirming previous findings by Benner et al. (2002). A large supporting data set allowed for the dissolved gas data to be incorporated into long-term reactive transport modeling of the site, providing additional information regarding the long-term treatment material consumption within the PRB. MIN3P simulations provided strong evidence that degassing and ebullition are likely significant processes occurring within the PRB.

If residence times are short, the value of dissolved gas data lies primarily in its use as a transport tracer. At Site II, a zone of low flow could be identified within the PRB. The gas composition in this zone could be explained by recharge through the clay cap and into the PRB, though these observations could also be explained by ingress of atmospheric gases due to diffusion from the unsaturated zone, and/or entrapment of atmospheric gases caused by water table fluctuations.

If residence times are long, the value of dissolved gas data lies primarily in its use as a reaction tracer. At Site III, the strong resemblance of water composition upgradient and downgradient of the PRB suggests that residence times are long and that there is little flow through the PRB. Although significantly elevated methane concentrations have been observed within the PRB, dissolved N_2 and Ar concentrations do not show significant trends in the horizontal direction through the aquifer and PRB. These data suggest that gas production and reaction rates may be relatively insignificant in this

system, although it has to be noted that CO_2 initially present in the system or produced by sulfate reduction is predominantly converted to bicarbonate in this PRB, and may therefore inhibit degassing and accounting for sulfate reduction. Very little can be said with respect to sulfate reduction in this barrier. The horizontal gradients at the site have not been well characterized, making it difficult prove or disprove dissolved gas data interpretation.

Although dissolved gas analysis answer all of the questions outlined in the objectives for each site, several generally applicable conclusions can be drawn from this study.

1. Degassing does leave a signature within and downgradient of a PRB if residence times are sufficiently long relative to reaction rates to allow gas production and degassing.
2. The gas composition was most useful as a proxy for residence times at Sites I and II. At Site I, dissolved gas data could be compared to results from previous tracer studies conducted by Benner et al. (2002), confirming findings on zones of preferential flow. At Site II, residence times were short, and the lack of a degassing signature in the water provided insight into the zones of preferential flow. To some extent the gas composition was useful as a tracer at site III, by indicating that all residence times were long.
3. Dissolved gas data could only be used to determine treatment material consumption attributed to each reaction process at Site I. The organic carbon treatment material consumption could be described using two overall reactions.

The Fe^0/organic carbon mixed PRBs of Sites II and III proved to be a system with too many variables for dissolved gas analysis to be conclusive.

4. Dissolved gas data can be used to determine rates of the reaction processes occurring within the PRB for certain systems, if residence times can be determined from groundwater flow modeling. Site I was the only PRB system where this could be employed, using a 4-gas degassing model and a reactive transport model.
5. The degree of degassing does provide some indication as to whether or not ebullition is occurring. Ebullition was observed at Site I, and dissolved gas analysis and reactive transport modeling indicate that it may be an important process. At Site II and Site III, limited degassing within the PRB indicated that ebullition was not significant.
6. The success and failures at Sites I-III can be used to create a set of criteria under which dissolved gas analysis is useful for PRB systems designed to treat acid mine drainage. The following points should be considered to determine if dissolved gas analysis would be informative:

Treatment material suitability:

Organic carbon PRBs – these systems have a near neutral pH, which means that a significant portion of the carbonate produced within the PRB will remain as CO_2. If sufficient gas is produced within the barrier, dissolved gas data can assist in evaluating processes contributing to the consumption of the organic carbon material.

Fe^0/Organic Carbon PRBs – these systems have a high pH, causing CO_2 produced within the barrier to form bicarbonate or carbonate. This leads to less degassing, and less of a signature in the dissolved gas data.

Dissolved gas composition of the influent groundwater:

The influent groundwater to the PRB at Site I had near atmospheric concentrations of Ar and N_2, and low concentrations of other gases. This made Ar and N_2 useful indicators. N_2 and Ar were already depleted upon entering the PRBs at both Sites II and III, which decreases the sensitivity of the method.

Residence times within the PRB:

Dissolved gas data is particularly useful, if residence times in the PRB are sufficiently long to allow gas production and degassing. If residence times are short, the value of dissolved gas data lies primarily in its use as a transport tracer. If transport rates are slow, the value of dissolved gas data lies primarily in its use as a reaction tracer.

In summary, dissolved gas analysis proved useful at all sites, with Site I having the best results. Residence times were sufficiently long to provide information on both reaction and transport processes, while at Sites II and III, residence times were either too short or too long, providing only information on the transport or reaction processes within the PRB. Furthermore, the treatment material within the PRB and the composition of the dissolved gases of the influent groundwater at Site I provided a system that was suitable for using dissolved gas analysis.

Appendix A

Sample Location	CH_4 error			CO_2 error			Argon Error			N_2 Error			Total Pressure Error		
	obs. (atm)	mod. (atm)	error	obs. (atm)	mod. (atm)	error	obs. (atm)	mod. (atm)	error	obs. (atm)	mod. (atm)	error	obs. (atm)	mod. (atm)	error
29_2	0.30	0.2429	18.9	0.24	0.2625	11.6	0.007	0.008	13.6	0.49	0.4869	0.3	1.03	1.00	2.6
29_8	0.14	0.2561	83.9	0.36	0.2781	21.8	0.007	0.007	4.3	0.47	0.4597	3.1	0.98	1.00	2.5
30_a	0.34	0.3695	7.6	0.32	0.4685	48.5	0.003	0.003	22.4	0.17	0.1588	6.8	0.83	1.00	20.2
30_4	0.09	0.2128	142.6	0.29	0.2311	20.1	0.008	0.008	1.3	0.53	0.5481	3.7	0.91	1.00	9.4
30_3	0.62	0.2674	57.0	0.25	0.2937	16.8	0.007	0.007	1.8	0.45	0.433	3.2	1.33	1.00	24.6
30_b	0.23	0.1337	43.0	0.15	0.1677	11.7	0.010	0.009	6.2	0.71	0.69	3.0	1.11	1.00	9.5
31_2	0.40	0.344	14.8	0.30	0.4581	54.5	0.004	0.004	4.4	0.22	0.1976	9.9	0.92	1.00	8.7
31_a	0.84	0.3615	57.2	0.40	0.4696	17.1	0.003	0.003	0.2	0.17	0.1657	0.1	1.41	1.00	29.3
31_4	0.17	0.1099	36.1	0.22	0.1518	30.6	0.010	0.010	9.1	0.74	0.7282	2.2	1.15	1.00	12.8
31_b	0.33	0.1953	40.3	0.24	0.2153	12.1	0.009	0.008	8.9	0.61	0.5806	5.4	1.20	1.00	16.4
Slow Path Ave.			31.1			29.7			8.5			4.0			17.1
Fast Path Ave.			69.2			19.3			6.0			3.5			10.1
Overall Average			50.1			24.5			7.2			3.8			13.6

Table A1. Observed and modeled partial pressures and total pressures in atmospheres for sampling locations within the barrier. Model estimates assume a 16 : 1 ratio of sulfate reduction to methanogenesis, and a pH of 6.5 within the barrier. Error is determined as the percent difference in the modeled and observed result divided by the observed value.

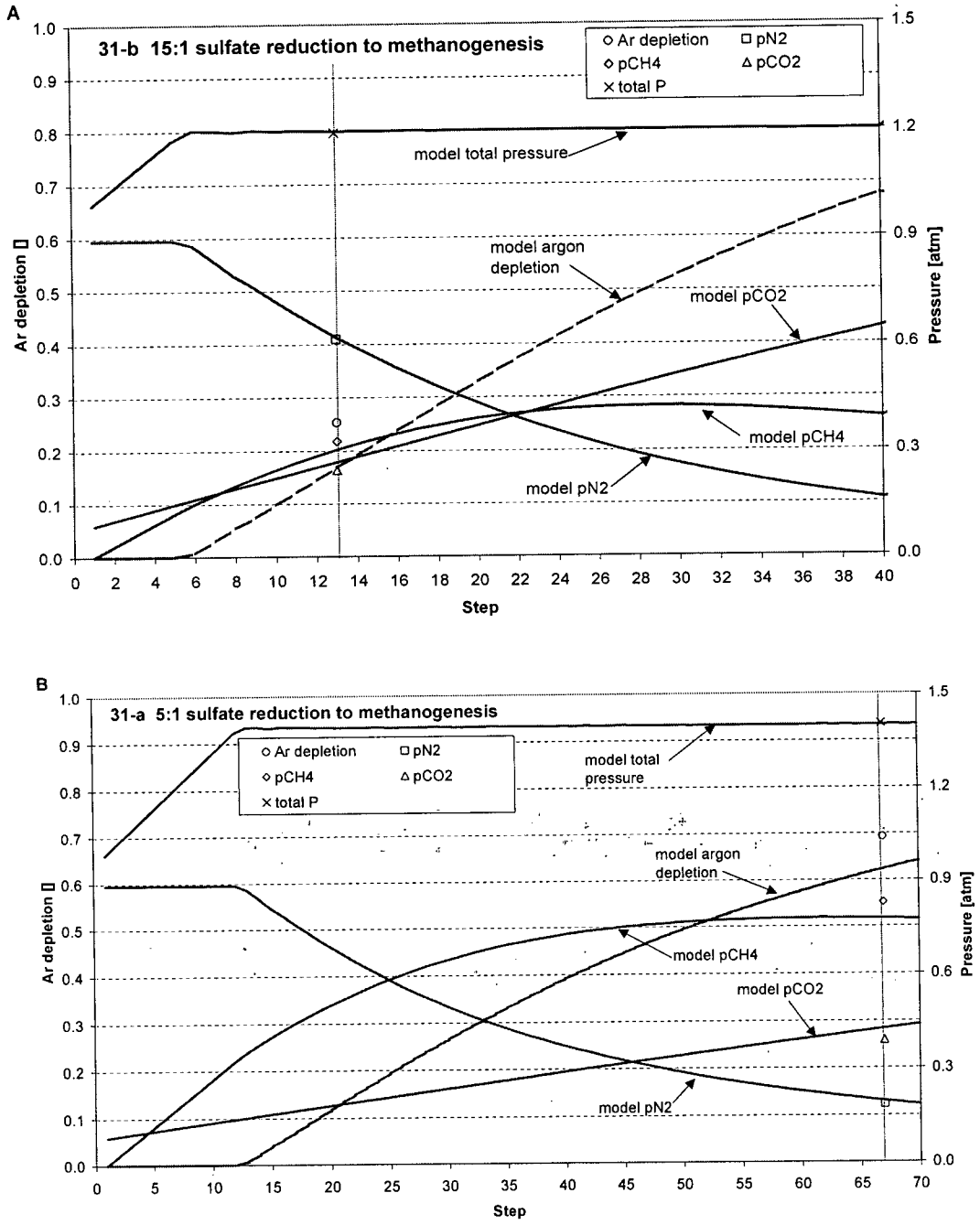

Figure A1. 4-gas model partial pressure results (N_2, CH_4, CO_2, Ar depletion, and total pressure) for differing ratios of sulfate reduction to methanogenesis at an assumed pH of 6.5, plotted against observed sampling location results (A) 31-b and (B) 31-a within the barrier.

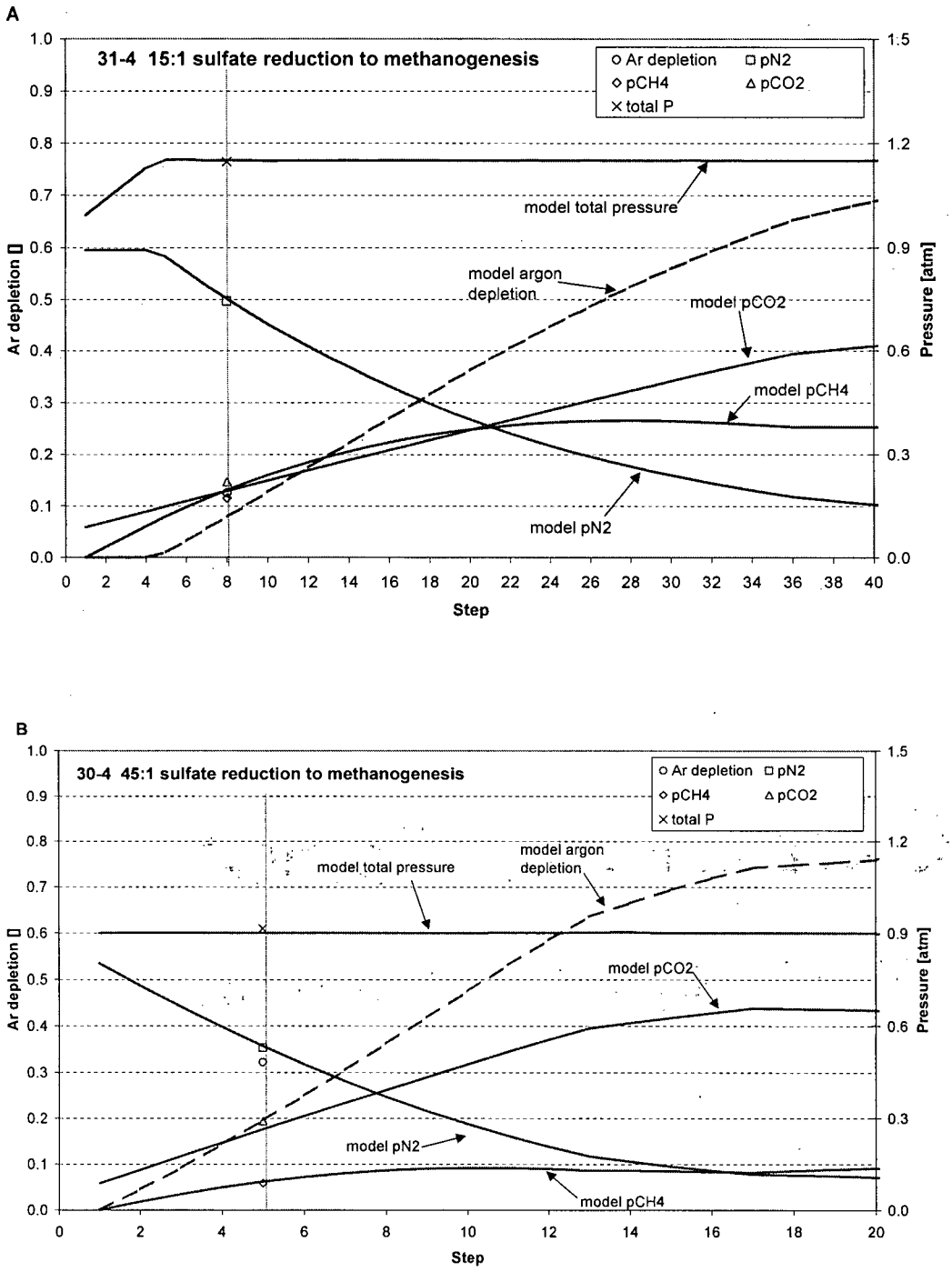

Figure A2. 4-gas model partial pressure results (N_2, CH_4, CO_2, Ar depletion, and total pressure) for differing ratios of sulfate reduction to methanogenesis at an assumed pH of 6.5, plotted against observed sampling location results (A) 31-4 and (B) 30-4 within the barrier.

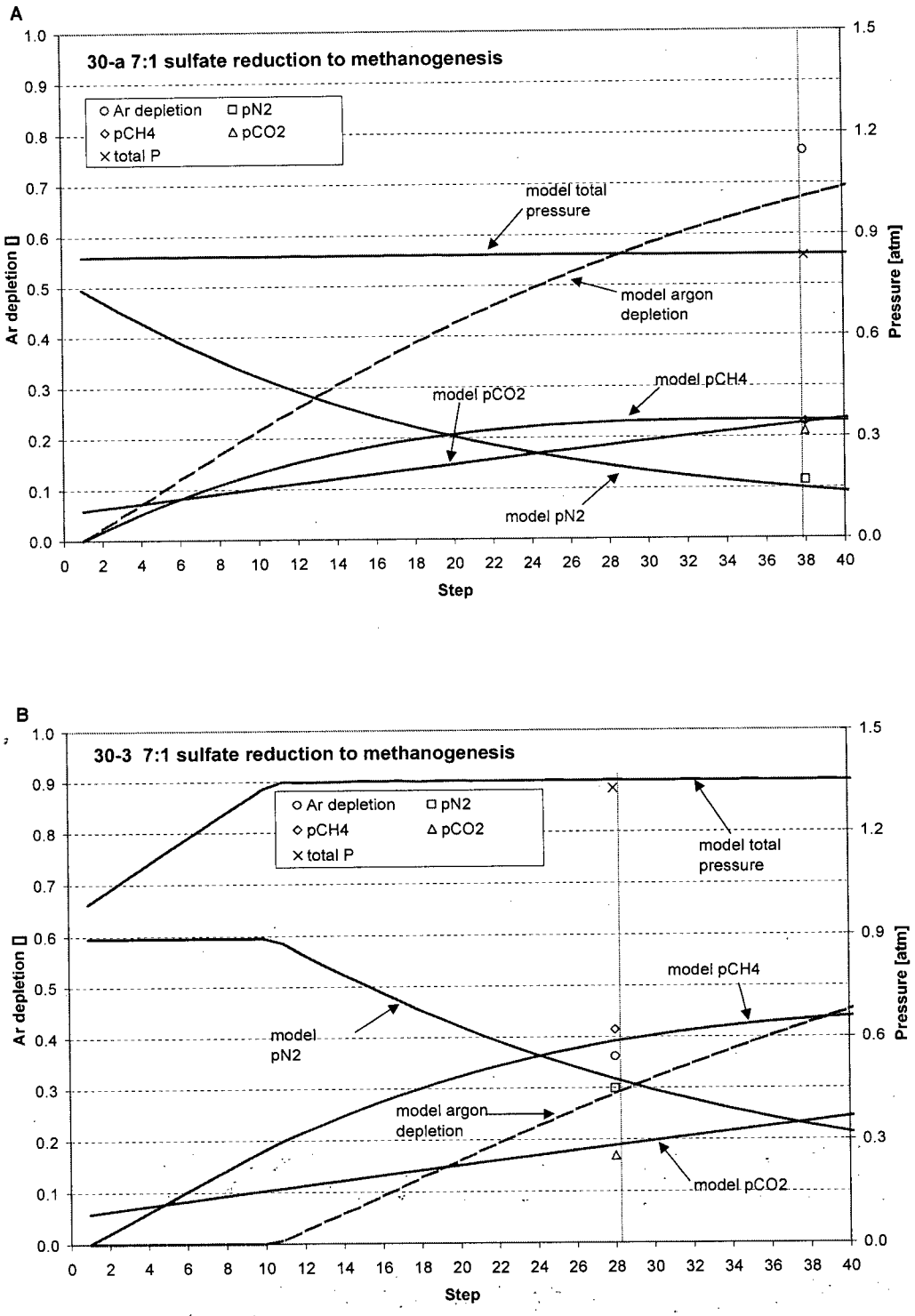

Figure A3. 4-gas model partial pressure results (N_2, CH_4, CO_2, Ar depletion, and total pressure) for differing ratios of sulfate reduction to methanogenesis at an assumed pH of 6.5, plotted against observed sampling location results (A) 30-a and (B) 30-3 within the barrier.

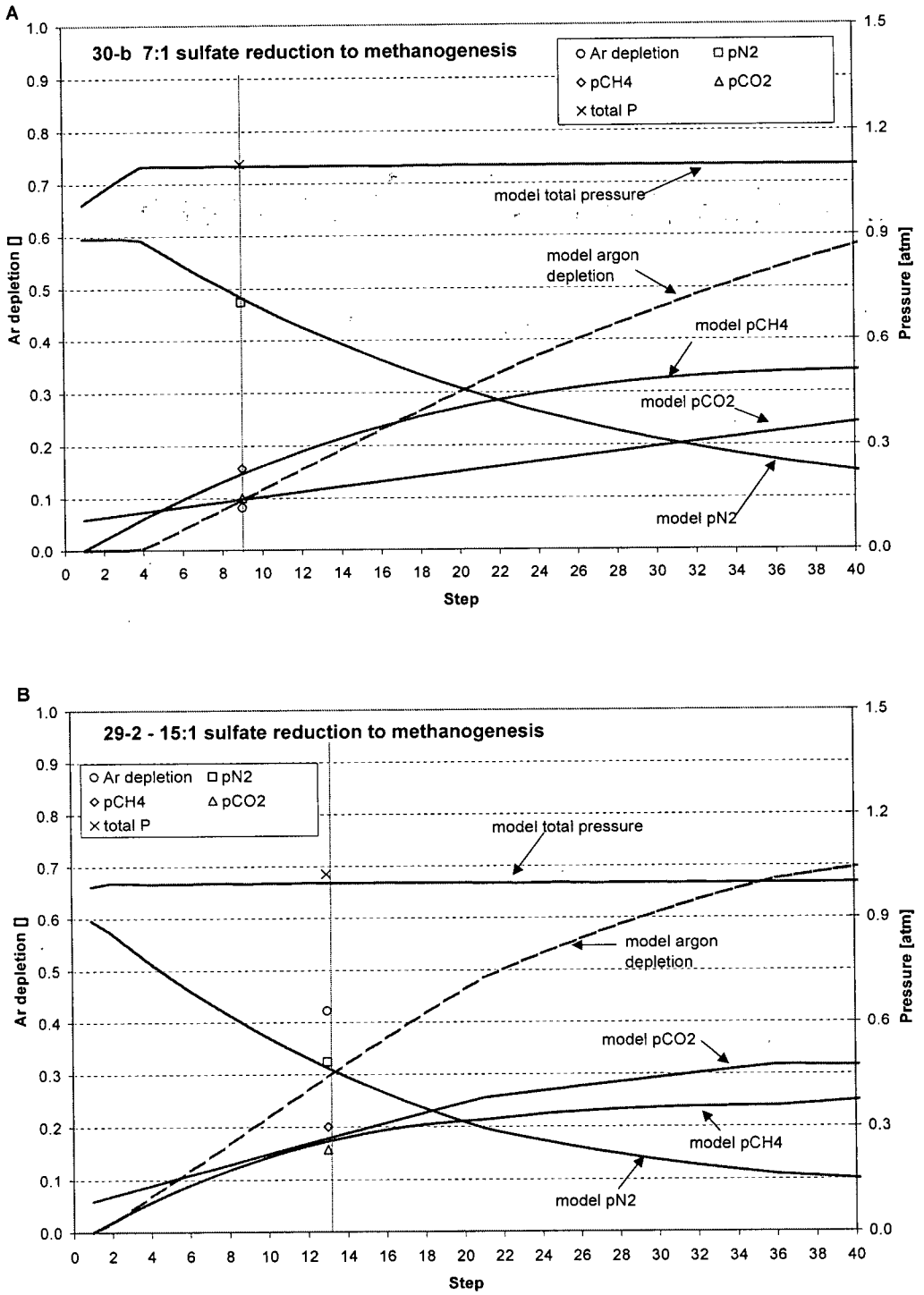

Figure A4. 4-gas model partial pressure results (N_2, CH_4, CO_2, Ar depletion, and total pressure) for differing ratios of sulfate reduction to methanogenesis at an assumed pH of 6.5, plotted against observed sampling location results (A) 30-b and (B) 29-2 within the barrier.

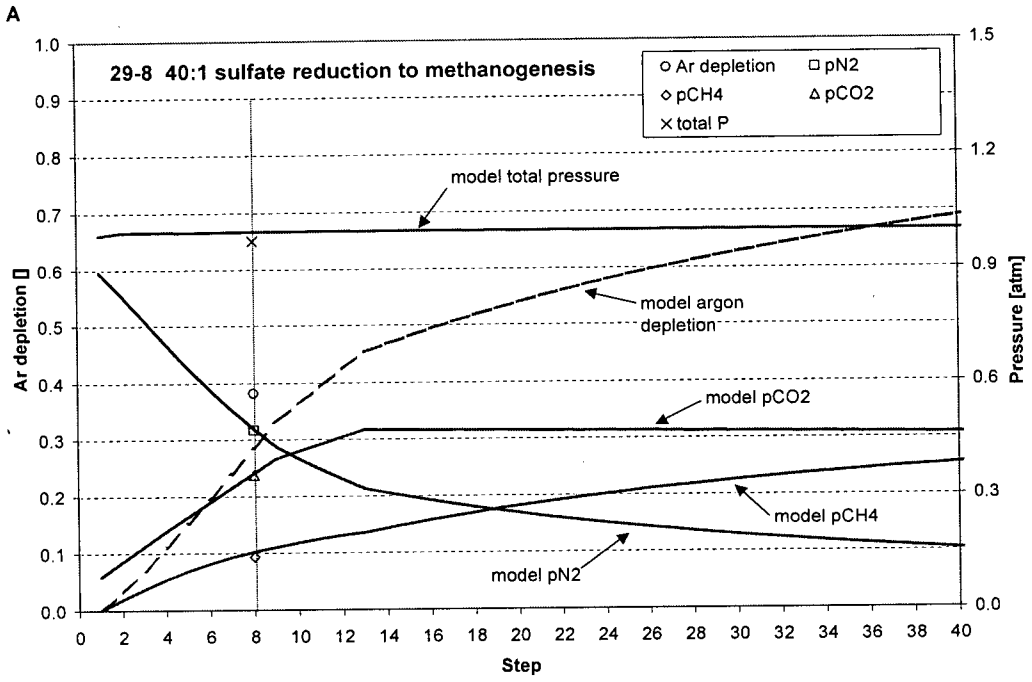

Figure A5. 4-gas model partial pressure results (N_2, CH_4, CO_2, Ar depletion, and total pressure) for differing ratios of sulfate reduction to methanogenesis at an assumed pH of 6.5, plotted against observed sampling location results for 29-8 within the barrier.

Sample Location	CH_4 Error			CO_2 Error			Argon Error			N2 Error			Total Pressure		
	obs. (atm)	mod. (atm)	error	obs. (atm)	mod. (atm)	error	obs. (atm)	mod. (atm)	error	obs. (atm)	mod. (atm)	error	obs. (atm)	mod. (atm)	error
29_2	0.30	0.26	13.5	0.24	0.27	13.3	0.007	0.007	10.9	0.49	0.48	2.0	1.03	1.01	1.8
29_8	0.14	0.15	9.9	0.36	0.36	1.5	0.007	0.008	7.0	0.47	0.48	0.9	0.98	1.00	2.4
30_a	0.34	0.35	1.5	0.32	0.34	7.8	0.003	0.003	15.3	0.17	0.15	13.1	0.83	0.84	1.0
30_4	0.09	0.09	6.5	0.29	0.26	8.9	0.008	0.008	2.7	0.53	0.54	1.2	0.91	0.90	1.5
30_3	0.62	0.59	5.6	0.25	0.28	12.2	0.007	0.007	7.9	0.45	0.48	6.2	1.33	1.35	1.8
30_b	0.23	0.22	6.5	0.15	0.15	2.8	0.010	0.009	3.8	0.71	0.72	1.9	1.11	1.10	0.5
31_2	0.40	0.38	5.8	0.30	0.29	2.0	0.004	0.004	15.6	0.22	0.22	2.5	0.92	0.90	2.5
31_a	0.84	0.78	8.0	0.40	0.42	4.8	0.003	0.004	16.7	0.17	0.20	20.7	1.41	1.40	1.0
31_4	0.17	0.20	13.5	0.22	0.19	11.6	0.010	0.010	7.6	0.74	0.75	1.1	1.15	1.15	0.4
31_?	0.33	0.30	7.4	0.24	0.27	9.4	0.009	0.009	5.6	0.61	0.62	0.9	1.20	1.20	0.3
Slow Path Ave.			6.9			8.0			13.3			8.9			1.6
Fast Path Ave.			8.7			6.8			5.3			1.2			1.0
Overall Average			7.8			7.4			9.3			5.1			1.3

Table A2. Observed and modeled partial pressures and total pressures in atmospheres for sampling locations within the barrier. Model estimates assume of pH of 6.5 within the barrier, and a ratio of sulfate reduction to methanogenesis that is specific to that sample location. Error is determined as the percent difference in the modeled and observed result divided by the observed value.

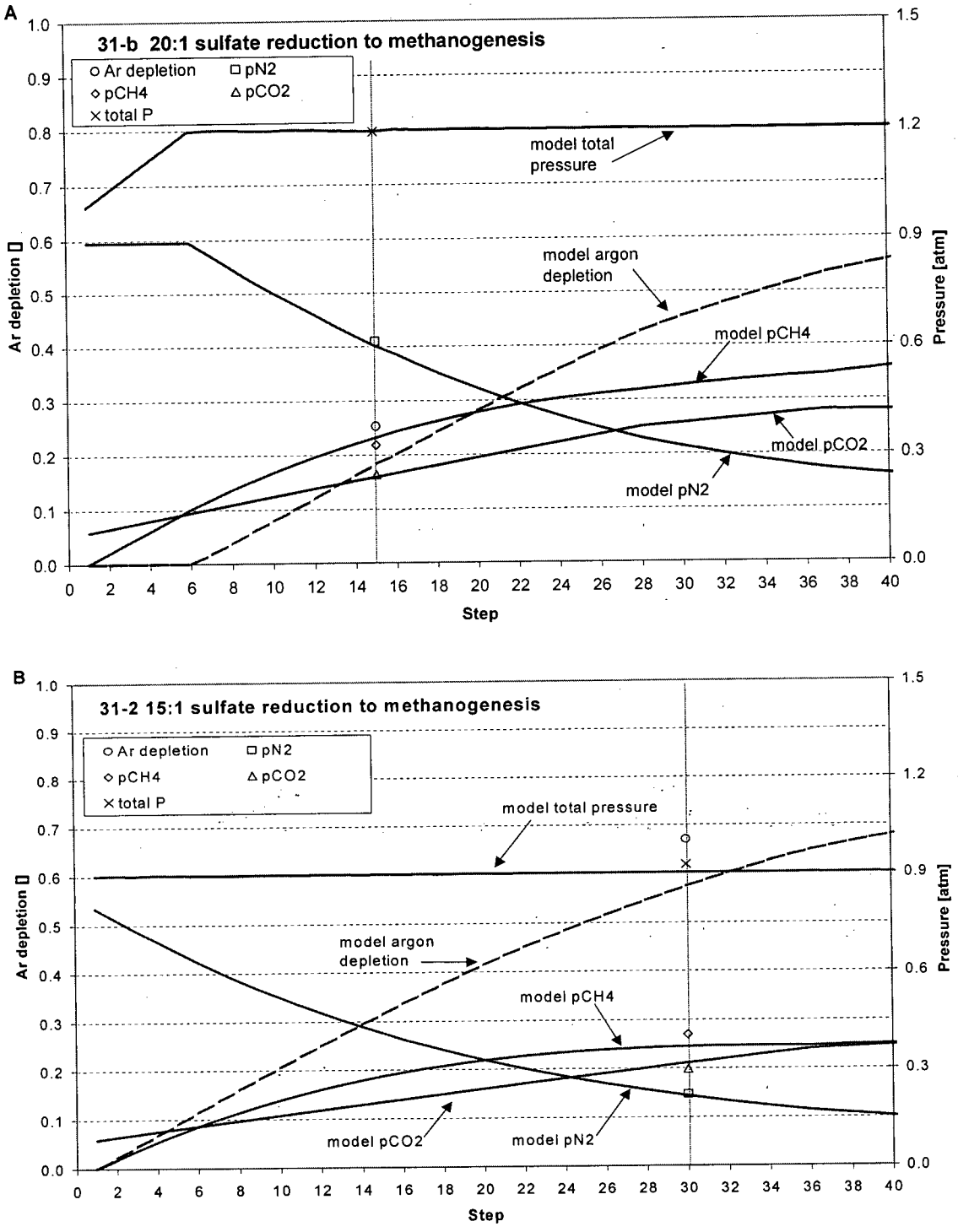

Figure A6. 4-gas model partial pressure results (N_2, CH_4, CO_2, Ar depletion, and total pressure) for differing ratios of sulfate reduction to methanogenesis at an assumed pH of 6.9, plotted against observed sampling location results (A) 31-b and (B) 31-2 within the barrier.

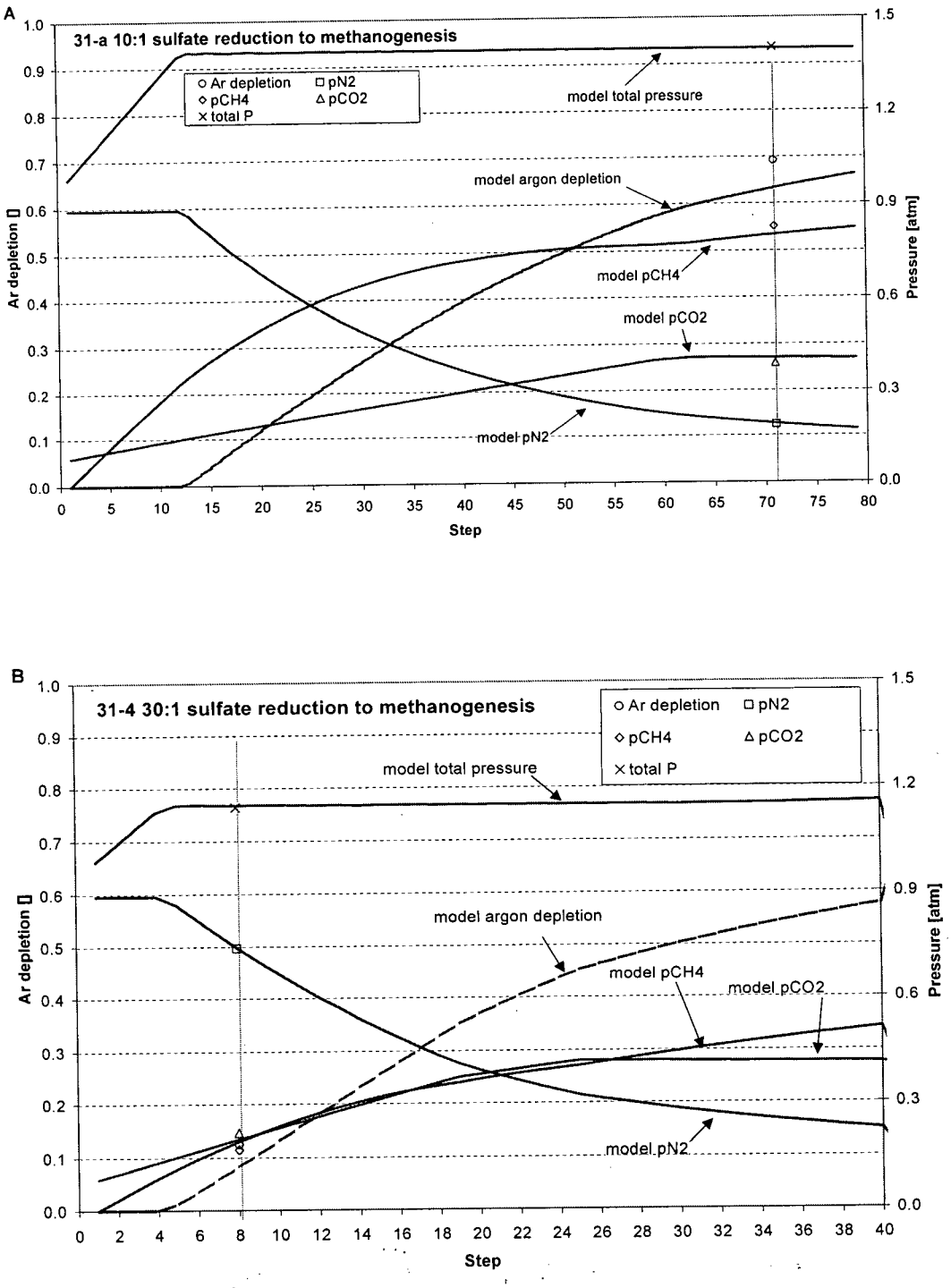

Figure A7. 4-gas model partial pressure results (N_2, CH_4, CO_2, Ar depletion, and total pressure) for differing ratios of sulfate reduction to methanogenesis at an assumed pH of 6.9, plotted against observed sampling location results (A) 31-a and (B) 31-4 within the barrier.

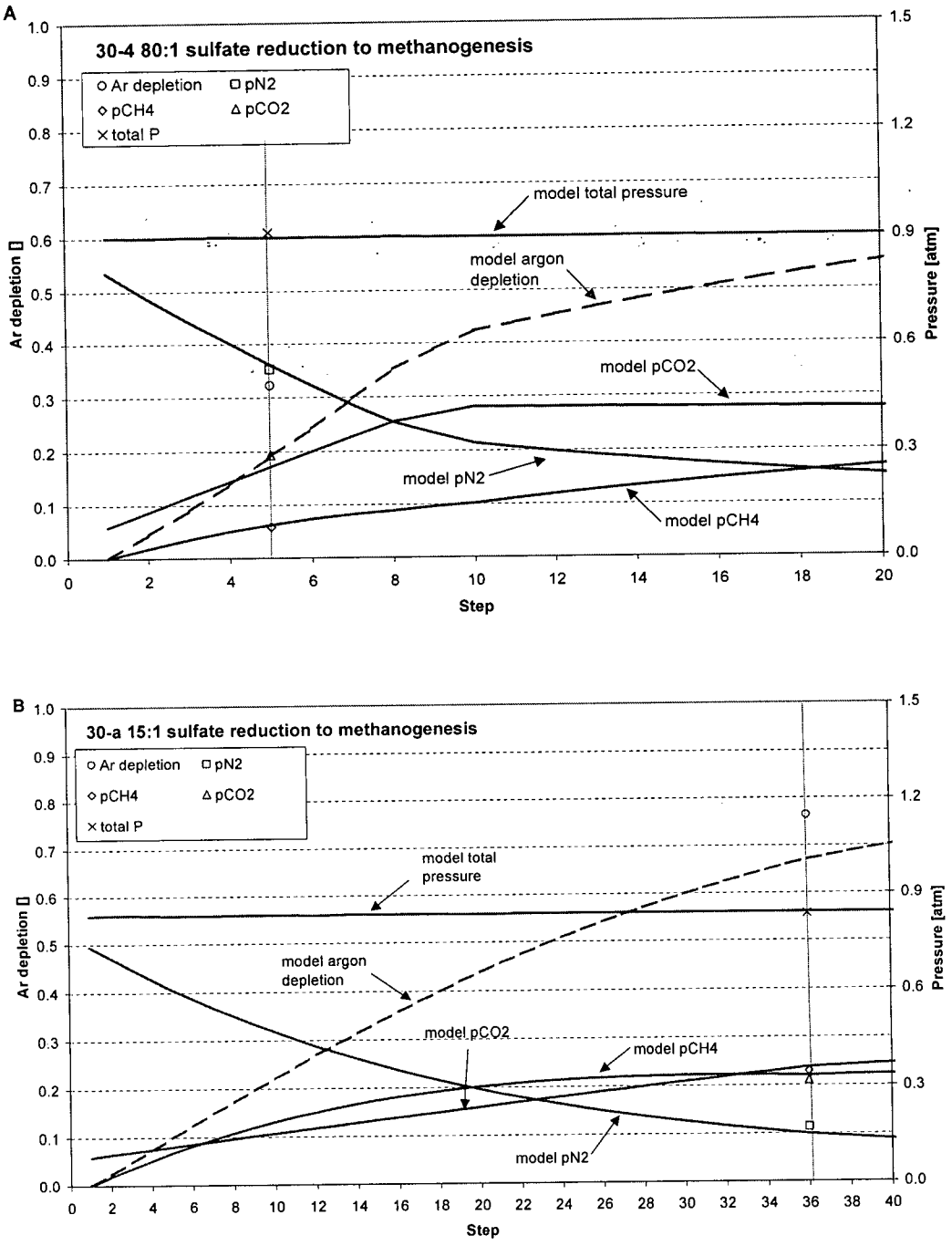

Figure A8. 4-gas model partial pressure results (N_2, CH_4, CO_2, Ar depletion, and total pressure) for differing ratios of sulfate reduction to methanogenesis at an assumed pH of 6.9, plotted against observed sampling location results (A) 30-4 and (B) 30-a within the barrier.

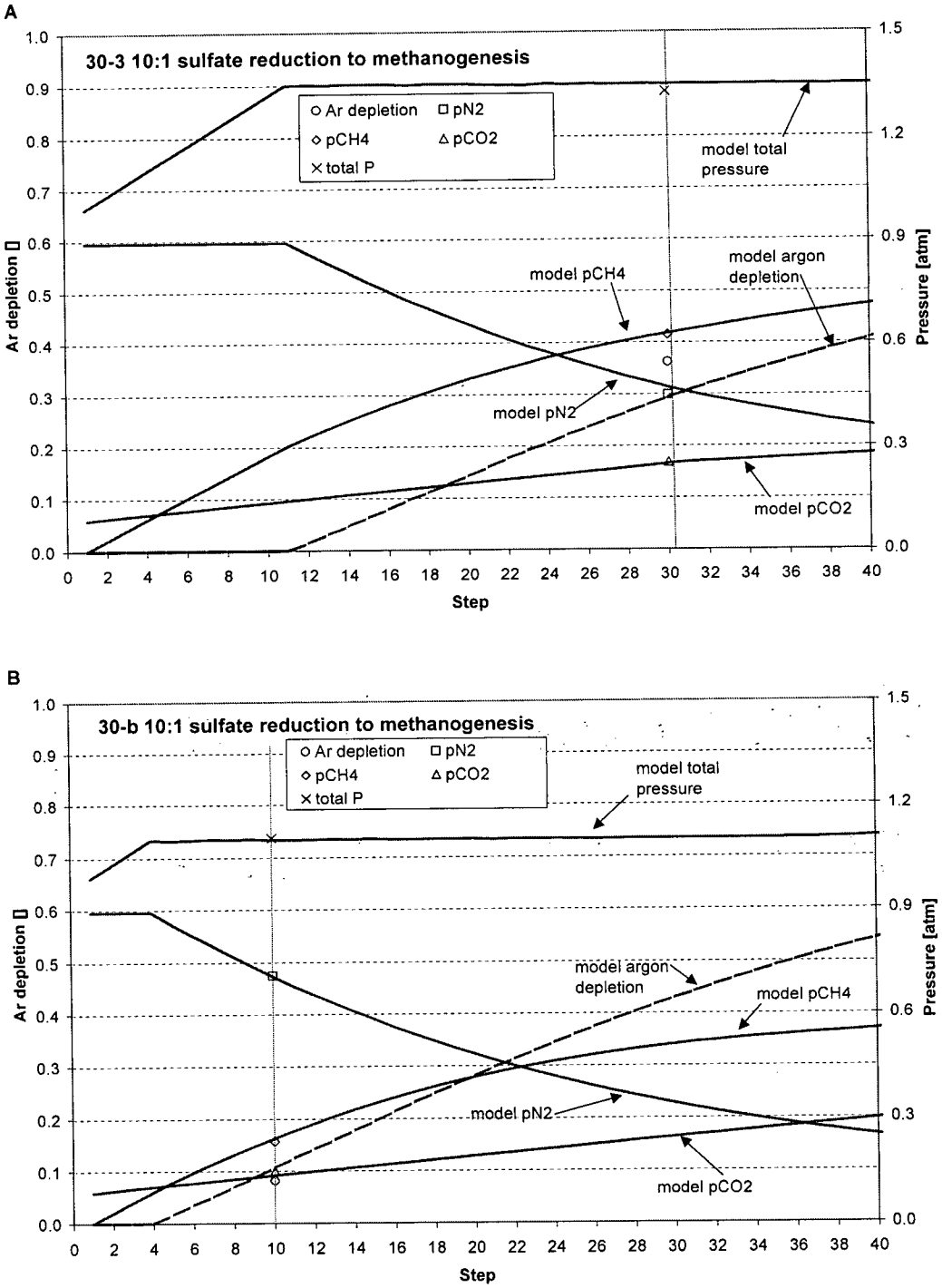

Figure A9. 4-gas model partial pressure results (N_2, CH_4, CO_2, Ar depletion, and total pressure) for differing ratios of sulfate reduction to methanogenesis at an assumed pH of 6.9, plotted against observed sampling location results (A) 30-3 and (B) 30-b within the barrier.

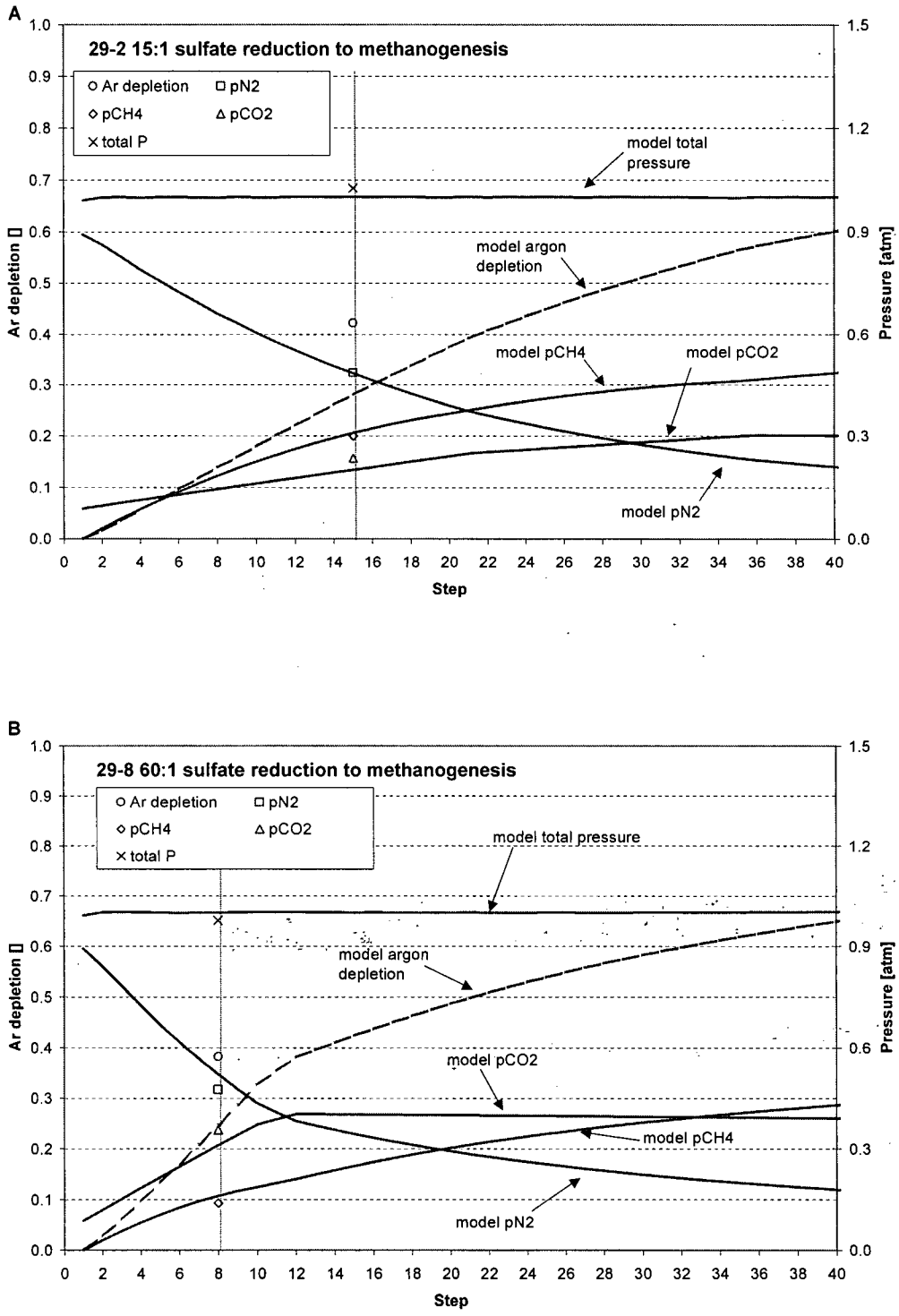

Figure A10. 4-gas model partial pressure results (N_2, CH_4, CO_2, Ar depletion, and total pressure) for differing ratios of sulfate reduction to methanogenesis at an assumed pH of 6.9, plotted against observed sampling location results (A) 29-2 and (B) 29-8 within the barrier.

Sample Location	CH_4 Error			CO_2 Error			Argon Error			N_2 Error			Total Pressure		
	obs. (atm)	mod. (atm)	error	obs. (atm)	mod. (atm)	error	obs. (atm)	mod. (atm)	error	obs. (atm)	mod. (atm)	error	obs. (atm)	mod. (atm)	error
29_2	0.60	0.61	3.2	0.53	0.50	14.9	0.31	0.31	13.5	0.78	0.76	6.0	1.33	1.27	5.4
29_8	0.44	0.46	15.7	0.66	0.61	13.1	0.31	0.31	12.9	0.77	0.82	10.0	1.28	1.30	2.7
30_a	0.64	0.63	3.8	0.61	0.66	13.3	0.30	0.30	16.2	0.47	0.45	12.9	1.13	1.14	1.3
30_4	0.39	0.39	7.4	0.59	0.56	11.5	0.31	0.31	2.4	0.83	0.84	2.6	1.21	1.20	1.9
30_3	0.92	0.92	1.0	0.55	0.55	2.3	0.31	0.31	7.4	0.75	0.77	5.2	1.63	1.65	1.9
30_b	0.53	0.54	4.3	0.45	0.44	8.7	0.31	0.31	5.2	1.01	1.01	0.6	1.40	1.40	0.9
31_2	0.70	0.67	9.5	0.60	0.61	6.7	0.30	0.30	11.7	0.52	0.51	2.6	1.22	1.20	2.8
31_a	1.14	1.10	5.4	0.70	0.71	1.7	0.30	0.30	11.9	0.46	0.49	14.5	1.71	1.70	1.3
31_4	0.47	0.49	13.3	0.52	0.50	8.5	0.31	0.31	8.4	1.04	1.04	0.4	1.45	1.45	0.7
31_?	0.63	0.65	6.6	0.54	0.54	2.9	0.31	0.31	7.5	0.91	0.90	2.4	1.49	1.49	0.3
Slow Ave			4.6			7.8			12.1			8.2			2.5
Fast Ave			9.5			8.9			7.3			3.2			1.3
Average			7.0			8.4			9.7			5.7			1.9

Table A3. Observed and modeled partial pressures and total pressures in atmospheres for sampling locations within the barrier. Model estimates assume a pH of 6.9 within the barrier and a ratio of sulfate reduction to methanogenesis that is specific to that sample location. Error is determined as the percent difference in the modeled and observed result divided by the observed value.